

Dissertation zur Erlangung des Doktorgrades
der Fakultät für Chemie und Pharmazie
der Ludwig-Maximilians-Universität München

**Mechanisms of rabies virus to escape the IFN system -
main actor: the phosphoprotein P**



Martina Rieder
aus Freising, Deutschland

2012

Erklärung

Diese Dissertation wurde im Sinne von §7 der Promotionsordnung vom 28. November 2011 von Herrn Prof. Conzelmann betreut und von Herrn Prof. Beckmann vor der Fakultät für Chemie und Pharmazie vertreten.

Eidesstattliche Versicherung

Diese Dissertation wurde eigenständig und ohne unerlaubte Hilfe erarbeitet.

München, den

.....

(Unterschrift des Autors)

Dissertation eingereicht am:	17.01.2012
Erstgutachter:	Prof. Dr. Karl-Klaus Conzelmann
Zweitgutachter:	Prof. Dr. Roland Beckmann
Tag der mündlichen Prüfung:	07.03.2012

This thesis has been prepared in the laboratory of Prof. Karl-Klaus Conzelmann at the Max von Pettenkofer-Institute and Gene Center of the Ludwig-Maximilians-University Munich.

Danksagung

Viele Menschen haben mich auf dem Weg der Doktorarbeit begleitet.

Allen voran möchte ich meiner Familie danken. Meinen Eltern, die mir ein Studium im Ausland und den langen Weg zum Dokortitel ermöglicht haben. Meinen älteren Geschwistern, die mich gut vorbereitet haben auf einen anspruchsvollen Werdegang.

Ganz besonders danke ich Prof. Dr. Karl-Klaus Conzelmann für die interessanten Projekte, die Unterstützung, und die Grillfeste, und Prof. Dr. Roland Beckmann für die Vertretung meiner Doktorarbeit. Meiner Arbeitsgruppe, d.h. Alex, Anika, Kerstin, Nadin, Vanessa, Konstantin, Moni, Christian, Lisa und Adriane, danke ich für den unglaublich starken Zusammenhalt und dass der Spass nie zu kurz gekommen ist.

Die Zeit im Labor 2.65 aka "Elba" aka "Harmony-Lab" wird mir, durch meine Koszi-Arbeitskollegen Jens, Bernd und Lisa, die super Praktikanten, die gute Musik, und viele Gespräche, immer besonders in Erinnerung bleiben.

Aus meiner Doktorarbeitszeit nicht wegzudenken ist Lisa, die immer ein offenes Ohr hat(te) und mir bei diversen Ausflügen auf das Dach mit gutem Rat zur Seite stand. Letztendlich haben mich Freundschaften wie diese in dieser Zeit gestärkt. An diesem Punkt möchte ich mich bei meinen Mädels bedanken, Silvi, Chrissy, Celine, Nadja M., Nadja D., Jeanny, Julia, Alex und Simone, die schon seit 15 Jahren an meiner Seite sind und in allen Lebenslagen für mich da sind.

Der Erfolg im letzten Jahr meiner Doktorarbeit wurde durch einen Menschen stark beeinflusst, der mir immer das Gefühl gegeben hat dass ich alles schaffen kann. Danke Beni!! Finanziert wurde der größte Teil meiner Arbeit durch das DFG Graduiertenkolleg 1202, unter der Leitung von Prof. Dr. Stefan Endres. Das Kolleg hat mir viele zusätzliche Weiterbildungen ermöglicht und Optionen eröffnet, und ich möchte mich bei Prof. Endres für das Engagement bedanken, mit dem er mich unterstützt und gefördert hat.

Table of contents

List of publications and oral presentations	IV
Summary	V
1 Introduction	1
1.1 Rabies virus (RABV) and the Lyssavirus genus.....	1
1.1.1 Lyssavirus taxonomy	1
1.1.2 Lyssavirus structure and genomes	4
1.1.3 Lyssavirus pathogenicity.....	5
1.1.4 RABV life cycle	7
1.1.5 RABV phosphoprotein P	10
1.2 Immune response to RABV.....	13
1.2.1 The interferon (IFN) system	13
1.2.2 Activation of RLR signaling by RABV.....	20
1.3 RABV countermeasures to inhibit IFN	23
1.4 Aim of this thesis	25
2 Materials and Methods.....	26
2.1 Materials.....	26
2.1.1 Chemicals.....	26
2.1.2 Kits.....	28
2.1.3 Enzymes and buffers	29
2.1.4 Oligonucleotides.....	30
2.1.5 Antibodies	31
2.1.6 Cell lines and media.....	32
2.1.7 Bacteria and media.....	34
2.1.8 Plasmids.....	34
2.1.9 Recombinant proteins	43
2.1.10 Viruses	44
2.1.11 Equipment	45
2.1.12 Miscellaneous.....	47
2.2 Methods.....	48
2.2.1 Cell culture.....	48
2.2.2 Plasmid construction: cloning and mutagenesis.....	48
2.2.3 Transfection and infection	52
2.2.4 Purification of recombinant proteins.....	53

2.2.5	Generation of recombinant viruses	54
2.2.6	Minigenome assay.....	55
2.2.7	Titration of virus stocks	55
2.2.8	Virus growth curves.....	55
2.2.9	RNA isolation and reverse transcription (RT) PCR.....	56
2.2.10	Northern blot.....	57
2.2.11	Quantitative real time-PCR (qRT-PCR).....	57
2.2.12	Luciferase reporter gene assay	59
2.2.13	Co-immunoprecipitation (Co-IP)	59
2.2.14	Denaturing polyacrylamide gel electrophoresis (SDS-PAGE).....	61
2.2.15	Native PAGE.....	61
2.2.16	Coomassie staining.....	62
2.2.17	Western blot analysis (semi-dry).....	62
2.2.18	Immunodetection.....	62
2.2.19	Immunofluorescence (IF)	63
2.2.20	<i>In vitro</i> ATPase assays.....	63
2.2.21	<i>In vitro</i> transcription.....	64
3	Results.....	65
3.1	Mechanisms of RABV P to inhibit IFN induction.....	65
3.1.1	Inhibition of IFN induction by RABV P depends on an internal domain	65
3.1.1.1	Deletion of RABV P amino acids 176-186 results in loss of IFN β inhibition	66
3.1.1.2	Amino acids 176-186 are essential to efficiently inhibit TBK1- and IKKi-induced IRF3 phosphorylation	67
3.1.2	Generation of recombinant viruses harboring deletions of amino acids 176-186	68
3.1.2.1	P Δ Ind proteins support viral growth	69
3.1.2.2	SAD Δ Ind viruses can grow in IFN-incompetent and IFN-competent cells	70
3.1.2.3	SAD Δ Ind viruses are inducers of IFN β , yet with diverging capacities.....	72
3.1.2.4	SAD Δ Ind1, a strong inducer of IFN β , has a characteristic transcription and replication profile, and is highly attenuated <i>in vivo</i>	73
3.1.3	RABV P interacts with proteins of the RLR signaling cascade: Interaction with RLRs.....	75
3.1.3.1	RABV P interacts with MDA5 and to a lesser extent Lgp2.....	76
3.1.3.2	RABV P interacts with the CARD/HD junction of MDA5 and the HD of Lgp2.....	77
3.1.3.3	RABV P _{NTD} and P _{CTD} regions confer interaction with MDA5.....	79
3.1.3.4	RABV P Δ Ind1 is able to interact with MDA5.....	80

3.1.3.5	Activation of RIG-I allows for RABV P association	81
3.1.3.6	Interaction of RABV P with RIG-I or MDA5 does not inhibit their ATPase activity...	84
3.1.4	RABV P interacts with proteins of the RLR signaling cascade: Interaction with IRF3	86
3.1.4.1	RABV P interacts with IRF3 depending on its activation	86
3.1.4.2	RABV P/IRF3 interaction inhibits phosphorylation of IRF3 at serine 386 while allowing phosphorylation at serines 396 and 398	89
3.1.4.3	Site directed mutagenesis of IRF3 serines 396/398 to alanine reduces interaction with RABV P	91
3.1.4.4	RABV P/IRF3 interaction involves helices H3/H4 of the IRF association domain	93
3.1.4.5	RABV P Δ Ind mutants unable to inhibit serine 386 phosphorylation can still interact with IRF3	95
4	Discussion.....	98
4.1	Inhibition of type I IFN induction by RABV P depends on amino acids 176-186.....	99
4.2	Inhibition of IRF3 activation is important for pathogenicity	101
4.3	RABV P interacts with RIG-I-like helicases depending on their conformational state	102
4.4	MDA5 holds a conformation that allows for basal signaling without activation	106
4.5	RABV P interacts with an activation intermediate of IRF3, depending on S396/S398 phosphorylation	107
4.6	RABV P binds to the H3/H4 helix of IRF3.....	110
4.7	RABV P binding to IRF3 H3/H4 shields adjacent S385/S386 from phosphorylation	112
4.8	Conclusion and future perspectives	113
5	Appendix	117
6	List of figures and tables	130
7	List of abbreviations.....	132
8	References	137

List of publications

- **Rieder M**, Finke S, Conzelmann KK. Interferon in lyssavirus infection. *BMTW*. In press.
- Marcinowski L, Lidschreiber M, **Rieder M**, et al. Real-time transcriptional profiling of cellular and viral gene expression during lytic cytomegalovirus infection. Manuscript in preparation.
- **Rieder M**, Conzelmann KK (2011). Interferon in rabies virus infection. *Adv. Virus Res.* 79:91-114. PMID: 21601044.
- **Rieder M**, Brzózka K, Pfaller CK, Cox JH, Stitz L, Conzelmann KK (2011). Genetic dissection of interferon-antagonistic functions of rabies virus phosphoprotein: Inhibition of IRF3 activation is important for pathogenicity. *J. Virol.* 85:842–852.
- **Rieder M**, Drechsel L, Conzelmann KK (2009). Rabies virus evasion of the interferon system. in: *Rabies: Symptoms, treatment and prevention*, Chapter 3. © Nova Science Publishers, Inc. ISBN: 978-1-61668-250-7.
- **Rieder M**, Conzelmann KK (2009). Rhabdovirus evasion of the interferon system. *JICR.* 29(9):499-509.

List of oral presentations

- National Symposium on Zoonosis Research, Berlin (Oct. 2011).
- 21th Annual Meeting of the Gessellschaft für Virologie, Freiburg (March 2011).
- DFG (Deutsche Forschungsgemeinschaft) -Graduiertenkolleg 1202 Annual Retreats (June 2010, June 2011).
- Meeting of the DFG with delegates from leading USA Universities. Oral presentation to represent the DFG Graduiertenkolleg 1202, Munich (June 2010).
- DFG-Graduiertenkolleg 1202 Results Colloquium, Munich (July 2009, Dec. 2010, Nov. 2011).
- Max von Pettenkofer Seminar Series, Munich (Feb. 2008, July 2009, Nov. 2010, Nov. 2011).
- Gene Center Seminar Series, Munich (Feb. 2008, July 2009, Oct. 2011).
- SFB Junior Faculty Retreat, Waging (June 2008).

Summary

The neurotropic rabies virus (RABV) of the *Lyssavirus* genus in the *Rhabdoviridae* family is the main causative agent of rabies, a long known zoonotic infectious disease, which still accounts for more than 55,000 human deaths each year. The virulence of RABV depends on various factors, including multiple mechanisms to counteract the antiviral type I interferon system (α -/ β -interferons) (IFN) of hosts, which are exerted by the viral phosphoprotein P.

In virus-infected cells IFN is induced after recognition of viral RNAs by pattern recognition receptors (PRR), like the RIG-I-like helicases (RLR), which induce downstream signaling leading to activation of the transcription factor IRF3 by the kinases TBK1 and IKKi. Secreted IFNs induce JAK/STAT signaling, which ultimately leads to expression of numerous antiviral and immunestimulatory proteins. RABV P can inhibit both IFN-mediated JAK/STAT signaling and RLR-mediated IRF3 activation and thus induction of IFN transcription. The aim of this work was to elucidate the molecular mechanisms of P to prevent IFN induction.

As revealed by site-directed mutagenesis experiments, the RABV P amino acids (aa) 176-186 are essential for its ability to inhibit IFN induction. RABV P constructs lacking aa 176-181, 182-186, and 176-186, were unable to inhibit IRF3 activation and IFN β transcription, while other multiple functions of P, such as inhibition of JAK/STAT signaling and support of virus replication, were not affected. Recombinant RABV carrying the respective mutations (SAD Δ Ind1, Δ Ind2 and Δ Ind1/2) were strong inducers of IFN and were attenuated after intracerebral injection into mice, illustrating an essential contribution of IFN inhibition to the pathogenicity of RABV.

The mechanisms applied by RABV P were further elucidated through the identification of cellular targets. This study provides first evidence for an interaction of RABV P with RLRs and with IRF3. Co-IP experiments revealed an interaction with the RLRs MDA5 and Lgp2 in non-alerted cells. Moreover, an interaction of P and RIG-I was revealed upon stimulation with RIG-I ligands, including 5'-ppp RNA. Interestingly, this finding is in concordance with the proposed structural models of RIG-I activation, in which ligand binding confers structural changes required for downstream signaling, probably unmasking domains

for P binding. In contrast, the conformation of latent MDA5 allows for both, basal signaling and P binding in the absence of a ligand.

Furthermore, it was shown for the first time that RABV P binds to a novel activation-intermediate form of IRF3, explaining the powerful inhibition of TBK1-mediated IRF3 activation. P was found to bind IRF3 dependent on the degree and time of stimulation of the RLR pathway. P-bound IRF3 revealed phosphorylation of C-terminal residues (S396, S398), while phosphorylation of S386, which is critical for IRF3 transcriptional activity, was prevented. Mutagenesis of IRF3 S396 and S398 resulted in reduced P binding. These data provide evidence for an obligatory sequential phosphorylation of IRF3 in which phosphorylation of the C-terminal Ser residues is required to release an auto-inhibitory domain (including helix 5) to allow S386 phosphorylation. Notably, however, C-terminal phosphomimetic IRF3 mutants still required stimulation to confer substantial P binding, strongly suggesting the existence of further unknown modifications required for full IRF3 activation, and P binding. As revealed by the use of IRF deletion mutants lacking all known auto-inhibitory structures (helix 1 and helix 5) the P binding interface of IRF3 involves helix 3 and 4.

1 Introduction

1.1 Rabies virus (RABV) and the *Lyssavirus* genus

Rabies is an acute and lethal encephalitis and appeared in the history of human threats already before 2000 B.C., as found in annotations by the Egyptians. This makes rabies one of the oldest documented diseases of humans. The pathogen associated to the disease was discovered by Remlinger and colleagues in 1903 and turned out to be a virus, consequently named rabies virus (RABV) (Rupprecht et al., 2002). RABV, which is actually one of the 30 first discovered viruses, belongs to the order *Mononegavirales* due to its non-segmented negative-strand RNA genome, and was annotated to the *Lyssavirus* genus of the family *Rhabdoviridae*. *Rhabdoviridae* are composed of a growing number of viruses, which comprise several livestock pathogens such as vesicular stomatitis virus (VSV; *Vesiculovirus* genus) or bovine ephemeral fever virus (BEFV; *Ephemerovirus* genus), many of which are of economic importance. Particularly appreciable, however, is RABV, the prototype of the *Lyssavirus* genus, which is a zoonosis and remains a constant and global threat for human health although effective vaccines and post-exposure prophylaxis (PEP) are available. Typically, lyssaviruses are associated with bats as reservoir species and restricted to certain geographical areas. However, RABV is endemic throughout the world and mainly infects terrestrial warm-blooded mammals found in wildlife, such as dogs, foxes, raccoons, skunks, jackals, mongooses etc. Human lyssavirus infections are still mainly associated with RABV, yet sporadic cases of rabies-like encephalitis have been reported from rabies-related lyssaviruses (Johnson et al., 2010). The factors involved in limiting the host range and being responsible for crossing the species barrier still remain unknown, especially as a very close genetic relationship between RABV and rabies-related viruses is obvious.

1.1.1 *Lyssavirus* taxonomy

Since the first isolation of a rabies-related virus in Africa 1956, ten viruses have been assigned to the *Lyssavirus* genus in addition to RABV and new isolates are analyzed in

ongoing attempts. The relatedness of the first African isolates to RABV was suggested 14 years later in an electron microscopy study from 1969/1970, where the bullet shape morphology characterized the viruses as rhabdoviruses (Shope et al., 1970). Up to date, serotyping and genotyping are the common methods to assign lyssaviruses, yet also their pathogenicity and immunogenicity are considered (Badrane et al., 2001). Nowadays, a great variety of other rabies-related viruses have been isolated, mostly from bats and from all around the world. Distinct viruses show prevalence for specific regions and bat species (see table 1). Interestingly, RABV has also been found in bats, however, apparently only in the Americas (Hughes et al., 2005). The reasons for this geographical separation and the evolution of bat lyssaviruses still remain elusive. In view of the close phylogenetic relationship, it is assumed that all lyssaviruses emerged from bat. Though only two of the viruses have been isolated from terrestrial animals, namely RABV and Mokola virus (MOKV), an evolutionary genetic adaptation seems obvious. Evolutionary relationships amongst the lyssaviruses are depicted in a phylogenetic tree (Fig. 1-1).

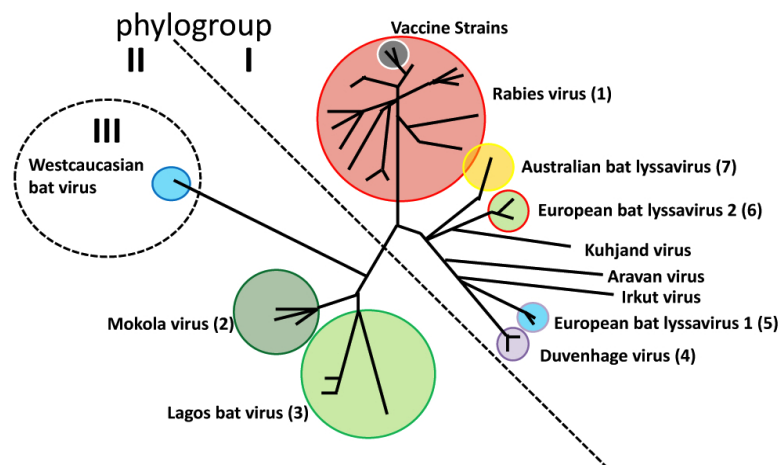


Figure 1-1: Phylogenetic tree of the lyssaviruses genus. Lyssaviruses are grouped into three phylogroups (I, II and III), according to their evolutionary relationship. Lyssaviruses are further assigned to specific genotypes based on their nucleotide sequence, immunogenicity and pathogenicity (in brackets or in table (1)). Assignment of ARAV, KHUV and IRKV (also SHIBV and BBLV; not shown) to specific Genotypes still has to be performed (figure adapted from (Badrane et al., 2001)).

Lyssaviruses are grouped into phylogroups I, II and III, and further annotated to distinct genotypes (table 1) due to their nucleotide sequence, immunogenicity and pathogenicity. Phylogroup I comprises RABV, and the closely related Australian bat lyssavirus (ABLV) (Fraser et al., 1996), Aravan virus (ARAV) (Kuz'min et al., 1992),

Khujand virus (KHUV) (Kuzmin et al., 2002), and European bat lyssavirus 2 (EBLV-2) (Lumio et al., 1986). Additionally, it contains Irkut virus (IRKV) (Botvinkin et al., 2003), Duvenhage virus (DUVV) (Meredith et al., 1971) and EBLV-1 (Schneider et al., 1985). Phylogroup II includes the more distinctly related Lagos bat virus (LBV) (Boulger and Porterfield, 1958) and MOKV (Shope et al., 1970). Two further viruses, namely Shimoni bat virus (SHIBV) (Kuzmin et al., 2010) and Bokeloh bat virus (BBV) (Freuling et al., 2011), have been recently proposed to belong to the *Lyssavirus* genus. Shimoni bat virus, which is highly related to LBV, has recently been grouped into phylogroup II, yet it might even be assigned as genotypic subgroup of LBV. The West Caucasian bat virus (WCBV) (Botvinkin et al., 2003), has specific genetic differences to other lyssaviruses, thus phylogroup III was established. WCBV also needs to be further characterized for final annotation. The genotypes and epidemiology of all annotated lyssaviruses are depicted in table 1 (for review see (Banyard et al., 2011)).

Table 1. Lyssavirus genotypes (GT) and epidemiology

Virus	GT	1 st Isolate	Spread	Reservoirs
RABV	1	Cow (PV strain), France, 1882	Worldwide	mammals, chiroptera
LBV	2	Bat <i>Eidolon helvum</i> , Nigeria, 1956	Sub-Saharan Africa	chiroptera
MOKV	3	Shrew, Nigeria, 1968	Sub-Saharan Africa	?
DUVV	4	Human, South Africa, 1970	Southern Africa	chiroptera
EBLV 1	5	Bat <i>Eptesicus serotinus</i> , Germany, 1986	Europe	chiroptera
EBLV 2	6	Human, Finland, 1986	Europe	chiroptera
ABLV	7	Bat <i>Pteropus alecto</i> , Australia, 1996	Australia	chiroptera
ARAV		Bat <i>Myotis blythi</i> , Kyrgyzstan, 1991	Kyrgyzstan	chiroptera
KHUV		Bat <i>Myotis mystacinus</i> , Tajikistan, 2001	Tajikistan	chiroptera
IRKV		Bat <i>Murina leucogaster</i> , Russia, 2002	Eastern Siberia	chiroptera
WCBV		Bat <i>Miniopterus schreibersi</i> , Russia, 2002	Western Caucasus Mountains	chiroptera
SHIBV		Bat <i>Hipposideros commersoni</i> , Kenya, 2009	Kenya	chiroptera
BBLV		Bat <i>Myotis nattererii</i> , Germany, 2009	Germany	chiroptera

1.1.2 Lyssavirus structure and genomes

Lyssaviruses, and all other *Rhabdoviridae*, are characterized by a rod- or bullet-shaped morphology. Their negative sense RNA genome forms a helical nucleocapsid (NC) or ribonucleoprotein (RNP) that is covered by a lipid envelope containing trimeric glycoprotein spikes. The 12 kb RNA genome encodes only five genes in the conserved order 3'-N-P-M-G-L-5'; these are transcribed to subgenomic mRNAs and translated to the respective proteins: the nucleoprotein (N), which encloses the viral RNA concurrent with its synthesis to form the NC; the phosphoprotein (P), a crucial non-catalytic cofactor for the viral RNA (vRNA) polymerase and for chaperoning soluble N protein (N⁰); the matrix protein (M), which is essential for virus assembly, budding, and regulation of RNA synthesis; the trimeric transmembrane glycoprotein (G) that attaches to target cells and induces membrane; and the "large" protein (L), the catalytic subunit of the viral RNA polymerase.

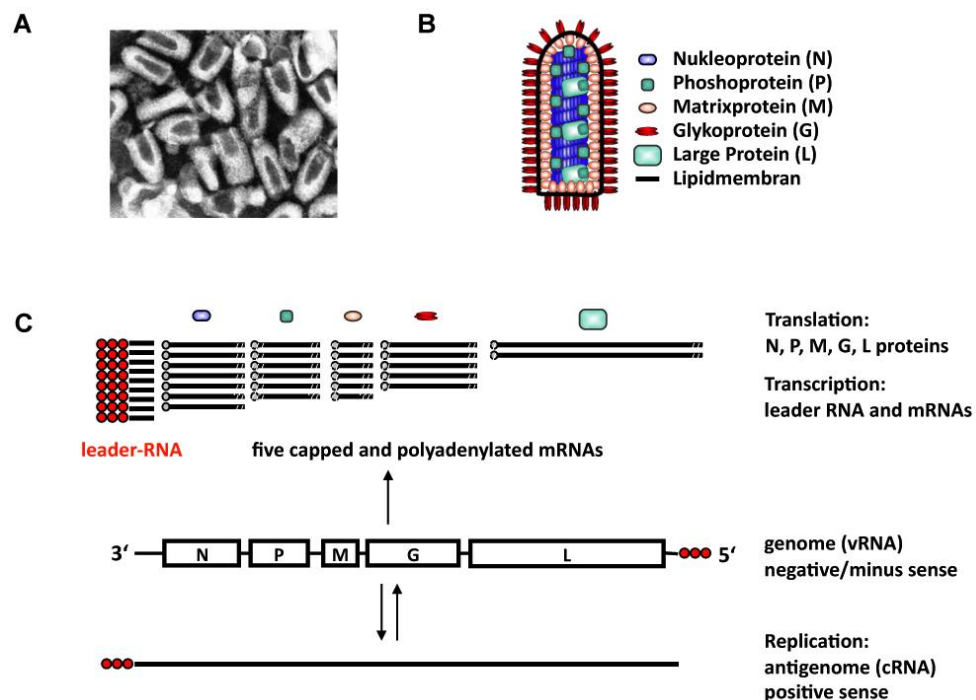


Figure 1-2: Rabies virus structure, genome and replication. (A) Electron micrograph of negatively stained rabies virions, purified from an infected cell culture (adapted from F. A. Murphy, School of Veterinary Medicine, University of California). (B) Illustration of a RABV particle showing virion organization. The viral RNP is composed of the RNA genome, the nucleoprotein (N), and the phosphoprotein (P) and forms the helical core. The matrix protein (M) forms a linkage between the RNP and the envelope, which is composed of a lipid membrane and the glycoprotein (G). (C) Organization of RABV RNA genome. The genome has a negative orientation, and comprises the genes N, P, M, G, L. Upon infection, sequential transcription of a 58 nt long 5'-ppp leader RNA and five capped and polyadenylated mRNAs takes place. mRNAs are translated into respective proteins. Replication of a full-length antigenome (cRNA) and subsequently genome (vRNA) takes place.

Inside the virion, the genome is encapsidated by the nucleoprotein N to form the NC and is present in a condensed, superhelical conformation, most likely held together by the M protein, which makes it very tight and stable (Naeve et al., 1980). When the NC is released into the cytoplasm for replication and transcription, it takes up a relaxed form, which allows for RNA synthesis. In this form, the N protein still binds tightly to the viral genome to protect it from cellular compounds, like RNases or small interfering RNAs, however, the N-RNA shielding is transiently released such that the polymerase complex (L/P) can access the RNA (Albertini et al., 2006, 2008). This highly controlled and transient access of the viral polymerase to the RNA apparently also avoids production of immune-stimulatory long dsRNAs (Weber et al., 2006). Transcription of five subgenomic, monocistronic mRNAs takes place that are 5'-capped and 3'-polyadenylated, just like cellular mRNAs. Transcription proceeds exclusively in the 3'-5' direction, and due to eventual dissociation of the viral polymerase at the intergenic regions a gradient of the mRNAs is generated (for review see (Whelan et al., 2004)). Prior to transcription of the N gene, synthesis of a 58 nt long 5'-pppRNA occurs, which is named leader RNA (Leppert et al., 1979). Subsequently, translation into viral proteins takes place. The genome RNP serves as a template for the generation of full-length anti-genome RNP, which in turn serves as template for the production of novel genomic RNPs that may serve for secondary transcription, replication, or assembly of new virions (see Fig. 1-2).

1.1.3 Lyssavirus pathogenicity

Although lyssaviruses are closely related, RABV is a unique member of the *Lyssavirus* genus. As opposed to other lyssaviruses, which are mainly associated to bats, RABV emerged as a threat for humans and terrestrial animals. The development of inactivated RABV vaccines for humans and pets, live attenuated viruses for wildlife, and post-exposure prophylaxis, has eradicated RABV in developed countries (Schneider and Cox, 1994). However, despite the availability of an effective vaccine, RABV still accounts for more than 50,000 human deaths per year, mainly occurring in poor rural regions of Africa and Asia and is largely transmitted by dogs (canine rabies). Due to its well-established host reservoir in Africa, Eurasia and North

America, including skunks, foxes, raccoons, dogs, jackals, bats etc., and the lack of structured vaccination programs in poor countries, an eradication of RABV appears difficult.

RABV is in most cases transmitted via bites or scratches from infected animals. Transport of the virus to the CNS causes acute encephalitis and death in > 99 % of the cases. A key strategy of RABV to effectively reach the CNS is to avoid cytotoxicity by restraining innate immunity and inflammation, therefore maintaining the integrity of the neuronal network (Finke and Conzelmann, 2005). Indeed, compared to other virus induced encephalitides, little inflammation is observed in rabies. It is actually believed that clinical signs result from neuronal dysfunction rather than from cytotoxic damage of neurons (Fu and Jackson, 2005). In mutation studies, distinct viral proteins have been identified to affect virulence and neuroinvasiveness. For instance, the G proteins from distinct RABV strains differ in sequence and receptor use (Dietzschold et al., 2008), stimulation of apoptosis (Lafon, 2008), and neuroprotective activities (Prehaud et al., 2010).

For unknown reasons, the incubation period can vary from approximately 1 week till up to 6 years, yet it generally takes 1-3 months until clinical signs appear, depending on the location of viral entry. First symptoms include fever, pain, and paraesthesia at the place of injury. Later hydrophobia, paralysis, or coma can follow.

The etiological agent of rabies encephalitis was thought to be exclusively RABV, until first rabies-related viruses were isolated from European insectivorous bats (Jelesic and Nikolic, 1956) and from West African fruit bats (Boulger and Porterfield, 1958) in 1956. Clinical signs have not only been detected in terrestrial animals and humans; in apparently rare cases, infected bats also showed signs of disease, such as atypical aggressiveness and finally death (Baer and Smith, 1991). Actually, many lyssaviruses have been detected as a result of bats exhibiting such clinical signs (Banyard et al., 2009). The transmission between bat conspecifics, showing clinical signs or not, is suggested to occur in their roosts, however, the actual route of transmission is still speculative. Apparently, all lyssaviruses are transmitted by direct contact of their hosts, which is in contrast to all other rhabdoviruses that are transmitted by insects.

Alarming, despite RABV, which is known to cause most cases of human rabies, sporadic cases of human rabies-like encephalitis caused by other lyssaviruses, namely EBLV-1, EBLV-2, ABLV and IRKV (all phylogroup I), have been reported (for review see (Banyard et al., 2011)).

Despite the obvious relatedness amongst lyssaviruses, the factors limiting their host range and enabling host switching, thus a spill-over from bats to terrestrial mammals, are unclear. However, the potential of non-rabies lyssaviruses to infect mammals, including humans, indicates a limited susceptibility, which is the first prerequisite to further adaptation to other host species. Interestingly, vaccinations against RABV are also effective against other viruses of phylogroup I but not against phylogroup II or III (Badrane et al., 2001).

1.1.4 RABV life cycle

RABV entry:

Although *in vivo* RABV and other lyssaviruses are renowned for their high neurotropism, resulting in their neuroinvasive character, *in vitro* they can infect nearly any cell type. The cell tropism is mainly determined by the transmembrane glycoprotein (G), which recognizes specific receptors via its ectodomain and induces membrane fusion (Gaudin, 1995). Receptors identified so far that facilitate cellular entry of RABV *in vitro*, are the nicotinic acetylcholine receptor (nAChR), the neural cell adhesion molecule (NCAM), and the neurotrophin receptor (p75NTR) (for review see (Lafon, 2005)). However, the importance of p75NTR *in vivo* has been questioned in a recent study (Tuffereau et al., 2007). Internalization of RABV and other lyssaviruses occurs via receptor-mediated endocytosis, generating vesicles/endosomes that contain complete virus particles. In neurons, these vesicles are transported along axonal microtubules in a retrograde fashion towards the cell body (Klingen et al., 2007). Generation of an acidic pH in the endosome leads to fusion of viral and endosomal membrane, release of the virus genome and replication in the cell body. New virus particles are formed, which are exclusively transmitted via synaptic connections to pre-synaptic neurons (Astic et al., 1993) until reaching the CNS.

RABV replication:

Once the RNP is released into the cytoplasm, it converts from a supercoiled to a relaxed form. As already described in part 1.1.2 of this thesis, this transition and the transient opening on the N-RNA clamping allows access of the viral RNA polymerase to the RNA genome, which serves as template for transcription and replication. Transcription of the N, P, M, G, and L gene starts at characteristic transcription start sites and continues until the polymerase encounters a stop/polyadenylation signal, characterized by a stretch of U residues. The polymerase stutters back and forth to generate an approximately 50–150 nt long poly(A) tail. The transcriptional stop/polyadenylation signal and the start signal of the neighboring gene are typically separated by so-called “intergenic regions” composed of only few, probably non-transcribed nucleotides, where the polymerase eventually dissociates (Finke et al., 2000). This generates a gradient of subgenomic, monocistronic mRNAs with a 5'-cap and 3'-poly(A) tail (Li et al., 2006; Ogino and Banerjee, 2007) that are translated into viral proteins. Finally, novel virions assemble at the plasma membrane (for review see (Whelan et al., 2004)).

The switch from transcription to replication goes along with two distinct forms of the polymerase, referred to as “transcriptase” and “replicase”, in which the L protein associates with P alone (L/P), or with P and N (L/P/N), respectively. From a 58 nt long region at the genome 3'-end, upstream of the N gene, an abundant amount of 5'-ppp leader RNA (see part 1.1.2) is synthesized. Previously, it was believed that synthesis of the 5'-ppp leader RNA is required for transcription, however, independent studies suggest that a leader-independent transcription initiation is possible. It was proposed that the transcriptase can directly enter at the leader/N junction, or scan from the 3'-end to the leader/N junction to initiate transcription of N mRNA without synthesis of leader RNA (Curran and Kolakofsky, 2008; Whelan, 2008).

Accumulation of the N protein and encapsidation of newly synthesized leader RNA by N (N-RNA) serves as a threshold for the initiation of replication of full-length genome. In case of vesicular stomatitis virus (VSV), the 5'-ppp leader RNA was found to be partially associated to N. Therefore, 5'-pppRNA may represent abortive replication products, generated due to insufficient amounts of N protein for encapsidation

(Blumberg et al., 1983). Product control may lead to the release of the leader RNA product from the polymerase and induces transcription at the leader/N gene junction (Vidal and Kolakofsky, 1989). However, in the presence of sufficient levels of N, the elaborate encapsidation of the leader RNA leads to formation of the “replicase” complex, which ignores the N gene start signal and induces replication to produce a full-length positive RNA strand complementary to the complete virus genome (Fig. 1-2C; for review see (Whelan et al., 2004)). Positive-strand antigenomes are also encapsidated by N protein and serve as template for generation of negative-stranded genomes. This is driven from a promoter located in the 3'-end of the antigenome, complementary to the leader RNA, called trailer RNA. The affinity of the P-L complex to the N-trailer RNA is stronger than to the N-leader RNA, producing an up to 50-fold excess of genomes over antigenomes (Finke and Conzelmann, 1997).

RABV assembly and budding:

During assembly of new virus particles, the nascent RNA is encapsidated by the N protein. The P protein facilitates polymerization of the N protein on the vRNA by the formation of N-P heterodimers in the cytoplasm. P is hereby acting as chaperone for N that specifically targets nascent vRNA, thus preventing the N protein from binding to cellular RNA and from aggregating (Peluso and Moyer, 1988). The M protein, which has been identified to be the major player in virus budding and morphogenesis, is able to recognize newly formed RNPs (Mebatsion et al., 1996, 1999). The G protein, which is transported to the plasma membrane via the ER and Golgi, plays rather a supportive role. On the plasma membrane, the M protein accumulates on the cytoplasmic side of G-enriched microdomains. During budding, RNPs attached to M condense into supercoiled structures, which, together with exocytic activity of the G protein, induce membrane curvature to form the bud site (Garoff et al., 1998). Viral egress is believed to occur with help of the host Nedd4 E3 ligase, which recruits the cellular vacuolar protein sorting (VPS) machinery to the bud site, inducing separation of the virus particle from the cell (Jayakar et al., 2004; Okumura and Harty, 2011).

When viral replication in the CNS commences, anterograde axonal transport of virus to the skin and salivary glands takes place, and transmission to further hosts is possible.

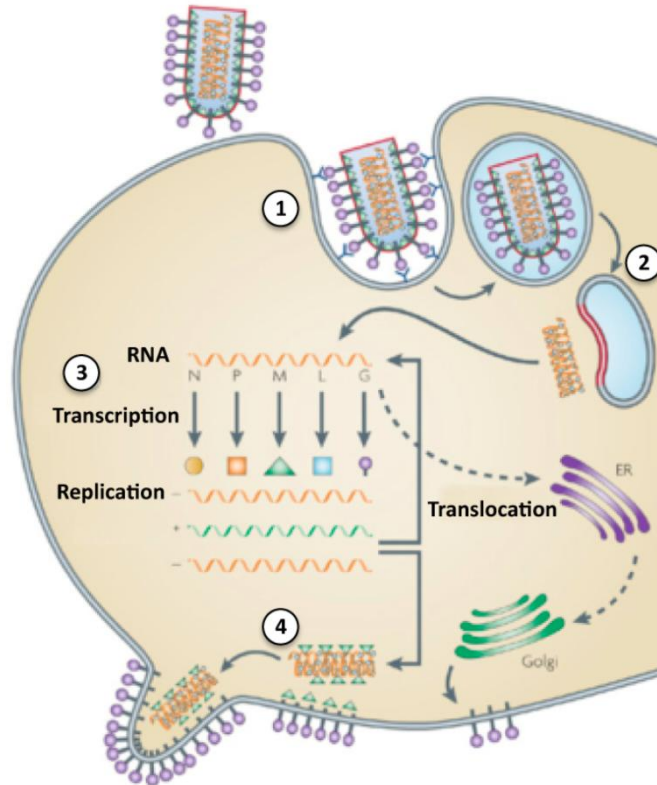


Figure 1-3: Simplified overview of the RABV life cycle. The virus enters the cell via receptor-mediated endocytosis (1). Subsequent pH-dependent membrane fusion leads to release of the viral genome into the cytoplasm (2). Transcription, translation, and replication produce novel virion components (3). Assembly of viral components takes place at the plasma membrane, budding occurs, and new virions are released (4) (adapted from (Schnell et al., 2010)).

1.1.5 RABV phosphoprotein P

The RABV phosphoprotein P is a multifunctional protein with important roles in transcription and replication, but also in counteracting specific steps leading to IFN gene expression and IFN-induced STAT signaling. Generally, the P proteins of *Mononegavirales* are critically involved in RNA synthesis, by acting as a non-catalytic cofactor of the polymerase complex L-P. In addition, RABV P binds to soluble N protein (N^0) thereby aiding the specific encapsidation of viral RNA (Chenik et al., 1994). Moreover, P is a binding partner of various cellular proteins, including dynein light chain, indicating a role in intracellular transport of viral components. The

diversity of functions and binding partners define P as a “hub” protein, crucial to the virus life cycle.

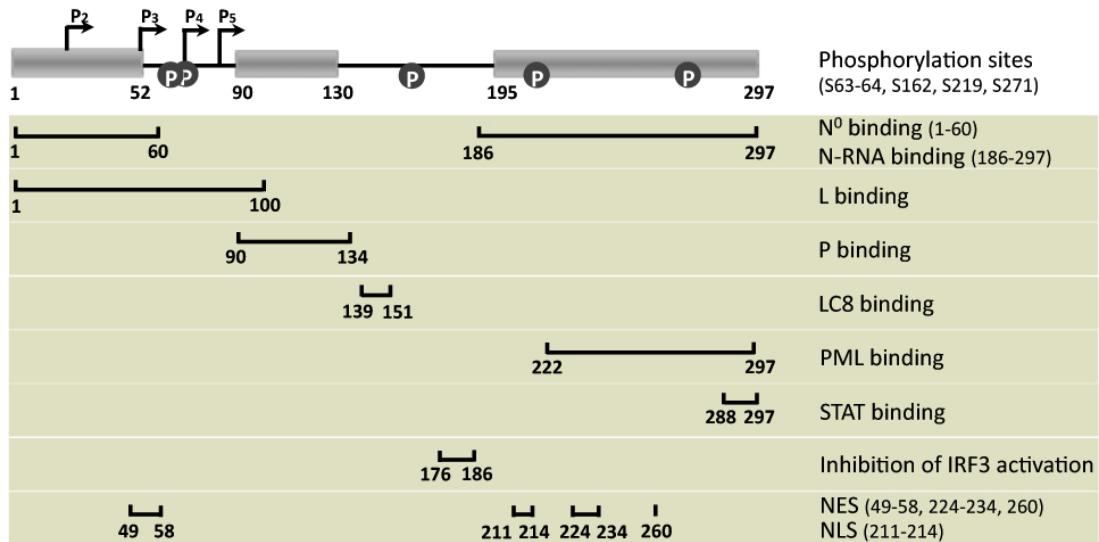


Figure 1-4: Overview of RABV phosphoprotein P domains and functions. On top, the RABV P protein is illustrated with its three structured domains, the N-terminal domain (P_{NTD}), the central domain (P_{CED}), and the C-terminal domain (P_{CTD}), separated by two intrinsically disordered domains. Truncated P forms and their respective transcription start sites are indicated by arrows. Phosphorylation sites are indicated and positions described. In the beige box the interacting domains, NLS and NES, and the aa that antagonize IRF3 activation are shown (adapted from (Rieder and Conzelmann, 2011)).

In addition to the full-length P protein, which is the major product from the P mRNA, leaky scanning by the ribosome generates further truncated P proteins from downstream in-frame translation initiation codons (AUG). These P forms are named P₂, P₃, P₄, and P₅ and their initiation codons are located at aa 20, 53, 69, and 83, respectively (Chenik et al., 1995). RABV P is a 297 aa phosphoprotein that contains three structured domains located at the N-terminus (P_{NTD}), the center of the protein (P_{CED}), and the C-terminus (P_{CTD}), separated by two intrinsically disordered domains, which provide flexibility.

The phosphoprotein P deduces its name from its phosphorylated moieties, containing phosphorylation sites at S63/S64, S162, S219, and S271. In contrast to VSV P, phosphorylation of RABV P is not required for transcription. The N-terminal residue S63, which is phosphorylated by a so far unidentified cellular rabies virus-specific kinase (Gupta et al., 2000), did not reveal a functional relevance yet (Gerard et al., 2009). Phosphorylation of C-terminal residues (S162, S210 and S271) by protein kinase C (PKC) was found to influence the nucleocytoplasmic distribution of P

(Moseley et al., 2007a). While P is entirely located in the cytoplasm, the lack of an N-terminal NES in P₃ - P₅ can result in nuclear localization (Pasdeloup et al., 2005; Vidy et al., 2007).

P_{NTD} comprises the binding sites for L and N⁰, and is therefore important for the polymerase co-function and RNA encapsidation. The central P_{CED} contains a P binding domain for the formation of elongated P homodimers both *in vitro* and *in vivo* (Gerard et al., 2009; Jacob et al., 2001; Ivanov et al., 2010). Self-association of full-length P dimers was shown to be dispensable for transcription (Jacob et al., 2001). However, dimerization has been shown to be essential for the cellular localization of P₃ and its association with cytoplasmic microtubules (Moseley et al., 2009). Further interaction domains include a strong dynein light chain 8 (DLC; LC8) binding site, located in the second disordered P domain (Jacob et al., 2000; Raux et al., 2000). RABV mutants lacking the DLC binding site appear to have defects in efficient virus transcription in neurons (Tan et al., 2007) and subcellular location of P forms seems to be distorted (Moseley et al., 2007b). The large P_{CTD} mediates binding to the N-RNA complex, and is therefore probably important for linking the polymerase P-L complex to the template (Schoehn et al., 2001; Mavrakis et al., 2004; Gerard et al., 2009; Ribeiro Jr. et al., 2008; Mavrakis et al., 2006).

As already mentioned, RABV P is counteracting IFN gene transcription and IFN-induced STAT signaling and is therefore a major factor in viral escape of the innate immune system and inflammation. RABV P interacts with STAT1/2 via its C-terminal aa 288-297 (Brzózka et al., 2006). Furthermore, binding of the P_{CTD} to the promyelocytic leukemia (PML) protein (also named TRIM19), was found to play a role in antiviral activity (Blondel et al., 2002). In this study, the molecular basis of P-mediated inhibition of IFN induction was addressed (Rieder et al., 2011).

1.2 Immune response to RABV

1.2.1 The interferon (IFN) system

The host defense against viruses depends on the recognition of “nonself” structures of pathogens, so-called pathogen-associated molecular patterns (PAMPs), by pattern recognition receptors (PRR) (Janeway Jr. and Medzhitov, 2002). These receptors induce signal transduction pathways leading to the secretion of the potent antiviral type I IFNs (IFN α/β) but also type III IFNs (IFN λ) and proinflammatory cytokines, like TNF and IL12 (Kawai and Akira, 2010; Pichlmair and Sousa, 2007). Type I IFNs are antiviral cytokines (Isaacs and Lindemann, 1957) that comprise the single IFN β and the IFN α family (14 subtypes) of partially homologous proteins (Calam, 1980). However, besides their essential role in innate immunity, type I IFNs are also able to stimulate adaptive immunity by inducing immune-modulatory genes, supporting activation of dendritic cells (DC), stimulating macrophages, increasing major histocompatibility complex class-I expression, and stimulating antibody secretion. These alterations support a Th1-biased immune response, thus integrating innate and adaptive immunity (for review see (Goodbourn et al., 2000)).

RLR and TLR signaling:

Although it is long known that dsRNA, or the synthetic dsRNA analogue poly(I:C), are potent inducers of type I IFN (Field et al., 1967), the receptors responsible for recognition of nonself RNA, the signaling cascades induced and the transcription factors involved have only been discovered in the past 10 years. PRRs of two families could be assigned to recognize viral RNA, namely the endosomal transmembrane Toll-like receptors (TLRs) 3, 7 and 8, and the cytoplasmic retinoic acid inducible gene-I (RIG-I)-like receptors (RLRs) RIG-I and MDA5 (melanoma differentiation-associated gene 5) (for reviews see (Kawai and Akira, 2010; Yoneyama and Fujita, 2010)). The virus-induced TLRs and RLRs trigger distinct signaling pathways that, however, eventually merge in the activation of the IFN regulatory transcription factor (IRF)3 (or IRF7), which activates transcription of type I and III IFNs (Honda and Taniguchi, 2006). Furthermore, these pathways lead to canonical activation of the nuclear factor- κ B (NF- κ B), which is not only the major transcription factor of a variety of

proinflammatory cytokines, such as TNF- α and interleukins, but also supports transcription of the early IFNs, such as IFN β and IFN α 4 (Perkins, 2007).

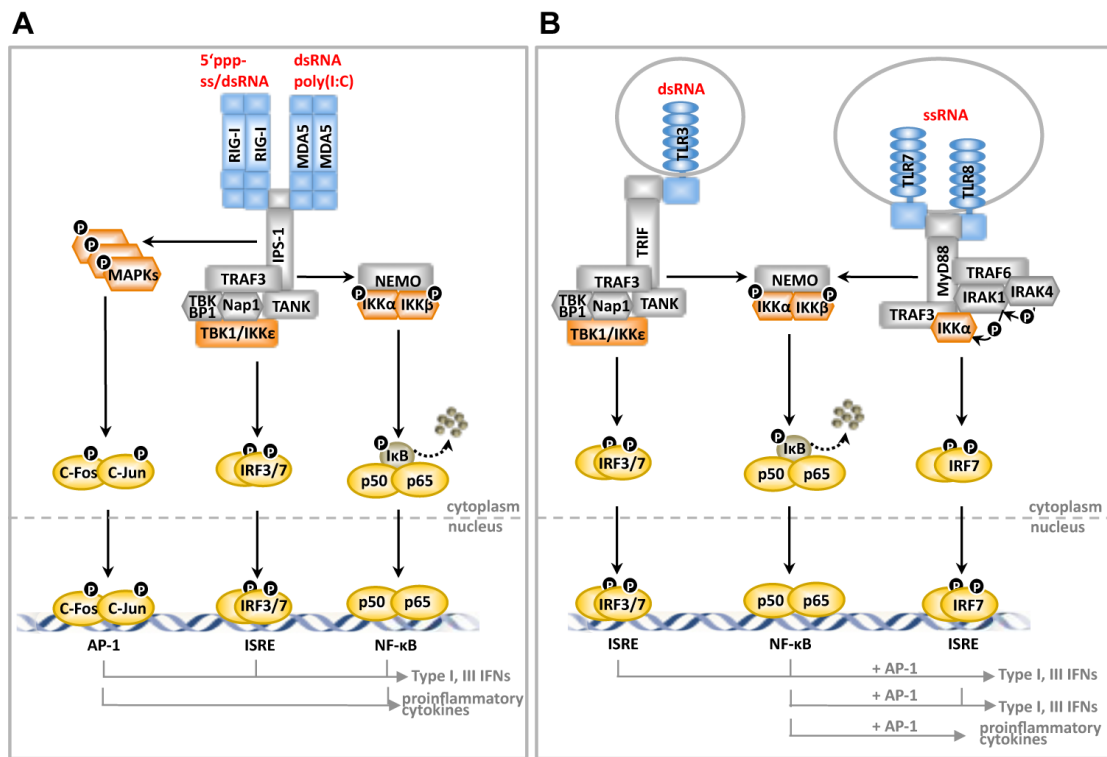


Figure 1-5: Induction of IFN and proinflammatory cytokines. The RLRs RIG-I and MDA5 (A) and the TLRs TLR3/7/8 (B) detect specific viral RNAs (red letters). This induces the formation of downstream signaling complexes (grey), which recruit and activate associated kinases (orange). The kinases TBK1 and IKKi phosphorylate and thus activate IRF3/7, whereas IKK α only activates IRF7. The IRFs form homo- or hetero-dimers and bind to the IFN α/β promoter in the nucleus. Simultaneously, the IKK $\alpha/\beta/\gamma$ (IKK γ =NEMO) complex is activated, which induces the ubiquitination of I κ B so that NF- κ B is released and translocates to the nucleus. NF- κ B and AP-1 also associate to the IFN α/β promoter, allowing the full capacity of IFN α/β transcription.

The RLRs RIG-I and MDA5 are cytoplasmic receptors, and therefore recognize cytoplasmic viral RNA. Upon activation, the N-terminal caspase activation and recruitment domains (CARDs) of RIG-I or MDA5 interact with the CARD of the mitochondrial adaptor IPS-1 (also called MAVS, VISA, or Cardif (Kawai et al., 2005)). Subsequently, TRAF3 associates to the C-terminal region of IPS-1, resulting in the formation of a large signaling complex with TRADD (Michallet et al., 2008), TANK (Pomerantz and Baltimore, 1999), NAP1 (Fujita et al., 2003), and SINTBAD (Ryzhakov and Randow, 2007). Complex formation is a pre-requisite for the poorly understood activation of the ubiquitous kinase TBK1, and the related IKKi (also named IKK ϵ ; largely expressed in immune cells), which then phosphorylates and thus activates IRF3 or IRF7 at multiple residues of the C-terminus, inducing transcription of IFN α/β .

As opposed to IRF3, IRF7 is not present ubiquitously but expression is upregulated by IFN signaling. Furthermore, a protein named MITA (also called STING or MPYS), which interacts with RIG-I, IPS-1, and possibly IRF3, has been found crucial for RLR signal transduction, and was suggested to act as scaffold protein (Bowzard et al., 2009).

An additional complex is formed on IPS-1 upon RLR activation, where TRADD associates with FADD1 and Rip1 (Balachandran et al., 2004). This leads to the activation of the latent IKK α / β / γ complex, which phosphorylates the inhibitor of NF- κ B (I κ B α) at serines 32 and 36, leading to the proteasomal degradation of the inhibitor and activation of NF- κ B (Traenckner et al., 1995).

TLR3/7/8 recognize RNA in endosomal compartments and subsequently associate to adaptor proteins containing a TIR domain. TLR3 detects dsRNA and consequently interacts with the adapter protein TRIF. This is followed by the recruitment of TRAF3, TANK, and the kinase TBK1, which in turn phosphorylates IRF3/7 for activation. The ssRNA recognizing TLR7/8 use a common signaling complex, formed on the adapter protein MyD88 (Honda et al., 2004), which recruits TRAF6 (Kawai et al., 2004) and TRAF3 (Oganesyan et al., 2006), IRAK1 (Uematsu et al., 2005), IRAK4 (Kim et al., 2007), as well as IKK α (Hoshino et al., 2006). IKK α recruits IRF7 to the signaling complex and leads to its activation. TLR3, 7, and 8 also induce activation of NF- κ B.

Activation of IRF3:

IRF3 belongs to the IRF family (IRF1-9) and is composed of a DNA-binding domain (DBD) containing a nuclear localization signal (NLS), a proline-rich domain containing a nuclear export signal (NES), a C-terminal IRF association domain (IAD) and several regulatory phosphorylation sites (Lin et al., 1999). IRF3 is ubiquitously expressed and exists latently in a monomeric form. Although a constant shuttling of IRF3 between the cytoplasm and the nucleus (through interaction with exportin CRM1 and importin- α members, respectively) takes place, in resting cells the export is prevailing. This generates an equilibrium on the part of the cytoplasm (Kumar et al., 2000). Upon virus infection, phosphorylation of IRF3 by TBK1 or IKKi occurs, inducing IRF3 activation.

It was shown that the chaperone heat shock protein (Hsp)90 interacts with IRF3 and TBK1, hereby probably bringing TBK1 and IRF3 into proximity which facilitates IRF3 phosphorylation by TBK1 (Yang et al., 2006). Interestingly, the protein translocase of outer membrane 70 (Tom70), a mitochondrial import receptor, was found to interact with Hsp90 but also IPS-1 upon RNA virus infection. This interaction is crucial for activation of TBK1 and IRF3 and it is therefore assumed that Tom70 acts as a critical adaptor linking IPS-1 to TBK1/IRF3/Hsp90 (Liu et al., 2010). Furthermore, *in vitro* analyses revealed that cyclophilin (Cyp)B, a protein that facilitates protein folding by its cis-trans peptidyl-prolyl isomerase activity, interacts with the auto-inhibitory domain of IRF3. This interaction was shown to be essential for virus-induced IRF3 activation (Obata et al., 2005).

Diverse reports indicate that specific phosphorylation events induce conformational changes that lead to homo/hetero-dimerization of IRF3/7 and association with the co-activators of transcription CBP (CREB-binding protein) or p300. This interaction is assumed to mask the IRF NES, leading to accumulation in the nucleus (Kumar et al., 2000). IRF3 binding to PRDIII-I of the IFN β enhancer is sufficient to induce IFN β transcription (Schafer, 1998), however, simultaneous binding of NF- κ B and AP1 transcription factors to PRDII and PRDIV, respectively, forms the IFN β enhanceosome that fully activates transcription from the IFN β promoter (Kim et al., 2000).

Phosphorylation of IRF3 is believed to be the major modification *in vivo* required for transcriptional activation. Activation involves conformational changes that unshields the IAD from constraints by auto-inhibitory structures (helices H1 and H5 of the IAD) (Qin et al., 2003). Distinct hypotheses are discussed that describe the specific phosphorylation events essential for activation. In previous studies involving IRF3 mutants, mass-spectrometry, or phospho-specific antibodies it was suggested that phosphorylation of Ser and Thr residues clustered in two regions of the IRF3 C-terminus, named site 1 (S385/S386) and site 2 (S396, S398, S402, T404, and S405), are decisive. Particularly the S385/S386 phosphorylation is characteristic for the active form of IRF3, as it is found in IRF3 dimers and in IRF3 bound to CBP. Furthermore, mutation of S385/S386 to non-phosphorylatable alanine abolishes activity, stressing their importance in transcriptional activity (Yoneyama et al., 1998).

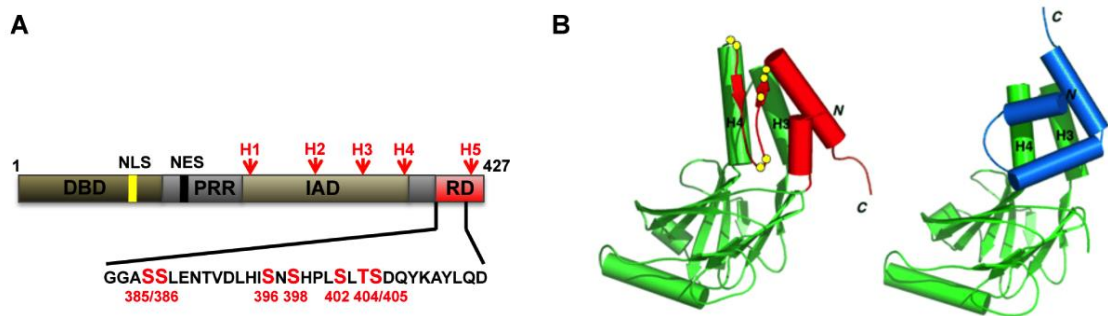


Figure 1-6: Structure of IRF3. (A) IRF3 comprises an N-terminal DNA binding domain (DBD) that contains an NLS, a central proline rich region (PRR) that contains an NES, and a C-terminal IRF association domain (IAD) and regulatory domain (RD) containing helices H1-H5. Phosphorylation of serine and threonine residues in the RD, such as S385/386 (site 1) and S396, S398, S402, T404, and S405 (site 2) by the virus induced kinases TBK1/IKKi, are involved in the activation of IRF3 (adapted from (Hiscott, 2007)). (B) *Left:* Ribbon diagram of IRF3 IAD in its inactive state where the IAD auto-inhibitory helices H1 and H5 (red) confer hydrophobic interactions with the H3 and H4 helices. C-terminal phosphorylation sites are shown in yellow (shown on the left). *Right:* Conformational changes lead to the interaction of the IAD helices H3 and H4 with the IRF-binding domain (IBiD) of CBP (blue) ((Hiscott, 2007) figure provided by Dr. Kai Lin).

Given that IRF3 mediates expression of various cytokines upon viral infection and ultimately modulates the immune response, the activation of IRF3 is subject to multiple regulations. For example, dsRNA induced IRF3 transcriptional activity was shown to be terminated by ubiquitinylation. It is suggested that phosphorylation of IRF3 at Ser339/Pro340 promotes interaction with the peptidyl-prolyl isomerase Pin1 (peptidyl-prolyl *cis/trans* isomerase, NIMA-interacting 1) that might catalyze conformational changes of IRF3 finally inducing polyubiquitinylation and proteasome-dependent degradation. Since phosphorylation of Ser 396 precedes the phosphorylation of Ser 339, it is assumed that phosphorylation of cluster II probably exposes Ser 339 favoring its subsequent phosphorylation. Ser 339 phosphorylation initially results in the fully active IRF3 that homodimerizes and associates with CBP/p300. In this state IRF3 is furthermore recognized by Pin1 leading to degradation (Bibeau-Poirier et al., 2006; Clément et al., 2008; Saitoh et al., 2006).

Further proteins have been demonstrated to regulate IRF3 activation. A negative regulator of IRF3 is for example the suppressor of IKKi (SIKE) that interacts with IKKi and TBK1, thus disrupting their interactions with TRIF, RIG-I and IRF3. Virus induced disruption of the binding of SIKE to TBK1/IKKi allows for IRF3 activation (Huang et al.,

2005). On the other hand, also positive regulators were identified, such as TRIM21 which interferes with the Pin1/IRF3 interaction, thus preventing IRF3 ubiquitination and degradation to sustain IRF3 activation during antiviral response (Yang et al., 2009). Furthermore, HERC5, an ISG15 E3 ligase, binds IRF3 upon viral infection and induces ISGylation of IRF3. This modification also inhibits ubiquitylation and degradation of IRF3 (Shi et al., 2010).

In a recent study, a further role of IRF3 has been elucidated besides its role as a transcription factor, which however is also induced via the RLR-signaling cascade. In virus-infected cells and in the additional presence of TRAF2 and TRAF6 which interact with the IPS-1/TRAF3/TBK-1 complex, IRF3 induces apoptosis by direct interaction with Bax at the mitochondria (via a BH3 domain in the IRF3-IAD H4 helix). This pro-apoptotic role of IRF3 is independent of the events leading to its transcriptional activity but is assumed to depend on distinct, yet unknown phosphorylation events by TBK1 (Chattopadhyay et al., 2010).

IFN signaling:

Secreted type I and II IFN acts in an autocrine and paracrine fashion by binding to the IFN α/β or IFN γ receptor (IFNAR, IFNGR), respectively, and activating the canonical JAK/STAT pathway, which induces the transcription of hundreds of interferon-stimulated genes (ISG), several of which have antiviral and immune stimulatory activity. IFN α/β bind to IFNAR which results in binding of TYK2- and JAK1 and subsequent tyrosine phosphorylation of the latent transcription factors STAT1 and STAT2. This causes formation of a heteromeric complex (IFN-stimulated gene factor 3 [ISGF3]) containing STAT1, STAT2, and IRF9. In the case of IFN γ binding to IFNGR, a JAK1 and JAK2 dependent tyrosine phosphorylation of STAT1 causes the association to STAT1 homodimers called the gamma-activated factor. ISGF3 and gamma-activated factor bind to DNA sequences called interferon stimulated response element (ISRE) and gamma-activated sequences (GAS), respectively, which are present in the promoters of many genes, hence promoting their transcription. IFN-induced JAK/STAT signaling stimulates the expression of many components of the PAMP-sensing machinery, hence providing a feedback loop increasing the magnitude

of sensing and IFN response (for review see (Kawai and Akira, 2008)).

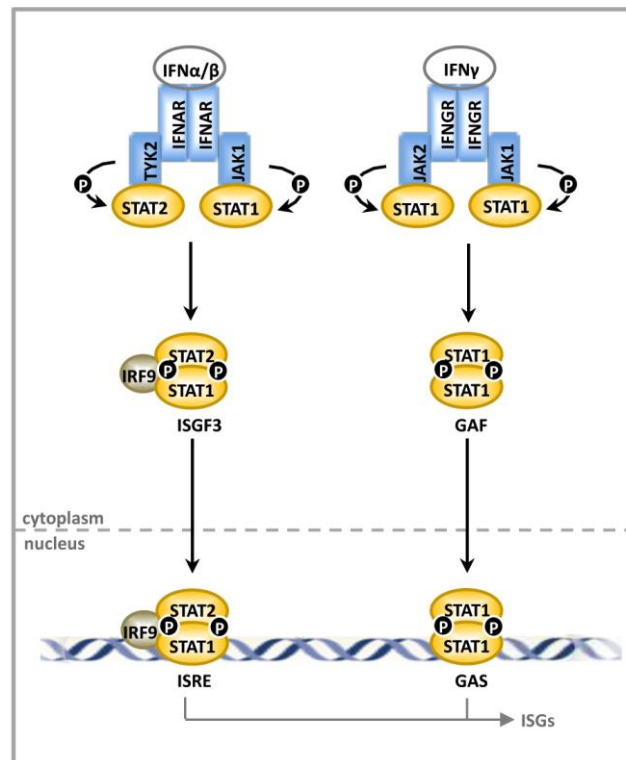


Figure 1-7: IFN α/β - and IFN γ -induced JAK/STAT signaling. IFN α/β and IFN λ act in an auto- and paracrine fashion by binding to cell surface IFNAR1/2 and IFNGR1/2, respectively. This results in activation of receptor-associated kinases JAK1/TYK2 and JAK1/JAK2, respectively, inducing phosphorylation of STAT1 and STAT2 transcription factors. In case of IFNAR signaling, STAT1 and STAT2 dimerize and recruit IRF9 (to form ISGF3), which leads to nuclear translocation and transcriptional activation of ISRE genes. IFNGR signaling leads to STAT1 homodimerization, translocation to the nucleus and transcription of GAS genes. ISGs are expressed, including many antiviral proteins.

Proteins encoded by ISGs include, for instance, IRF7 and RLRs, and direct antiviral proteins, such as PKR, 2'-5' OAS and RNaseL, or Mx proteins (Haller et al., 2007b; Sandrock et al., 2001; Silverman, 2007; Williams, 1999). The 2'-5' OAS/RNase L system degrades viral and cellular RNAs. PKR is activated by dsRNA (Kerr et al., 1974; Lebleu et al., 1976) or by proteins like PACT (Sen and Peters, 2007) and limits viral translation by phosphorylating the initiation factor eIF-2. Mx proteins are dynamin-like GTPases effective against a broad variety of positive- and negative-strand RNA viruses (Haller et al., 2007a).

Furthermore, the PML protein, which is a component of nuclear multiprotein complexes named PML nuclear bodies (NBs), has been found to be induced by type I and type II IFNs. In PML knockout MEFs, the infectious titers of the RABV strain CVS

were significantly increased (Blondel et al., 2002). Additionally, overexpression of the PML isoforms IV and IVa, but not other isoforms, resulted in reduction of RABV replication, indicating specific antiviral activities (Blondel et al., 2010).

1.2.2 Activation of RLR signaling by RABV

While expression of TLRs is mostly limited to specialized immune cells, such as dendritic cells and macrophages, the RLRs appear to be ubiquitous. RLR signaling emerges to be the major path for inducing an IFN response upon RNA virus infection, while involvement of TLRs is rather specialized.

TLR3/7/8 were shown to be involved in recognition of various viruses, including respiratory syncytial virus (TLR3) (Rudd et al., 2006) and VSV (TLR7) (Lund et al., 2004), which may gain access to the endosomal receptor by autophagy (for review see (Kawai and Akira, 2010)). However, their role in recognition of RABV is controversial (Edelmann et al., 2004). A certain role of TLR3 in response to RABV infection was shown when TLR3 was upregulated after RABV infection of mice and in the human cerebellar cortex tissues (Jackson et al., 2006). However, a recent study with TLR3 knockout mice showed that TLR3 does not contribute to IFN production in DC during RABV infections (Faul et al., 2010). It is even possible, that TLR3 might have a proviral role as it is involved in the generation of RABV Negri bodies (Menager et al., 2009). TLR7/8 was also excluded to be involved in RABV recognition. It was shown that the lack of TLR7/8 did not alter IFN expression in RABV-infected mouse DC (Faul et al., 2010). Furthermore, TLR7- dependent activation of IFN expression by RABV in isolated human pDC was not observed (Hornung et al., 2004).

The importance of RLRs in the antiviral response was illustrated by generation of RLR knockout mice where an adequate antiviral immunity to RNA viruses, including rhabdoviruses, could not be mounted (Kato et al., 2006; Kumar et al., 2006). RIG-I, MDA5 and laboratory of genetics and physiology 2 (Lgp2) are DExD/H box RNA helicases/translocases belonging to the superfamily 2 (SF2) helicases or ATPases (Kang et al., 2002; Yoneyama et al., 2004; Rothenfusser et al., 2005). All RLRs contain a C-terminal regulatory/repressor domain (RD or CTD) and an ATP-dependent

specific viral ligands of MDA5 and also RIG-I, and a tentative interplay between the two receptors, are still highly discussed. RNA transfection experiments suggested differential activation of RLRs. RIG-I was activated by *in vitro*-transcribed RNAs which, like rhabdoviral leader and genome RNAs, contain a 5'-ppp (Hornung et al., 2006) but also requires a base-paired region of at least 18-20 nucleotides (5'-ppp-dsRNA) (Schmidt et al., 2009). Lgp-2 also recognizes dsRNA, independent of 5'-ppp (Pippig et al., 2009). MDA5 was shown to recognize dsRNA lacking 5'-terminal phosphates as seen in picornaviruses, which produce RNAs that lack a 5'-ppp and instead have a protein (Vpg) linked covalently to the 5'-terminus (Gitlin et al., 2006). Further studies suggested that MDA5 prefers longer dsRNA, whilst RIG-I prefers shorter dsRNA (Kato et al., 2008). However, recent findings indicate that RIG-I also recognizes much longer (>200 bp) dsRNAs not necessarily bearing a 5'-ppp (Binder et al., 2011). The existence of such RNAs in infected cells is however controversial, and binding apparently occurs with much lower affinity.

In order to elaborate the molecular understanding of the RLR activation, diverse structural studies have been undertaken. Crystal structures of individual RLR domains, in part complexed with specific RNAs, ATP analogues, zinc etc. (Civril et al., 2011; Cui et al., 2008; Jiang et al., 2011; Pippig et al., 2009; Takahashi et al., 2009; Li et al., 2009), but also of full-length RIG-I (Kowalinski et al., 2011; Luo et al., 2011) could be successfully resolved. Taken these data together a gross model of general RLR activation and a more elaborate model of RIG-I activation is suggested. In the absence of a ligand, RIG-I exists in an auto-inhibited state where the CARDs fold back to the C-terminal part of RIG-I, probably being shielded from downstream signaling by interactions with the HD (or the RD, or both). This conformation sterically hinders dsRNA binding to the helicase and K63-polyubiquitylation of the CARDs, which is required for interaction with IPS-1 (Gack et al., 2007). The first step of activation is the recognition of 5'-ppp-dsRNA by the flexible RD (much higher affinity compared to 5'-OH-dsRNA), which leads to co-operative binding of dsRNA and ATP to the HD. A conformational switch occurs, driven by ATP hydrolysis that releases the CARDs, allowing for their polyubiquitylation and downstream signaling (Hopfner and Michaelis, 2007). It is also suggested that RIG-I forms dimers or oligomers along the dsRNA. The ligand specificity could be explained by the distinct residues in the

generally conserved RD RNA binding loop. For example, RIG-I, but not MDA5 or Lgp2, contains a lysine residue that is critically required for triphosphate binding.

1.3 RABV countermeasures to inhibit IFN

In order to restrain damage of neuronal circuits for efficient virus spread to the CNS, RABV pursues various strategies. In the past years the importance of viral counteractions against the host type I interferon system in order to establish an infection became evident. RABV phosphoprotein P takes up a key role in the viral evasion of the IFN system. In distinct experiments it was shown that RABV P directly interferes with IFN induction and also IFN signaling.

RABV P inhibits IFN induction:

The shifting of individual rhabdoviral genes to distinct positions in the genome can be used as a tool to control expression levels of RABV proteins due to a possible dissociation of the viral polymerase at the intergenic regions and the resulting attenuated transcription of genes. The expression of RABV P was manipulated by generating a recombinant RABV expressing P from the most downstream position (SAD Δ PLP: 3'-N-M-G-L-P-5'; wt: 3'-N-P-M-G-L-5') so that very little amounts of P are expressed, just sufficient to support RNA replication. SAD Δ PLP was only slightly attenuated in an IFN incompetent cell line but completely failed to replicate in IFN-competent cells. This effect was correlated with efficient transcription of IFN β mRNA in SAD Δ PLP infected cells, whereas in wt RABV-infected cells IFN β transcription was hardly detectable. In addition, SAD Δ PLP infection resulted in phosphorylation of S386 and dimerization of the critical transcription factor IRF3 as opposed to wt virus. Ectopic expression of P from plasmids inhibited IRF3 activation, and IRF7 activation to a lesser extent, after TBK1 overexpression (Brzózka et al., 2005).

RABV P inhibits IFN signaling:

In cells infected with RABV the induction of ISGs and of ISRE- or GAS-controlled luciferase by IFN α/β or IFN γ treatment was found to be almost completely abolished as opposed to cells infected with SAD Δ PLP. This demonstrates that RABV P is a potent IFN signaling antagonist. Overexpression of P from plasmid could also inhibit

ISG promoter activation after stimulation of the cells with IFN α or IFN γ , reinforcing the inhibitory role of P. Interestingly, despite the lack of ISRE and GAS-controlled gene expression in wt RABV-infected cells, effective phosphorylation of both STAT1 and STAT2 was observed after IFN treatment. Moreover, the phosphorylated isoforms of STATs accumulated in RABV infected cells, whereas in mock-infected cells phospho-STATs were rapidly de-phosphorylated. This could be explained in immunofluorescence studies after RABV infection or P cDNA transfection, which demonstrated STAT and RABV P co-localization in the cytoplasm. Individual studies suggested that RABV P associates with activated STATs, thereby sequestering the transcription factor in the cytoplasm, unable to bind its promoter (Brzozka et al., 2006; Vidy et al., 2005).

Not only full-length P but also the N-terminally truncated P₃ can bind to STAT1 and retain it in the cytoplasm. Here, P₃ associates with microtubules and thereby prevents STAT nuclear import. Furthermore, though representing a minor fraction of total P products, nuclear P₃ can bind STAT1 thereby inhibiting its binding to the promoter of the ISGs (Vidy et al., 2007). An intriguing finding was that P₃ that is localized to the nucleus exists as a monomer, whereas cytoplasmic P₃ exists as a dimer. Dimerization of P₃ in the cytoplasm is essential for the stable association of P₃ with microtubules (Moseley et al., 2009).

Interplay of RABV with antiviral ISGs:

Inhibition of RABV and other lyssaviruses by otherwise potent antiviral ISGs, such as PKR and the 2'-5' OAS/RNase L system, has not been observed so far. Although IFN α / β induced bovine Mx was reported to inhibit specific strains of RABV, human Mx protein does not seem to inhibit lyssaviruses (Leroy et al., 2006). The only antiviral ISG identified so far to be effective against RABV is PML. However, RABV P of the CVS strain has been shown to bind to the PML protein. It is suggested that this interaction retains PML in the cytoplasm and hereby inhibits the IFN-induced antiviral activities of PML (Blondel et al., 2002; Chelbi-Alix et al., 1998; Everett and Chelbi-Alix, 2007).

1.4 Aim of this thesis

It was shown that RABV P is a potent inhibitor of the RLR-induced IFN-induction pathway and the IFN-induced JAK/STAT pathway. The mechanism of RABV to inhibit IFN signaling has been ascribed to the binding of RABV P aa 288-297 to activated STAT1/2 and the resulting retention of STATs in the cytoplasm (Brzózka et al., 2006). Furthermore, P₃ can bind to STAT in the nucleus (Vidy et al., 2007). These interactions inhibit binding of STAT transcription factors to promoters of target genes. It has also been revealed that RABV P inhibits IRF3 activation (Brzózka et al., 2005) and that the internal aa 176-186 are essential for this inhibition (Rieder et al., 2011).

The aim of this thesis is to elaborate the mechanisms of RABV P to inhibit the IFN induction pathway. RABV P deletion mutants and recombinant RABV lacking aa 176-186, which lost the ability to inhibit IFN induction, were characterized *in vitro* and the pathogenicity of recombinant viruses was analyzed *in vivo*. Cellular interaction partners of RABV P were identified and the mode of inhibitory action elucidated. From the data two models are proposed for the course of events leading to inhibition of IRF3 activation by RABV P: First, RABV P associates to RLRs depending on their conformational state, induced by the presence of an adequate ligand in case of RIG-I and independent of a ligand in case of MDA5 and Lgp2. Second, RABV P interacts with an activation intermediate of IRF3. Activation of IRF3 is conferred by conformational rearrangements that liberate domains essential for transcriptional activation of IRF3. The collected data indicates that the domains liberated are targeted by RABV P to circumvent transcription of IFN.

2 Materials and Methods

2.1 Materials

2.1.1 Chemicals

All general solutions and buffers are listed in the appendix.

Acetone p.a.	Roth
Acrylamide/Bisacrylamide 29:1 Rotiphorese Gel 40	Roth
Acetic acid glacial, Rotipuran® 100 % p.a.	Roth
Acetone, Rotipuran® 99.8 % p.a.	Roth
Acridine orange	Roth
Agarose, UltraPure	Invitrogen
Ammonium chloride (NH ₄ Cl)	Merck
Ammonium persulfate; (APS) ((NH ₄) ₂ S ₂ O ₈)	Amresco
Ampicillin sodium salt (Amp)	Roth
Bacto tryptone	Becton Dickinson
Bacto yeast extract	Becton Dickinson
β-Mercaptoethanol	Sigma-Aldrich
Brilliant blue	Biorad
Bromphenol blue	Sigma-Aldrich
BSA	Sigma-Aldrich
Calcium chloride dihydrate (CaCl ₂ •2H ₂ O)	Sigma-Aldrich
Chloramphenicol succinate sodium salt (CAM)	Sigma-Aldrich
Deoxychol acid (DOC)	Sigma-Aldrich
Disodium hydrogen phosphate dihydrate (Na ₂ HPO ₄ •2H ₂ O)	Merck
Dimethyl sulfoxide (DMSO), p.a.	Roth
DL-Dithiothreitol, BioUltra, ≥ 99.5 % (DTT)	Roth

Ethylenediamine tetraacetic acid (EDTA)	Sigma
Ethanol, p.a.	Merck
Ethidium bromide solution 1 %	Roth
Ficoll 400	Pharm. Fine Chem.
Formic acid, p.a.	Merck
Geneticin (G418)	Invitrogen Gibco
Glycerol , Rotipuran® ≥ 99.5 %	Roth
L-Glutamine	Invitrogen Gibco
Glyoxal	Sigma-Aldrich
Hydrochloric acid, Rotipuran® 37 % p.a.	Merck
Hygromycin B	Calbiochem
Imidazole	Merck
Isopropyl β-D-1-thiogalactopyranoside (IPTG)	Roth
Isopropanol, p.a.	Merck
Kanamycin monosulfate salt (Kan)	Sigma-Aldrich
Lithium chloride, p.a.	Merck
Leupeptin	Sigma-Aldrich
Magnesium chloride hexahydrate (MgCl ₂ •6H ₂ O)	Fluka
Magnesium sulfate heptahydrate (MgSO ₄ •7H ₂ O)	Merck
Methanol abs., p.a.	Roth
Milk powder, blotting grade	Roth
NP-40 substitute	Fluka
Orange G	Sigma / Fluka
Paraformaldehyde	Merck
Phenol red	Merck
Phenylmethylsulfonylfluorid (PMSF)	Serva
Polyethyleneimine (PEI), high MW, water-free	Sigma-Aldrich
Potassium acetate, extra pure (CH ₃ CO ₂ K)	Merck

Potassium chloride, p.a. (KCl)	Merck
Potassium dihydrogen phosphate, p.a. (KH ₂ PO ₄)	Merck
Potassium hydrogen carbonate (KHCO ₃)	Merck
Sodium citrate x 2H ₂ O	Merck
Sodium dodecyl sulfate (SDS)	Serva
Sodium acetate trihydrate, p.a. (NaOAc•3H ₂ O)	Merck
Sodium chloride, p.a. (NaCl)	Merck
Sodium hydrogen carbonate (NaHCO ₃)	Merck
Sodium hydroxid (NaOH)	Merck
Sodium orthovanadate (Na ₃ VO ₄)	Sigma-Aldrich
Sodium phosphate	Merck
Tetramethylethylenediamine (TEMED)	Roth
Tricine, Pufferan® > 99 %	Roth
Tris, Pufferan® ≥ 99.9 %	Roth
Trisodiumcitrate-dihydrate > 99 % p.a.	Roth
Triton X-100	Merck
Tween-20	Roth
Urea, Pufferan® ≥ 99.5 % p.a.	Roth
Xylene cyanol	Sigma-Aldrich

2.1.2 Kits

Plasmid purification:	
Nucleobond® Xtra Midi	Macherey&Nagel
DirectPrep® 96 Miniprep	Qiagen
Cloning:	
QIAquick® Gel Extraction Kit	Qiagen
QIAquick® Nucleotide Removal Kit	Qiagen

QIAquick® PCR Purification Kit	Qiagen
Luciferase reporter gene assay:	
Dual Luciferase® Reporter Assay System	Promega
<i>In vitro</i> transcription:	
MEGAscript Kit	Ambion
Northern blot:	
Ready prime II kit	GE healthcare
RNA isolation:	
RNeasy® Mini Kit	Qiagen
Real time PCR:	
Quantitect SYBR® Green PCR Kit	Qiagen
Transfection:	
Mammalian Transfection Kit	Stratagene

2.1.3 Enzymes and buffers

DNA polymerases:	
Pfu DNA Polymerase	Fermentas
10x Pfu Buffer	Fermentas
Phusion® High Fidelity DNA Polymerase	NEB
5x Phusion HF Buffer	NEB
Taq DNA Polymerase	biomaster
10x amplif. buffer incl. MgCl ₂ 25mM for Taq Pol.	biomaster
DNase/RNase:	
TURBO DNase Deoxyribonuclease I, RNase free	Fermentas
RNase A	Macherey&Nagel
RNA polymerases:	
Transcriptor Reverse Transcriptase	Roche
DNase/RNase inhibitors:	

SUPERase-In	Ambion
Restriction enzymes:	
Restriction Enzymes	NEB
NEBuffer 1, 2, 3, 4	NEB
Ligase:	
T4 DNA Ligase	NEB
T4 DNA Ligase Buffer	NEB
Phosphatase :	
Calf Intestine Alkaline Phosphatase (CIAP)	NEB
Protease Inhibitor:	
cComplete ULTRA Protease Inhibitor Cocktail Tablets	Roche

2.1.4 Oligonucleotides

Primers for PCR and sequencing were ordered from metabion. Primer sequences can be found in the appendix.

Miscellaneous:	
Deoxyribonucleotide triphosphate (dNTPs) mix	Bioline
Polyinosinic:polycytidylic acid (poly I:C)	Sigma
Oligo(dT)12-18 Primer	Invitrogen
dNTPs Set	Bioline
γ - ³² P-ATP	Hartmann Analytic
Oligonucleotides for <i>in vitro</i> transcription:	
MeV-leader +:	
5'-AATTCGCGTAATACGACTCACTATAACCAAACAAGTTGGGTAAGGATAGTT CAATCAATGATCATCTTCTAGTGCACTT-3'	
MeV-leader + template:	
5'-AAGTGCACTAGAAGATGATCATTGATTGAACTATCCTTACCCAACCTTTGTTTG GTTATAGTGAGTCGTATTACGCG-3'	
MeV-leader -:	

5'-AATTCGCGTAATACGACTCACTATAAAGTGCCTAGAAAGATGATCATTGATTG
AACTATCCTTACCCAACCTTTGTTTGGT-3'

MeV-leader – template:

5'-ACCAAACAAAGTTGGGTAAGGATAGTTCAATCAATGATCATCTTCTAGTGAC
TTTATAGTGAGTCGTATTACGCG-3'

2.1.5 Antibodies

Primary antibodies (dilution WB, IF):

Flag M2 polyclonal rabbit (1:20,000, 1:200)	Sigma-Aldrich
Flag M2 monoclonal mouse (1:20,000, 1:200)	Sigma-Aldrich
RABV P rabbit custom-made (P160-5) (1:50,000, 1:2000)	Finke Stefan
RABV RNP (against N, P) rabbit custom-made (S50) (1:20,000, -)	BFAV
RABV G rabbit custom made (HCA05/1) (1:10,000, -)	Metabion
RABV N rabbit custom made (S86) (1:10,000, -)	BFAV
RABV M rabbit custom made (M1B3) (1:10,000, -)	BFAV
RABV N (FITC-labeled) rabbit (Centocor™) (1:50,000, -)	FDI Fujirebio
IRF3 (FL-425) rabbit (1:1000, 1:50)	Santa Cruz
IRF3 phospho386 rabbit (1:1000, -)	IBL
IRF3 phospho396 rabbit (1:1000, -)	Cell signaling
IRF3 phospho396 rabbit (1:1000, -)	Upstate
IRF3 phospho398 rabbit (1:1000, -)	Upstate
TBK1 (N-term) rabbit (1:1000, -)	Epitomics
IKKε/IKKi (K-14) goat (1:100, -)	Santa Cruz
TANK (H-300) rabbit (1:200, -)	Santa Cruz
Nap1 rabbit (1:500, -)	ABR
MDA5 rabbit (1:1000, -)	BioCat
RIG-I rabbit (1:1000, -)	Cell signaling
Lgp2 rabbit (1:1000, -)	Proteintech Europe

NEMO/IKK γ (DA10-12) mouse (1:1000, -)	Cell signaling
Actin (20-33) rabbit (1:5000, -)	Sigma-Aldrich
GST (B14) mouse (1:1000, -)	Santa Cruz
HA rat (1:1000, -)	Roche
GFP rabbit (1:10,000, -)	Invitrogen

Secondary antibodies (dilution WB, IF):

Anti-mouse HRP (1:20,000, 1:1000)	Jackson ImmunoResearch Laboratories
Anti-rabbit HRP (1:20,000, 1:1000)	Jackson ImmunoResearch Laboratories
Anti-human HRP (1:20,000, 1:1000)	Jackson ImmunoResearch Laboratories
Anti-mouse Alexa 488 (-, 1:200)	Invitrogen
Anti-rabbit Alexa 488 (-, 1:200)	Invitrogen
Anti-rabbit Alexa 555 (-, 1:200)	Invitrogen
Anti-rabbit Alexa 633 (-, 1:200)	Invitrogen
Anti-mouse Alexa 633 (-, 1:200)	Invitrogen

Diverse immunoreagents (dilution IF):

TO-PRO-3 iodide (1:1000)	Invitrogen
--------------------------	------------

2.1.6 Cell lines and media

Cell lines:

HEK 293T: Human embryonic kidney cells expressing SV40 T-antigen (ordered from ATCC).

Huh7.5: Human hepatoma cells containing a point mutation leading to non-functional RIG-I (received from C. Rice).

HEp-2: Human epidermoid (laryngeal squamous) carcinoma cells (ordered from ATCC).

Vero: African green monkey kidney cells (ordered from ATCC).

MVi/It: Interscapular tumor cells from *Myotis velifer incautus* bat (ordered from ATCC).

TB1/Lu: Lung epithelial cells from *Tadarida brasiliensis* bat (ordered from ATCC).

BSR-T7/5: BHK21-derived (baby hamster kidney) cells expressing T7 polymerase (received from BFAV).

Media and additives:

D-MEM	Invitrogen
G-MEM	Invitrogen
Fetal Bovine Serum	Invitrogen
Newborn Calf Serum	Invitrogen
L-Glutamine 100x (200 mM)	Invitrogen
Tryptose phosphate	Invitrogen
MEM amino acids	Invitrogen
Penicillin/Streptomycin	Invitrogen
G418 sulfate	Calbiochem/Merck
0.25 % Trypsin-EDTA	Invitrogen

Medium for HEK 293T, Huh7.5, HEp-2:	<u>D-MEM+3:</u> D-MEM + 10 % (v/v) FCS + 2 mM L-Glutamine + 0.2 % (v/v) Penicillin/Streptomycin
Medium for BSR-T7/5:	<u>G-MEM+4:</u> G-MEM + 10 % (v/v) NCS + 4 % (v/v) Tryptose phosphate + 2 % (v/v) MEM amino acids + 0.2% (v/v) Penicillin/Streptomycin + 1 M G418 every second passage
Medium for MVi/It and TB1/Lu:	<u>D-MEM+2:</u>

D-MEM
 + 10 % (v/v) FCS
 + 0.2 % (v/v) Penicillin/Streptomycin

2.1.7 Bacteria and media

Bacteria:

Plasmid amplification: <i>E. coli</i> XL-1 Blue	Stratagene
Recombinant protein expression: <i>E. coli</i> Rosetta (DE3)	Novagen

Media for propagation of bacteria:

LB medium:	85 mM NaCl
	0.5 % Yeast extract
	1 % (w/v) Bactotryptone
	1 mM MgSO ₄
LB++:	85 mM NaCl
	0.5 % Yeast extract
	1 % (w/v) Bactotryptone
	1 mM MgSO ₄
	1 mM MgSO ₄
	10 mM KCl
LB plates:	1000 ml LB medium
	+ 15 g Agar

LB medium and LB plates were supplemented with the appropriate antibiotics: ampicillin (100 µg/ml), chloramphenicol (25 µg/ml), or kanamycin (25 µg/ml).

2.1.8 Plasmids

Commercially acquired plasmids:

pCR3: eukaryotic expression vector, CMV-promoter controlled	Invitrogen
pEGFP-N3: eGFP vector, CMV-promoter controlled	Clontech

p125-Luc: Firefly luciferase, IFN β promoter controlled	Promega
pISRE-Luc: Firefly luciferase, ISRE controlled	Clontech
pCMV-RL: <i>Renilla</i> luciferase, CMV-promoter controlled	Promega
pCMV-myc vector	Invitrogen

Plasmids kindly provided:

pCAGGs:

Cloning vector containing a β chicken actin promoter; A. Garcia-Sastre.

pCR3-RABV P:

Expression plasmid for RABV P cloned into pCR3 vector; K. Brzózka.

pCR3-RABV P Δ Ind1:

Expression plasmid for RABV P lacking aa 176-181 cloned into pCR3 vector (restriction sites *Acc65I/NotI*); K. Brzózka (Rieder et al., 2011).

pCR3-RABV P Δ Ind2:

Expression plasmid for RABV P lacking aa 181-186 cloned into pCR3 vector (restriction sites *Acc65I/NotI*); K. Brzózka (Rieder et al., 2011).

pCR3-RABV P-Ig:

Expression plasmid for RABV P-Ig cloned into pCR3-Ig vector (restriction site *HindIII*); K. Brzózka.

pCR3-Ig-RABV P:

Expression plasmid for RABV P cloned into pCR3-Ig vector (restriction sites *EcoRI/NotI*); K. Brzózka.

pCR3-Ig-RABV P₂:

Expression plasmid for RABV P₂ (aa 19-297) cloned into pCR3-Ig vector (restriction sites *EcoRI/NotI*); K. Brzózka.

pCR3-Ig-RABV P₃:

Expression plasmid for RABV P₃ (aa 52-297) cloned into pCR3-Ig vector (restriction sites *EcoRI/NotI*); K. Brzózka.

pCR3-Ig-RABV P₄:

Expression plasmid for RABV P₄ (aa 69-297) cloned into pCR3-Ig vector (restriction sites *EcoRI/NotI*); K. Brzózka.

pCR3-RABV P Δ 191-297:

Expression plasmid for RABV P 1-190 cloned into pCR3-Ig vector (restriction sites Acc65I/NotI); K. Brzózka.

pCR3-RABV P Δ 199-297:

Expression plasmid for RABV P 1-198 cloned into pCR3-Ig vector (restriction sites Acc65I/NotI); K. Brzózka.

pCR3-RABV P Δ 217-297:

Expression plasmid for RABV P 1-216 cloned into pCR3-Ig vector (restriction sites Acc65I/NotI); K. Brzózka.

pCR3-RABV P Δ 245-297:

Expression plasmid for RABV P 1-244 cloned into pCR3-Ig vector (restriction sites Acc65I/NotI); K. Brzózka.

pcDNA3.1-Flag-RIG-I:

Expression plasmid for human RIG-I cloned into pcDNA3.1-Flag vector (restriction sites EcoRV/XhoI, inserts SnaBI/XhoI); K. Brzózka.

pcDNA3.1-Flag-MDA5:

Expression plasmid for human MDA5 cloned into pcDNA3.1-Flag vector (restriction sites EcoRV/XhoI, inserts SnaBI/XhoI); K. Brzózka.

pcDNA3.1-Flag-Lgp2:

Expression plasmid for human Lgp2 cloned into pcDNA3.1-Flag vector (restriction sites EcoRV/XhoI, inserts SnaBI/XhoI); K. Brzózka.

pcDNA3.1-Flag-MDA5 Δ CARD:

Expression plasmid for human MDA5 with a deletion of the CARD domain cloned into pcDNA3.1-Flag vector (restriction sites EcoRV/XhoI, inserts SnaBI/XhoI); K. Brzózka.

pcDNA3.1-Flag-MDA5 HD:

Expression plasmid for human MDA5 helicase domain cloned into pcDNA3.1-Flag vector (restriction sites EcoRV/XhoI, inserts SnaBI/XhoI); K. Brzózka.

pcDNA3.1-Flag-Lgp2 HD:

Expression plasmid for human Lgp2 helicase domain cloned into pcDNA3.1-Flag vector (restriction sites EcoRV/XhoI, inserts SnaBI/XhoI); K. Brzózka.

pcDNA3.1-Flag-Lgp2 RD:

Expression plasmid for human Lgp2 regulatory domain cloned into pcDNA3.1-Flag vector (restriction sites EcoRV/XhoI, inserts SnaBI/XhoI); K. Brzózka.

pEBOS-RIG-I CARD (Δ RIG-I):

Expression plasmid of human RIG-I CARD domain (aa 1-284) cloned into pEBOS vector; A. Krug.

pCR3-Flag-MeV-V Δ C:

MeV-V containing a point mutation, which prevents coexpression of C cloned into pCR3 vector (restriction sites EcoRI/NotI); C. Pfaller.

pET-28M-SUMO3-GFP:

Bacterial expression vector for SUMO3-tagged constructs (EMBL); K.-P. Hopfner, S. Akira.

pM6P-HisD/Flag-Sintbad:

Expression plasmid for mouse Flag-Sintbad (Ryzhakov and Randow, 2007); G. Ryzhakov.

pM6P-HisD/Flag-Nap1:

Expression plasmid for mouse Flag-Nap1 (Ryzhakov and Randow, 2007); G. Ryzhakov.

pM6P-HisD/Flag-NEMO:

Expression plasmid for human Flag-NEMO (Ryzhakov and Randow, 2007); G. Ryzhakov.

pFlag-IRF3-5D :

Expression plasmid for constitutively active IRF3 with aa substitutions S396D, S398D, S402D, T404D and S405D (Lin et al., 1998); J. Hiscott.

pEF-p50-IRF3-J2A:

Expression plasmid for p50-IRF3 with aa substitutions S385A, S386A cloned into pEF vector (Takahasi et al., 2010); T. Fujita.

pEF-p50-IRF3-396A :

Expression plasmid for p50-IRF3 with aa substitution S396A cloned into pEF vector (Takahasi et al., 2010); T. Fujita.

pEF-p50-IRF3-2A :

Expression plasmid for p50-IRF3 with aa substitutions S396A and S398A cloned into pEF vector (Takahasi et al., 2010); T. Fujita.

pEF-p50-IRF3-3A :

Expression plasmid for p50-IRF3 with aa substitutions S402A, T404A and S405A, cloned into pEF vector (Takahasi et al., 2010); T. Fujita.

pEF-p50-IRF3-5A :

Expression plasmid for p50-IRF3 with aa substitutions S396A, S398A, S402A, T404A and S405A, cloned into pEF vector (Takahasi et al., 2010); T. Fujita.

pEF-p50-IRF3-J2A5D :

Expression plasmid for p50-IRF3 with aa substitutions S385A, S386A, S396D, S398D, S402D, T404D and S405D, cloned into pEF vector (Takahasi et al., 2010); T. Fujita.

pFlag-IRF3 S339A:

Expression plasmid for Flag-IRF3 with aa substitution S339A (Clément et al., 2008); M. J. Servant.

pFlag-IRF3 2A/S339A:

Expression plasmid for Flag-IRF3 with aa substitutions S396A, S398A and S339A (Clément et al., 2008); M. J. Servant.

pFlag-IRF3 3A/S339A:

Expression plasmid for Flag-IRF3 with aa substitutions S402A, T404A, S405A and S339A (Clément et al., 2008); M. J. Servant.

pFlag-IRF3 5A/S339A:

Expression plasmid for Flag-IRF3 with aa substitutions S396A, S398A, S402A, T404A, S405A and S339A (Clément et al., 2008); M. J. Servant.

pFlag-IRF3 396A/S339A:

Expression plasmid for Flag-IRF3 with aa substitutions S396A and S339A (Clément et al., 2008); M. J. Servant.

pFlag-IRF3 2D/S339A:

Expression plasmid for Flag-IRF3 with aa substitutions S396D, S398D and S339A (Clément et al., 2008); M. J. Servant.

pFlag-IRF3 5D/S339A:

Expression plasmid for Flag-IRF3 with aa substitutions S396D, S398D, S402D, T404D, S405D and S339A (Clément et al., 2008); M. J. Servant.

pEF-RIG-I:

Expression plasmid for RIG-I (wt) (Cui et al., 2008); A. Krug.

pFlag-IPS-1:

Expression plasmid for Flag-IPS-1; S. Akira.

pFlag-TBK1:

Expression plasmid for Flag-TBK-1; K. Brzózka, S. Marozin.

pSAD L16:

Expression plasmid containing the full-length RABV genome cDNA cloned into pSAD vector; S. Finke.

pSAD PΔInd1:

Expression plasmid containing the full-length RABV genome cDNA with deletion of aa 176-181 in the P gene (Rieder et al., 2011); K. Brzózka.

pSAD PΔInd2:

Expression plasmid containing the full-length RABV genome cDNA with deletion of aa 182-186 in the P gene (Rieder et al., 2011); K. Brzózka.

pSDI-HH-flash:

Expression plasmid containing the firefly luciferase gene flanked by leader and trailer sequence of RABV (Ghanem et al., 2011); A. Ghanem.

pTIT-RABV-L:

Expression plasmid for T7-dependent expression of RABV L (Finke and Conzelmann, 1999); S. Finke.

pTIT-RABV-N:

Expression plasmid for T7-dependent expression of RABV N (Finke and Conzelmann, 1999); S. Finke.

pTIT-RABV-P:

Expression plasmid for T7-dependent expression of RABV P (Finke and Conzelmann, 1999); S. Finke.

Plasmids generated during this thesis:

pCR3-Flag-RABV P:

Expression plasmid for RABV P cloned into pCR3 vector (restriction sites Acc65I/XhoI).

pCR3-RABV PΔInd1/2:

Expression plasmid for RABV P cloned into pCR3 vector (restriction sites Acc65I/NotI).

pCR3-Ig-RABV P 82-216:

Expression plasmid for RABV P aa 69-216 cloned into pCR3 vector (restriction sites EcoRI/NotI).

pCR3-Ig-RABV P 82-244:

Expression plasmid for RABV P aa 82-216 cloned into pCR3 vector (restriction sites EcoRI/NotI).

pCR3-Ig-RABV P 52-216:

Expression plasmid for RABV P aa 82-216 cloned into pCR3 vector (restriction sites EcoRI/NotI).

pCMV-myc-MDA5:

Expression plasmid of human MDA5 cloned into pCMV-myc vector (Invitrogen; restriction sites SfiI/XhoI).

pCAGGs-Flag-MDA5 CARD 1-350:

Expression plasmid of human MDA5 CARD domain (aa 1-350) cloned into pCAGGs vector (restriction sites Acc65I/XhoI).

pCAGGs-Flag-MDA5 1-449:

Expression plasmid of human MDA5 aa 1-449 cloned into pCAGGs vector (restriction sites Acc65I/XhoI).

pCAGGs-Flag-MDA5 287-449:

Expression plasmid of human MDA5 aa 287-449 cloned into pCAGGs vector (restriction sites Acc65I/XhoI).

pCAGGs-Flag-RIG-ICD/HD-MDA5RD:

Expression plasmid of the chimeric protein RIG-ICD/HD-MDA5RD with N-terminal Flag-Tag, cloned into pCAGGs vector (restriction sites Acc65I/XhoI).

pCAGGs-Flag-RIG-ICD/HD-Lgp2RD:

Expression plasmid of the chimeric protein RIG-ICD/HD-Lgp2RD with N-terminal Flag-Tag, cloned into pCAGGs vector (restriction sites Acc65I/XhoI).

pCAGGs-Flag-MDA5CD/HD-RIG-IRD:

Expression plasmid of the chimeric protein MDA5CD/HD-RIG-IRD with N-terminal Flag-Tag, cloned into pCAGGs vector (restriction sites Acc65I/XhoI).

pCAGGs-Flag-MDA5CD/HD-Lgp2RD:

Expression plasmid of the chimeric protein MDA5CD/HD-Lgp2RD with N-terminal Flag-Tag, cloned into pCAGGs vector (restriction sites Acc65I/XhoI).

pCAGGs-Flag-Lgp2HD-RIG-IRD:

Expression plasmid of the chimeric protein Lgp2HD-RIG-IRD with N-terminal Flag-Tag, cloned into pCAGGs vector (restriction sites Acc65I/XhoI).

pCAGGs-Flag-Lgp2HD-MDA5RD:

Expression plasmid of the chimeric protein Lgp2HD-MDA5RD with N-terminal Flag-Tag, cloned into pCAGGs vector (restriction sites Acc65I/XhoI).

pCAGGs-Flag-RIG-ICD-MDA5HD-RIG-IRD:

Expression plasmid of the chimeric protein RIG-ICD-MDA5HD-RIG-IRD with N-terminal Flag-Tag, cloned into pCAGGs vector (restriction sites Acc65I/XhoI).

pCAGGs-Flag-MDA5CD-RIG-IHD-MDA5RD:

Expression plasmid of the chimeric protein MDA5CD-RIG-IHD-MDA5RD with N-terminal Flag-Tag, cloned into pCAGGs vector (restriction sites Acc65I/XhoI).

pCAGGs-Flag-Sintbad:

Expression plasmid of mouse Flag-Sintbad cloned into pCAGGs vector (restriction sites EcoRI/NheI).

pCAGGs-Flag-Nap1:

Expression plasmid of mouse Flag-Nap1 cloned into pCAGGs vector (restriction sites EcoRI/NheI).

pCAGGs-Flag-NEMO:

Expression plasmid of human Flag-NEMO cloned into pCAGGs vector (restriction sites EcoRI/NheI).

pCAGGs-Flag-Rip1:

Expression plasmid of human Flag-Rip1 cloned into pCAGGs vector (restriction sites Acc65I/XhoI).

pFlag-IRF3:

Expression plasmid for pFlag-IRF3 cloned by mutagenesis PCR from pFlag-IRF3 S339A.

pFlag-IRF3 2A:

Expression plasmid for Flag-IRF3 with aa substitutions S396A and S398A, cloned by mutagenesis PCR from pFlag-IRF3 2A/S339A.

pFlag-IRF3 3A:

Expression plasmid for Flag-IRF3 with aa substitutions S402A, T404A and S405A, cloned by mutagenesis PCR from pFlag-IRF3 3A/S339A.

pFlag-IRF3 5A:

Expression plasmid for Flag-IRF3 with aa substitutions S396A, S398A, S402A, T404A and S405A, cloned by mutagenesis PCR from pFlag-IRF3 5A/S339A.

pFlag-IRF3 396A:

Expression plasmid for Flag-IRF3 with aa substitution S396A, cloned by mutagenesis PCR from pFlag-IRF3 396A/S339A.

pFlag-IRF3 398A:

Expression plasmid for Flag-IRF3 with aa substitution S398A, cloned by mutagenesis PCR from pFlag-IRF3.

pFlag-IRF3 AADDD:

Expression plasmid for Flag-IRF3 with aa substitutions S396A, S398A, S402D, T404D and S405D, cloned by mutagenesis from FI-IRF3 5D (Lin et al., 1998).

pFlag-IRF3 DDAAA:

Expression plasmid for Flag-IRF3 with aa substitutions S396D, S398D, S402A, T404A and S405A, cloned by mutagenesis from FI-IRF3 5D (Lin et al., 1998).

pCAGGs-Flag-IRF3 150-427:

Expression plasmid of human Flag-IRF3 aa 150-427 cloned into pCAGGs vector (restriction sites Acc65I/XhoI).

pCAGGs-Flag-IRF3 185-427:

Expression plasmid of human Flag-IRF3 aa 185-427 cloned into pCAGGs vector (restriction sites Acc65I/XhoII).

pCAGGs-Flag-IRF3 200-427:

Expression plasmid of human Flag-IRF3 aa 200-427 cloned into pCAGGs vector (restriction sites Acc65I/XhoII).

pCAGGs-Flag-IRF3 300-427:

Expression plasmid of human Flag-IRF3 aa 150-427 cloned into pCAGGs vector (restriction sites Acc65I/XhoII).

pCAGGs-Flag-IRF3 200-384:

Expression plasmid of human Flag-IRF3 aa 150-427 cloned into pCAGGs vector (restriction sites Acc65I/XhoII).

pFlag-IRF3 L192R, L195R, L196R:

Expression plasmid for Flag-IRF3 with aa substitutions L192R, L195R, and L196R, cloned by mutagenesis from pFlag-IRF3.

pFlag-IRF3 L322R, I326R, I330R:

Expression plasmid for Flag-IRF3 with aa substitutions L322R, I326R, and I330R, cloned by mutagenesis from pFlag-IRF3.

pFlag-IRF3 L375R, M378R, A379R:

Expression plasmid for Flag-IRF3 with aa substitutions L192R, L195R, and L196R, cloned by mutagenesis from pFlag-IRF3.

pET28M-SUMO3-RABV P:

Expression plasmid for purification of RABV P, cloned into pET28M-SUMO3-GFP (restriction sites AgeI, XhoI).

2.1.9 Recombinant proteins

Proteins purified during this thesis:

RABV P; purified from the expression vector pET28M-SUMO3-RABV P in Rosetta DE3 bacteria.

Proteins kindly provided:

His-RIG-I, purified from the Baculovirus expression vector (pFBDM) in High Five™ cells (Cui et al., 2008); A. Kirchhofer.

His-MDA5, purified from the Baculovirus expression vector (pFBDM) in High Five™ cells (Cui et al., 2008); A. Kirchhofer.

Commercially acquired proteins:

GST-TBK1; Abnova.

GST-Nap1; Abnova.

2.1.10 Viruses

Viruses kindly provided:

SAD L16:

Recombinant rabies virus with the nucleotide sequence of the attenuated vaccine strain SAD B19 (gene bank accession M31046.1), generated by rescue from a full-length cDNA plasmid (Schnell et al., 1994); K.K. Conzelmann.

SAD Δ PLP:

Recombinant rabies virus derived from SAD L16 generated by deletion of the P gene, and insertion of the P gene after a sequence resembling the N/P gene border downstream of the L ORF. The full-length cDNA plasmid was used for rescue (Brzózka et al., 2005); K. Brzózka.

SAD Δ Ind1:

Recombinant rabies virus derived from SAD L16, harboring the aa deletion 176-181 in the phosphoprotein, generated by rescue from a full-length cDNA plasmid (Rieder et al., 2011); K. Brzózka.

SAD Δ Ind2:

Recombinant rabies virus derived from SAD L16, harboring the aa deletion 182-186 in the phosphoprotein, generated by rescue from a full-length cDNA plasmid (Rieder et al., 2011); K. Brzózka.

Sendai virus (DI)-H4:

Defective interfering particles of Sendai virus (SeV DI-H4) used for induction of IFN β (Strahle et al., 2006); D. Garcin.

Viruses generated during this thesis:

SAD Δ Ind1/2:

Recombinant rabies virus derived from SAD L16, harboring the aa deletion 176-186 in the phosphoprotein, generated by rescue from a full-length cDNA plasmid.

2.1.11 Equipment

Apparatuses:

Bacteria shaker ISF-1-W	Kuhner
Centrifuge 5417C (rotor F45-30-11)	Eppendorf
Centrifuge Evolution RC (SLC6000 and SS34 rotors)	Sorvall
Centro LB 960 plate luminometer	Berthold
CO ₂ Incubator	SANYO
Digital Sonifier W-250 D	Branson
Fireboy plus	Integra Biosciences
Forma Scientific Water-Jacketed Incubator 3250	Labotect
Forma ULT deep freezer	Thermo Scientific
Freezer GU1202	Liebherr
Fridge KU1710	Liebherr
Fusion FX7	Vilber Lourmat
Gel Doc System	Biorad
GJ Balance	Kern
Horizontal gel electrophoresis system S/M/L/XL	Peqlab/OWL
iShin Deep freezer	Nunc
IX71 UV-light microscope	Olympus
Jobin Yvon FluoroMax-P fluorimeter	Horiba
LightCycler 2.0	Roche
LSM 510 Meta Laser Scanning Microscope	Carl Zeiss
Mini Quick Spin RNA Columns	Roche
NanoDrop ND-1000 Spectrophotometer	Peqlab
Neubauer improved counting chamber	Marienfeld
Optimax Typ TR developing machine	MS Laborgeräte
PIPETBOY acu	IBS
Pipettes (2, 10, 20, 100, 200, 1000 µl)	Gilson
Pipettes (2, 10, 20, 100, 200, 1000 µl)	Eppendorf
Roller mixer SRT2	Stuart
Scientifica Magnetic Stirrer/heater Unit	VELP

Semidry Blotting System	Peqlab
Superdex 75 column	GE Healthcare
Sterilguard Class II Type A/B3 sterile workbench	The Baker Company
Standard Power Pack P25	Biometra
Swip SM25 Shaker	Edmund Bühler
Thermocycler T3	Biometra
Thermomixer 5436	Eppendorf
TMS light microscope	Nikon
Typhoon 9400 Variable Mode Imager	GE Healthcare
Vacu-Blot system	Biometra
Varifuge 3.0 R	Heraeus
Vertical gel electrophoresis system	Biorad
Disposables:	
12-well plates	BD Falcon
24-well plates	BD Falcon
96-well plates	BD Falcon
6-well plates	BD Falcon
50 ml Falcons	BD Falcon
15 ml Falcons	BD Falcon
Amicon Ultra-15 Centrifugal filter devices (MWCO 10,000)	Millipore
Capillary pipet tips 200 µl	Biozym
Cell culture flasks (T25, T75, T175)	BD Falcon
Combitips plus 10 ml	Eppendorf
Combitips plus 5 ml	Eppendorf
Coverslips 18 x 18 mm	Roth
Cuvette: UVette	Eppendorf
Microscope slides 76 x 26 mm	Roth
PCR Softstrips 0,2 ml	Biozym
Polypropylene reaction tubes (0.25, 0.5, 1.5, 2 ml)	Eppendorf
Roche LightCycler Capillaries 20 µl	Roche
Safe-Lock Tubes (0.5, 1.5, 2 ml)	Eppendorf
SafeSeal®-Tips (2,5 µl, 10 µl, 20 µl, 200 µl, 1,000 µl)	Biozym

2.1.12 Miscellaneous

1 kb DNA Ladder	NEB
0.5 – 10 kb RNA ladder	Invitrogen
Alexa Fluor 488-5(or 7-) UTP	Invitrogen
Anti-Flag® M2-Agarose from Mouse	Sigma-Aldrich
Dialysis membrane Zellutrans (MWCO 8,000-10,000)	Roth
DPBS	Invitrogen
Duralon-UV™ membranes	Stratagene
Gel Blotting Paper	Machery-Nagel
Gravity flow Strep-Tactin Superflow Column	IBA BioTAGnology
His6-SEN2CD	Boston Biochem
HiTrap Q HP ion exchange column	GE Healthcare
Hyperfilm ECL	GE Healthcare
Immobilon-P blotting membrane (PVDF)	Millipore
Immobilon-FL blotting membrane (PVDF)	Millipore
Lipofectamine™ 2000	Invitrogen
Ni-NTA Agarose	QIAGEN
Nitrocellulose membrane Protran BA 83 Whatman	GE healthcare
Oligo(dT)12-18 Primer	Invitrogen
PCR Marker	NEB
Precision Plus Protein Standards	Biorad
Protein A-Sepharose CL-4B	GE Healthcare
Serological pipettes (5, 10, 25 ml)	Costar
Streptavidin-Agarose	Sigma-Aldrich
Universal type I Interferon (IFN alpha A/D)	PBL
Vectashield® Mounting Medium for Fluorescence	Vector Laboratories
Western Lightning Plus-ECL	PerkinElmer

2.2 Methods

2.2.1 Cell culture

The cell lines used were stored in incubators at 37 °C and with 5 % CO₂. The work performed on all cell lines was always under sterile conditions. For experiments the cells were cultivated in T25 or T75 flasks in their described media. The cell cultures were passaged every three days by splitting them in an appropriate ratio generally ranging from 1:6 – 1:10.

2.2.2 Plasmid construction: cloning and mutagenesis

Polymerase chain reaction (PCR)

DNA polymerases synthesize the DNA strand by multiple cycles of denaturation of the dsDNA (95-98 °C), annealing of specific primers to the free 3'-OH-end of the template (depending on primer: usually 45-50 °C) and elongation (68-72 °C), resulting in synthesis of the complementary strand. Correct size of PCR products can be validated by agarose gel electrophoresis.

For standard PCR a 100 µl PCR-mix was prepared:

Components	amount
DNA-template	1 pg - 10 ng
5' primer (10 µM)	5 µl
3' primer (10 µM)	5 µl
5x Buffer HF	20 µl
DMSO	3 µl
dNTP-mix	0.8 µl (0.2 mM per nucleotide)
Phusion polymerase	1 µl (2 U)
H ₂ O	ad 100 µl

The PCR-program was comprised of the following steps:

Step	Temp.	Time	
1.	98 °C	30 sec	
2.	98 °C	30 sec	← 30x
3.	50 °C	30 sec	
4.	72 °C	15 sec/kbp	
5.	72 °C	10 min	
6.	4 °C	∞	

For purification of standard PCR products the QIAquick PCR Purification Kit was applied, following the protocol of the producer.

For mutagenesis PCR a 100 μ l PCR-mix was prepared:

Components	amount
DNA-template	1 pg - 10 ng
5' primer (10 μ M)	2.5 μ l
3' primer (10 μ M)	2.5 μ l
10x Buffer with MgCl ₂	10 μ l
dNTP-mix	1 μ l (0.25 mM per nucleotide)
bioPfu polymerase	1 μ l (2 U)
H ₂ O	ad 100 μ l

The PCR-program was comprised of the following steps:

Step	Temp.	Time	
1.	95 °C	30 s	
2.	95 °C	10 s	
3.	50 °C	30 s	← 18x
4.	68 °C	4 min/kbp	
5.	68 °C	30 min	
6.	4 °C	∞	

Subsequently, DNA was digested with DpnI restriction enzyme for at least 3 hours at 37 °C to remove all methylated template DNA (5'-GATC-3' methylation generated during bacterial plasmid DNA amplification). 10 μ l newly synthesized mutated plasmid DNA was directly transformed into bacteria for amplification.

For contamination control PCR a 25 μ l PCR-mix was prepared:

Components	amount
DNA-template	100 pg
5' primer i.e. hAc for (10 μ M)	0.625 μ l
3' primer i.e. hAc rev (10 μ M)	0.625 μ l
10x Buffer with MgCl ₂	2.5 μ l
DMSO	2.5 μ l
dNTP-mix	0.25 μ l (0.25 mM per nucleotide)
Taq polymerase	0.25 μ l (2 U)
H ₂ O	ad 25 μ l

The PCR-program was comprised of the following steps:

Step	Temp.	Time	
1.	95 °C	1 min	
2.	95 °C	30 sec	← 36x
3.	45 °C	30 sec	
4.	72 °C	45 sec/kbp	
5.	72 °C	10 min	
6.	4 °C	∞	

Restriction endonuclease digestion

For the site-directed insertion of a DNA fragment into a vector, or fusion of DNA fragments, digestion with specific restriction enzymes that create characteristic DNA ends (3' or 5' prime overhangs, sticky or blunt ends, depending on the enzyme), was applied. For this purpose, 5-10 µg PCR-product and the vector were incubated with restriction enzymes (time and temperature depending on the enzyme). To prevent re-ligation of the vector backbones, 10,000 U CIAP enzyme was subsequently added to the vector restriction digestion for further incubation (30 min, 37 °C). The digested DNA fragments of particular size were applied to agarose gel electrophoresis.

Agarose gel electrophoresis of nucleic acids

For the agarose gel, agarose powder was mixed with 1 x TAE buffer at a specific concentration, i.e. 1 % agarose for DNA fragments >500 bp and in case of <500 bp 2 % agarose. Samples containing DNA were mixed with 20 % Orange G loading buffer and loaded into the wells of the agarose gel. Additionally, a 1kb marker (1 % gel) or PCR marker (2 % gel) was loaded. In the meshwork of the agarose gel, DNA fragments were separated according to their size. Gels were run for 30 min to 1 hour at 120 V. For visualization of DNA by UV-light the running buffer contained 0.075 % ethidium bromide in 1 x TAE. Images were acquired on a BioRad GelDoc system. DNA fragments for ligation are excised from the gel and purified by the QIAquick Gel Extraction Kit following the protocol of the producer.

Ligation

Ligation of a specific DNA insert into a designated vector, cut with the same restriction enzymes, is carried out using the T4 DNA ligase (o/n, 16 °C) by the

formation of covalent phosphodiester-bonds between the free 5'-phosphate group and the free 3'-OH-group of the desoxyribose of the complementary ends.

For ligation a 20 μ l mix was prepared:

Components	amount
PCR-product (insert)	10 μ l
Linear vector	0.5 μ l
T4 DNA ligase	0.5 μ l
10x T4 DNA ligase buffer	2 μ l
H ₂ O	ad 20 μ l

To selectively amplify ligated plasmids or plasmid DNA in general, plasmids contain an antibiotic resistance gene. Plasmid DNA was transformed into bacteria, plated out onto LB-plates containing a suitable antibiotic, and bacteria were incubated at 37 °C o/n. Single colonies for plasmid preparations or for production of inoculum for protein expression were isolated.

Transformation of bacteria

50 μ l chemically competent bacteria of the *E. coli* strain XL-1 Blue or *E. coli* Rosetta DE3 were thawed on ice and 10 μ l ligation mix or 1 μ l plasmid DNA was added (20 min, on ice). After a heat shock (2 min, 42 °C) and another 2 min on ice, 200 μ l LB++ was added to the bacteria and shaken for 30 – 60 min at 37°C.

DNA-preparation (MINI-, MIDI-prep)

Colonies grown o/n were picked from the LB-plates and transferred into 1 ml (small scale MINI preparation) antibiotic containing LB-medium and shaken o/n at 37°C. To harvest the bacterial cells they were centrifuged (10 min, 4 °C, 2500 rpm). The bacterial pellet was resuspended in 200 μ l Flexi I, lysed with 200 μ l Flexi II (5 min, RT), and neutralized with 200 μ l Flexi III (5 min, on ice). In a centrifugation step (10 min, 4 °C, 14000 rpm) the cell debris was removed and the supernatant transferred to 400 μ l isopropanol to precipitate the DNA. DNA was pelleted (10 min, 4 °C, 14000 rpm), dried and solubilized in 50 μ l H₂O. To validate ligation of the correct insert, a control digest of 1 μ g DNA was carried out using the appropriate restriction enzymes and subjected to agarose gel electrophoresis. Size of insert and vector were validated using a 1kb marker as reference.

For large scale MIDI preparation, colonies or 75 μ l of the transformed bacterial suspension were transferred to 50 ml LB-medium (or 100 ml in case of recombinant protein expression), containing a specific antibiotic, and shaken o/n at 37 °C. Bacterial cells were pelleted (20 min, 4 °C, 3500 rpm) and the DNA was purified by using the Nucleobond Xtra Midi kit following the protocol of the producer. Concentration of the DNA was determined using the NanoDrop ND-1000 spectrophotometer.

Plasmid DNA sequencing was carried out by GATC biotech. Requested concentrations are 30-100 ng/ μ l plasmid DNA and 10 pmol/ μ l sequencing primer, both in 20 μ l volume. Software of DNAMAN 6.0 and Chromas 1.45 was applied to analyze acquired sequences.

2.2.3 Transfection and infection

A specific number of cells was initially seeded into an adequate culture dish or well-plate (6, 12, 24 or 96-well plate or 6 cm dish). For this purpose, cell numbers were counted using a Neubauer chamber or estimated due to the size of the culture flask and cell density. When cells are confluent, following cell numbers are designated to specific culture flasks: T25: 3×10^6 cells; T75: 9.4×10^6 cells. Cells were trypsinized, taken up in medium and seeded into the desired dish (incubation mostly o/n).

Culture dish	number of cells	volume of medium
6 cm dish	6×10^5	2 ml
6-well plate	3×10^5	2 ml
12-well plate	2×10^5	600 μ l
24-well plate	6×10^5	300-500 μ l
96-well plate	6×10^5	100-200 μ l

Transfection

Cells were transfected with appropriate transfection reagents. For transfection of less than two plasmids, polyethyleneimine (PEI) solution (1 mg/ml) was used. PEI was pre-incubated in D-MEM w/o additives for 5 min, subsequently mixed with the DNA (2 μ l PEI/ μ g DNA) for 20 min and added to the cells. For transfection of more than two plasmids, LipofectamineTM2000 (2.5 μ l Lipofectamine/ μ g DNA) was used. It was pre-

incubated with D-MEM w/o additives for 5 min. Plasmids DNA was diluted in D-MEM w/o additives and combined with diluted Lipofectamine/D-MEM mix. Following incubation of 20 min, the solution was added to the cells. For virus rescue, BSR-T7/5 cells were transfected with calcium phosphate using the Mammalian Transfection Kit following the protocol of the producer.

Infection

HEK 293T, BSR-T7/5 or HEp-2 cells were grown to a confluence of 60 to 80 % and infected at a specific multiplicity of infection (MOI). For luciferase assays and quantitative RT-PCR in HEK 293T cells, an MOI of 3 was applied. For growth curve analysis of recombinant RABVs in BSR-T7/5, HEp-2 or 293T cells, an MOI of 0.05, and for Western blot analysis of protein levels and immunofluorescence microscopy in HEp-2 cells, an MOI of 1 was used.

2.2.4 Purification of recombinant proteins

Purification of recombinant proteins was carried out by His-tag purification from *E. coli* Rosetta. Bacteria were transformed with pET28M-SUMO3-RABV P and grown in appropriate LB medium. 100 ml pre-culture was grown at o/n at 37 °C and 10 ml thereof transferred to 1 l LB medium. The culture was shaken at 37 °C until an OD600 of 0.6-0.8 was reached. Expression of the protein His6-SUMO3-RABV P was initiated by the addition of 0.5-1 mM IPTG (isopropyl- β -D-thiogalactopyranosid) and the bacteria were further incubated o/n at 18 °C. Bacteria were pelleted by centrifugation in a Sorvall SLC-6000 rotor (20 min, 4 °C, 4,000 g), resuspended in 13 ml of Buffer A and disrupted by sonification. The suspension was centrifuged again using the Sorvall rotor SS-34 (45 min, 4 °C, 10,000 g) to clear the lysate. 6 ml Ni-NTA agarose beads, which bind to the His-tag, were added (incubation at 4 °C on roller mixer, 1-2 h), and the mixture was transferred to a column. 30-60 ml buffer A was applied to wash the column. Subsequently, the protein was eluted with buffer B in five 3 ml fractions. Fractions of purified protein were analyzed by SDS-PAGE and Coomassie staining. Positive fractions were pooled and dialyzed in dialysis buffer (o/n, 4 °C), which contains the protease His-SEN2 (50 nM) to cleave off the His6-

SUMO-tag. The cleaved tag and the protease were removed by additional incubation with 6 ml Ni-NTA agarose (1-2 h, 4 °C), transferred to a column and washed with 10-20 ml buffer A. The flow-through was dialyzed again (o/n, 4 °C) and proper cleavage was verified by SDS-PAGE and Coomassie staining (see 2.2.14, 2.2.16). Finally, the protein suspension was transferred to an Amicon Ultra-15 Centrifugal filter device and concentrated by centrifugation (steps of 10 min, 4 °C, 3,500 rpm). To determine protein concentration, absorption at 280 nm was measured with the NanoDrop ND-1000 spectrophotometer, and multiplied with the protein's extinction coefficient (determined by ProtParam). Aliquots of purified proteins were shock frozen in liquid nitrogen and stored at -80 °C.

2.2.5 Generation of recombinant viruses

SAD Δ Ind1/2 was generated by using a reverse genetics approach. For this purpose, BSR-T7/5 cells were seeded in a 6-well plate and cultivated o/n. One hour before transfection, medium was changed to D-MEM. Cells were transfected with 10 μ g pSAD P Δ Ind1/2, 5 μ g pTIT-RABV N, 2.5 μ g pTIT-RABV P, and 2.5 μ g pTIT-RABV L using the Mammalian transfection kit. 4 hours post transfection (p.t.) the medium was changed again to G-MEM+4. 72 hours p.t. the supernatant was passaged; therefore, collected, centrifuged (10 min, 4 °C, 1600 rpm) to remove cell debris, and transferred to freshly seeded BSR-T7/5 cells (6-well plate). 2 ml of fresh G-MEM+4 medium was added to the transfected cells and incubated for further 72 hours. Supernatant was passaged again, and transfected cells were trypsinized for splitting. 75 % were split into a T25 cell culture flask and 25 % into a 6-well plate and incubated again for 72 hours. The transfected cells and supernatant passages in 6-well plates were fixed with acetone 80 % and analyzed for RABV N protein by incubation with Centocor™ (FITC-labeled anti-RABV N monoclonal antibody). Positive rescues were identified by scanning for virus foci, using a fluorescent microscope. Supernatant of cells grown in corresponding T25 cell culture flasks was collected, cleared from cell debris by centrifugation (10 min, 4 °C, 1600rpm), and stored in aliquots at -80 °C. To generate virus stock, BSR-T7/5 cells were seeded in T25 flasks and infected at an MOI of 0.01 to 1. 48 hours post infection (p.i.) the first harvest was carried out by taking the

supernatant and removing the cell debris by centrifugation (10 min, 4 °C, 1,600 rpm). Fresh medium was added and 96 hours p.i. the second harvest was collected the same way. Harvests were stored in aliquots at -80 °C.

2.2.6 Minigenome assay

BSR-T7/5 cells were seeded in a 6-well plate and cultivated overnight. One hour before transfection, medium was changed to D-MEM. Using the Mammalian transfection kit, cells were transfected with the helper plasmids pTIT-RABV N (5 µg), pTIT-RABV L (2,5 µg), and either one of pTIT-RABV P or pCR3 PΔInd1/2, or no P at all. In addition, 4 µg of the pSDI-HH-flash minigenome, composed of the firefly luciferase (FL) gene flanked by the RABV leader and trailer sequence, and 10 ng of the control plasmid pCMV-RL were transfected. 48 hours p.t., the cells were lysed in passive lysis buffer and subjected to dual luciferase detection by the luminometer.

2.2.7 Titration of virus stocks

For titration, virus stock was thawed and a 10-fold dilution series was prepared (7 x 900 µl G-MEM + 100 µl virus/virus dilution). BSR-T/7 cells were seeded into 96-well plates and after 2 hours infected with 100 µl of the virus dilution (in duplicates). 48 hours p.i., cells were fixed with acetone 80 % and stained for RABV N with Centocor. Foci were counted using a fluorescence microscope, and the titer, namely focus forming units per ml (ffu/ml), was calculated.

2.2.8 Virus growth curves

To analyze growth kinetics of distinct viruses, growth curves were undertaken. Therefore, BSR-T7/5 cells in G-MEM were seeded into a T25 flask and infected in suspension with an MOI 0.05. 6 hours p.i., medium was changed to G-MEM+4 and after 1 h 1 ml supernatant was collected as first time point. 24 h, 48 h, 72 h, and 96 h p.i., further supernatants were collected and frozen at -80 °C. Subsequently, supernatants are thawed again and titrated as described above to determine the

infectious titers at the given time points.

2.2.9 RNA isolation and reverse transcription (RT) PCR

Isolation of RNA from mammalian cells was carried out using the RNeasy® Mini Kit (QIAGEN) following the protocol of the producer. To determine RNA concentration, absorption at 240 nm was measured using the NanoDrop ND-1000 spectrophotometer. RNAs were stored at -80 °C. For further analysis, total RNA was transcribed to cDNA in a reverse transcription (RT) reaction. Prior to the RT, purified RNA was digested with DNase I (45 min, 37 °C; inactivation with EDTA 10 min, 65 °C) to avoid contamination with genomic DNA. In a contamination control PCR (see 2.2.2) absence of DNA was verified.

For RT PCR the following PCR-mix was prepared:

Reaction 1:

Components	amount
RNA	1 µg
Oligo-dT (100 ng/µl)	0.5 µl
H ₂ O	ad 7.1 µl

The first RT PCR-program was comprised of the following steps:

Step	Temp.	Time
1.	65 °C	10 min
2.	on ice	5 min

Reaction 2:

Components	amount
Reaction 1	7.1 µl
RT buffer 1x	2 µl
SUPERase-In	0.25 µl
dNTP-mix	0.4 µl (25 mM per nucleotide)

The second RT PCR-program was comprised of the following steps:

Step	Temp.	Time
1.	55 °C	30 min
2.	85 °C	5 min

cDNA was stored at -20 °C or analyzed directly. To confirm/exclude the presence of a

specific mRNA/cRNA, standard PCR was applied using the appropriate primers. For DNA-visualization, agarose gel electrophoresis (2.2.2) was carried out. For quantitative analyses of a certain gene, qRT-PCR was undertaken (2.2.11).

2.2.10 Northern blot

BSR-T7/5 or HEK 293T cells were infected with SAD L16, SAD Δ Ind1, SAD Δ Ind2 and SAD Δ Ind1/2, at an MOI of 3, and RNA was isolated 48 hours p.i. (described in 2.2.9). 2 μ g purified RNA in a total volume of 7.2 μ l was incubated with 3 μ l 5 x phosphate buffer and 1.8 μ l glyoxal solution (30-45 min, 56 °C). Finally, Blue juice was added. RNA samples were loaded onto an RNA agarose gel. For the gel, 2 g agarose (RNA grade) was dissolved in 167.3 ml H₂O (ultra pure) and 4 ml 50 x phosphate buffer by heating. The gel solution was cooled to approximately 30 °C, 26.7 ml formaldehyde 37 % were added (H₂O ad 200 ml), and filled into a 24 cm x 20 cm cast. Electrophoresis was carried out using 1 x phosphate buffer at 25 V o/n and RNA was stained using acridine orange solution. To visualize RNAs, the gel was washed with 1 x phosphate buffer to remove background staining. Subsequently, RNA was transferred and cross-linked to a nylon membrane (2 h, -100 mbar) using the Biometra® Vacu-Blot System. A RABV N-probe was generated by radioactive labeling of PCR products of RABV N (25 ng) with ³²P-CTP using the Ready prime kit II (GE healthcare). After pre-incubation of the membrane with Zeta hybridizing buffer (10 min, 68 °C), probes diluted in 8 ml Zeta hybridizing buffer were applied (o/n, 68 °C). The membrane was washed once with Zeta wash buffer 5 % and twice with Zeta wash buffer 1 % (68 °C, 20 min) before letting it dry. To analyze RNA profiles, the membrane was exposed to a PhosphoScreen (Molecular Dynamics) (2-72 h) and scanned by a STORM Scanner (Molecular Dynamics). Images were evaluated by ImageQuant and Microsoft Excel software.

2.2.11 Quantitative real time-PCR (qRT-PCR)

For quantitative analyses of cellular mRNA levels after transfection or infection, the total RNA was isolated 24 h p.t./p.i. and reverse transcribed to single strand cDNA

(2.2.8). Samples were diluted 1:5 and as reference a standard curve was generated by a 10-fold dilution series of one cDNA sample (5 dilutions 1:1, 1:10, 1:100, 1:1000, 1:10000). The dilutions were set to relative values for quantification of the samples. A master mix was prepared containing specific primers and SYBR Green, a cyanine dye which preferentially binds to newly transcribed dsDNA. To normalize the results, the same samples were subjected to qRT-PCR with primers for a (steady) housekeeping gene. The standards, the cDNA 1:5, and a no template sample (negative control) were distributed to LightCycler capillaries and placed into a rotor.

For qRT-PCR a 20 μ l PCR-mix was prepared:

Components	amount
cDNA	1 μ l
Primer 1	1 μ l
Primer 2	1 μ l
SYBR Green Master Mix	10 μ l
H ₂ O	ad 20 μ l

The qRT-PCR-program was comprised of the following steps:

Step	Temp.	Time	
1.	95 °C	15 min	
2.	94 °C	15 min	
3.	47-53 °C	20 sec	← 55x
4.	72 °C	10 sec	
5.	95 °C	10 sec	} Melting curve
6.	40 °C	20 sec	
7.	to 95 °C	10 sec (0.1 °C/s)	
8.	40 °C	30 sec	

Annealing temperatures for the gene of interest, in this case hIFN β , and the housekeeping gene GAPDH, were 47 °C and 53 °C, respectively. The LightCycler software 4.0 was used to obtain a relative quantification, and values of single samples were calculated from the standard curve. Finally, IFN β mRNA values were normalized against GAPDH. All qRT-PCR assays were carried out in duplicates (standard deviations depicted as error bars). Expression levels of corresponding proteins were analyzed by SDS-PAGE and Western blotting (see 2.2.14 and 2.2.17).

2.2.12 Luciferase reporter gene assay

To examine IFN induction and IFN signaling, the Dual Luciferase® Reporter Assay System was applied. In this system, the two individual reporter enzymes firefly luciferase (FL; correlates with evoked effects) and *Renilla* luciferase (RL; serves as baseline transfection control) are simultaneously expressed within a single cell culture system. For this purpose, cells were transfected or infected with compounds under investigation. To analyze IFN induction, a p125-luc reporter plasmid, with FL under the control of the IFN β promoter, was cotransfected with plasmids of interest, or 6 h p.i. (50 ng/ μ l p125-luc and 1 ng/ μ l p*Renilla*). For analysis of IFN α - or IFN γ -induced JAK/STAT signaling, 400 ng/ μ l pISRE-luc and 10 ng/ μ l p*Renilla* or 400 ng/ μ l pGAS-luc and 10 ng/ μ l p*Renilla* was transfected, respectively. In this case, the luciferase gene is downstream of the ISRE- or GAS-containing promoters. Cells were lysed in passive lysis buffer (Promega) 18-24 h p.t. or p.i. and 20 μ l cell lysate was subsequently incubated with 40 μ l firefly- and *Renilla* substrate in a Luminometer (Berthold) by which the luciferase-activities were measured. Corresponding expression levels were examined by SDS-PAGE and Western blotting (2.2.14 and 2.2.17).

2.2.13 Co-immunoprecipitation (Co-IP)

In order to identify protein interaction partners, Co-IP was applied. HEK 293T cells were seeded in a 6 cm dish and transfected with cDNAs coding for potential interaction partners. For analysis of viral interaction partners cells could also be infected. One day p.t./p.i. the cells were detached from the dish by 1 ml PBS + 5 mM EDTA. The cell suspension was centrifuged (5 min, 4 °C, 2,500 rpm) and the pellet lysed (1 h, 4 °C) with 300 μ l Co-IP buffer containing a protease inhibitor. Following lysis, the suspension was centrifuged again (15 min, 4 °C, 14,000 rpm) and the supernatant containing the proteins, free of separated cellular residues, was transferred to a new tube. 30 μ l of the supernatant was mixed with 30 μ l protein lysis buffer as a control (WCL=whole cell lysate) for the amount of total protein expression (10 %). For precipitation of proteins the remaining supernatant (90 %) was incubated

with a specific matrix (Flag or sepharose).

Incubation with a Flag-matrix and precipitation

The remaining supernatant (90 %) was incubated with 100 µl anti-Flag® M2-Agarose (o/n, 4 °C). This matrix is composed of agarose beads that are covalently linked to anti-Flag-antibody, thus capturing Flag-tagged proteins. In case the Flag-tagged protein interacts with another protein in the cell lysate, the whole complex stays captured to the matrix. Potential interacting partners were labeled with a distinct tag, such as a His-tag, or a specific antibody had to be used for subsequent detection. Any proteins not co-precipitated to the matrix were washed away with 3 x 500 µl Co-IP buffer (10 min, 4 °C and subsequent centrifugation 2 min, 4 °C, 14,000 rpm).

Incubation with a SepharoseA-matrix and precipitation

Besides using the Flag-matrix it is possible to precipitate proteins, for which a specific antibody exists, with Protein A-Sepharose. Protein A, which is covalently conjugated to sepharose, specifically binds to the Ig-part of antibodies. To prepare a Protein A-Sepharose-matrix, Sepharose A was washed with 2 x 50 ml buffer A (1.5 g Sepharose A/50 ml buffer) (30 min, 4 °C and centrifugation 2 min, 4 °C, 2,000 rpm) on a roller mixer. After a further centrifugation step, buffer A was removed and the beads incubated with 50 ml of buffer B (30 min, 4 °C). Afterwards, beads were centrifuged (2 min, 4 °C, 3,500 rpm), reconstituted in 7.5 ml buffer B and aliquots of 1 ml stored at 4 °C. Prior usage, the beads were washed with 3 x 500 µl Co-IP buffer and incubated with the antibody (concentration depending on antibody) specific for the protein of interest (o/n, 4°C). For precipitation of proteins, the cleared lysate (90 %) was incubated with 100 µl SepharoseA-matrix (o/n, 4 °C) and washed with 3 x 500 µl Co-IP buffer (10 min, 4 °C and subsequent centrifugation 2 min, 4 °C, 14,000 rpm).

Finally, the beads were pelleted (2 min, 4 °C, 14,000 rpm) and protein lysis buffer was added. SDS-PAGE and Western blot analysis (2.2.14 and 2.2.17) were applied to analyze whether proteins had been pulled down by the matrix (IP), and for identification of interaction partners (Co-IP).

2.2.14 Denaturing polyacrylamide gel electrophoresis (SDS-PAGE)

For analysis of endogenous protein expression or protein overexpression after transfection or infection, cells were lysed with an appropriate amount of SDS-containing protein lysis buffer.

Culture dish/matrix suspension	volume of protein lysis buffer
6-well plate	~ 600 μ l
12-well plate	~ 300 μ l
24-well plate	~ 150 μ l
100 μ l Co-IP matrix	~ 150 μ l

Subsequently, lysates were boiled (5 min, 95 °C) to denature the proteins. SDS surrounds the protein with a negative charge and the β -mercaptoethanol prevents the reformation of disulfide bonds. The protein samples were separated according to their molecular weight using Jagow-gels (polyacrylamide gels). In order to set up the apparatus (Peqlab) for electrophoresis, 4 % stacking gel, a non-restrictive large pore gel, was layered on top of a 10 % separating gel. The denatured proteins and Precision Plus Protein Standard as marker were loaded onto the gel and run o/n at ~50 volt. Jagow anode and cathode buffer were used as running buffers (see appendix for gels and buffers).

2.2.15 Native PAGE

In case proteins had to be analyzed in their native globular state, i.e. for analysis of dimerization, native PAGE was performed. A 7.5 % native gel was prepared in an appropriate gel apparatus (Peqlab) containing specific buffers and pre-run at 30 mA, 30 min. Cells were lysed in 100 μ l native lysis buffer for 1 h, 4 °C. Cell debris was removed by centrifugation (10 min, 4 °C, 14,500 rpm) and subsequent transfer of supernatant to new Eppendorf tubes. 10 μ l of the cell lysate was mixed with 10 μ l native loading buffer, loaded onto the native gel and run for 2 h at 150 mA (see appendix for gels and buffers).

2.2.16 Coomassie staining

To visualize proteins following SDS- or native-PAGE directly, the gel was incubated for 20 min in Coomassie staining solution and subsequently washed with Coomassie wash solution (3 x 20-60 min) until bands appeared.

2.2.17 Western blot analysis (semi-dry)

In order to make proteins accessible to antibody detection, they were transferred from within the gel onto a nitrocellulose membrane. For this step, the stacking gel was removed and the separating gel was put into semi dry buffer for 10 min for equilibration. The gel was then placed face-to-face with the membrane, sandwiched by Whatman paper (all soaked in semi-dry buffer) and electroblotted for 2 h at 400 mA/gel using a semi-dry blotting device (Peglab). Blotting results in the movement of charged proteins from within the gel onto the membrane while maintaining the organization they had within the gel. The proteins were exposed on a thin surface layer for detection. To avoid non-specific protein interactions of the antibody used for detection, the membrane was placed into a solution of 2.5 % milk powder in PBS-T (1 h, RT).

2.2.18 Immunodetection

For visualization of proteins on the membranes, the primary antibody was diluted in PBS-T (for appropriate dilutions see 2.1.5.) and applied to the nitrocellulose membrane for incubation (2 h, RT or o/n, 4 °C). Subsequently, the nitrocellulose membrane was washed with PBS-T (3 x 10 min) to remove unbound antibody. The membrane was then incubated with HRP-conjugated or fluorescently labeled secondary antibody, diluted in PBS-T (2 h, RT). The membrane was washed again (3 x 10 min) and ECL solution was applied according to supplier's manual. Membranes were either exposed to a Hyperfilm-ECL and developed or directly subjected to Vilber Lourmat Fusion FX7 to visualize protein bands due to Chemiluminescence. In case fluorescently labeled secondary antibody was applied, Typhoon 9400 variable Mode

Imager or Fusion FX7 were used to visualize protein bands. Immunodetection was also performed on fixed whole cells directly and investigated by fluorescent microscopy (see 2.2.19).

2.2.19 Immunofluorescence (IF)

Microscopic (confocal or non-confocal) analysis of cells was undertaken by applying immunodetection to specific endogenous or overexpressed proteins using fluorescently labeled secondary antibodies, or by overexpression of GFP-fusion proteins. For transfection/infection, HEp-2 or Vero cells were seeded on glass cover slips in a 24-well format. 24-30 h p.t./p.i., medium was removed and the cells washed with 1 x PBS. Subsequently, PBS was removed and cells fixed with 500 μ l 3 % PFA/PBS (20 min, RT). Cells were rinsed twice with 1 x PBS and the cell membrane was permeabilized with 500 μ l PBS/0.5 % Triton X-100 (5 min, RT). Then, 500 μ l PBS/2 % BSA/0.1 % Triton X-100 was applied for 20 min, RT. In case of immunodetection, primary antibody was diluted to appropriate concentrations (see 2.1.5.) in PBS/2 % BSA/0.1 % Triton X-100 and added to the cells for 1 h, RT. Cells were washed with PBS/0.1 % Triton X-100 (3 x 5 min) and incubated with fluorescently-labeled secondary antibody, diluted in PBS/2 % BSA/0.1 % Triton X-100, for 1h (in case of fluorescently-labeled primary antibody this step was skipped). Cover slips were then washed three times with PBS and once with H₂O and fixed on microscope slides using Vectashield mounting medium (Vector Labs) and nail varnish. Slides were dried at 4 °C and stored in the dark. Confocal microscopy was carried out on a Laser Scanning Microscope (Zeiss) using the LSM Meta software, and non-confocal UV microscopy on a UV microscope (Olympus) applying the analySIS software.

2.2.20 *In vitro* ATPase assay

ATPase activity of MDA5 and RIG-I was analyzed after stimulation with poly(I:C) and in absence or presence of RABV P. A 0.5-2 μ M solution of purified MDA5 or RIG-I in H₂O, and a 1 μ M solution of RABV P was prepared. 50 μ l ATPase dilution buffer containing or lacking poly(I:C) was mixed with 1 μ l purified RABV P, or no RABV P as

control (for buffer compositions see appendix). 1 μl $\gamma\text{-}^{32}\text{P}\text{-ATP}$ was added to 29 μl H_2O and 5 μl of the mix was added to the ATPase reaction mixes. The reaction was initiated by the addition of the enzymes MDA5 or RIG-I and incubation at 32 °C. A time course of ATP hydrolysis was made by applying 1 μl of the reaction mix to a polyethyleneiminecellulose plate (Merck, Darmstadt) at 5 min intervals. Air-drying of the mixture on the cellulose plate stopped the reaction instantly. ATP hydrolysis was evaluated by thin-layer chromatography (TLC) where the plate was incubated in 0.5 M LiCl/1.0 M formic acid to separate the hydrolyzed $\gamma\text{-}^{32}\text{P}$ from $\gamma\text{-}^{32}\text{P}\text{-ATP}$. The amounts of $\gamma\text{-}^{32}\text{P}$ and $\gamma\text{-}^{32}\text{P}\text{-ATP}$ were visualized with a phosphoimager (Amersham, Bioscience) and quantified using ImageQuant software. Reaction velocities were displayed as hydrolyzed $\gamma\text{-}^{32}\text{P}$ against time.

2.2.21 *In vitro* transcription

The MEGAscript Kit (Ambion) was applied for *in vitro* transcription as described in the manufacturer's instructions. Measles virus leader template DNA oligonucleotides (see 2.1.4) containing a T7 promoter sequence (100 μM) were annealed with T7 promoter antisense oligonucleotide (100 μM) in the ratio 1:1 by heating (95 °C, 5 min) and subsequent cooling. 2 μl of this oligonucleotide was subjected to *in vitro* transcription (37 °C, o/n). DNase was supplied to digest template DNA and recovered RNA was purified using Mini Quick Spin RNA Columns (Roche).

3 Results

3.1 Mechanisms of RABV P to inhibit IFN induction

RABV P takes up a dual role in the inhibition of innate immune signaling, inhibiting IFN α/β - and IFN γ -induced JAK/STAT signaling (Brzózka et al., 2006; Vidy et al., 2005), and also blocking the transcriptional activation of IFN itself by interfering with activation of the transcription factors IRF3 and IRF7 (Brzózka et al., 2005). While it is known that RABV P inhibits JAK/STAT signaling by binding to activated STATs, and that this inhibition is lost upon deletion of the 10 C-terminal aa 288-297 (Brzózka et al., 2006), the mechanism(s) and domain(s) responsible for inhibiting IRF3 activation so far remained elusive. Activation of IRF3 and IRF7 occurs through phosphorylation by the kinases TBK1 and IKKi and is triggered by various PRRs. In most cell types IRF3 is activated after induction of the RLR signaling cascade, or in case of certain viruses via the TLR3 signaling cascade. In pDC, IRF7 is furthermore activated by TLR7 signaling. Distinct studies provide evidence that RABV RNA does not induce TLR3 or TLR7 signaling. Only in the latter case RABV P has no inhibitory effects (Pfaller and Conzelmann, 2008). In the first part of my dissertation I analyzed P mutants unable to prevent IFN induction and showed the relevance of IFN inhibition for pathogenesis of recombinant RABV *in vivo* (Rieder et al., 2011). In the second part, molecular targets of P were identified and details on the inhibition mechanism revealed.

3.1.1 Inhibition of IFN induction by RABV P depends on an internal domain

P is a multifunctional protein involved in both IFN escape and viral RNA synthesis. In order to elucidate specific domain(s) or amino acids of RABV P involved in inhibition of IFN induction, previous work in the laboratory (by K. Brzózka) involved the generation of P mutants with small deletions. Initial screening for their ability to inhibit IFN β promoter activity in dual luciferase assays indicated that the integrity of a region between aa 162 and 186 is required for full activity. For a detailed analysis, different constructs (P Δ 176-181, P Δ 182-186, and P Δ 176-186) were constructed and

compared in dual luciferase assays and qRT-PCR experiments for their ability to inhibit IFN β induction, as well as in native gel experiments for their ability to inhibit phosphorylation and dimerization of IRF3.

3.1.1.1 Deletion of RABV P amino acids 176-186 results in loss of IFN β inhibition

In dual luciferase assays the expression of IFN β promoter-controlled firefly luciferase (FL) from p125-luc was analyzed after transfection of distinct stimulators of the IFN induction cascade, such as constitutively active RIG-I- or MDA5-CARDs, named Δ RIG-I (aa 1-284) and Δ MDA5 (aa 1-350), respectively, and TBK1. Each of the inducers was coexpressed with plasmids of RABV P, the P deletion constructs, or empty vector (EV), into HEK 293T cells. A strong induction of FL expression upon cotransfection of Δ RIG-I, Δ MDA5 and TBK1 with EV was detected (namely 19-, 9-, and 75-fold, respectively), which was almost completely abolished by cotransfection of P wt. However, P Δ 176-181 (P Δ Ind1) and P Δ 182-186 (P Δ Ind2) had lost the ability to inhibit IFN β promoter activation significantly as levels of FL activity reached about 75% of the stimulated EV controls. A third mutant, harboring a combined deletion of Δ Ind1 and Δ Ind2, named P Δ 176-186 (P Δ Ind1/2), also showed a loss of inhibition. Interestingly, the strongest residual inhibition was observed in the Δ Ind1/2 mutant, leading to the hypothesis that loss of inhibition is due to conformational alterations that somehow destroy the inhibitory mechanism, and is not directly conferred by the identified domains (Fig. 3-1A). In our recent publication, dual luciferase assays revealed that P Δ Ind1, P Δ Ind2 and P Δ Ind1/2 were also able to inhibit mouse IRF7-induced FL promoter activation when co-expressed with TBK1 (Rieder et al., 2011).

To corroborate these findings, qRT-PCR experiments were carried out, using IFN β -specific primers to evaluate levels of newly transcribed IFN β mRNA. Expression of Δ RIG-I from transfected plasmid led to a 760-fold increase of IFN β mRNA (100 %), compared to non-stimulated cells (control). This induction was strongly inhibited by coexpression of full-length RABV P, to about 1 %. However, in the presence of the deletion mutants P Δ 176-181, Δ 182-186, and Δ 176-186, transcription was not effectively inhibited, resulting in accumulation of IFN β mRNA to 83 %, 75 % and 43 %

of the control, respectively (Fig. 3-1). Supporting the results from the dual luciferase assay, also here, a higher inhibitory of the double deletion mutant $\Delta 176-186$ was apparent.

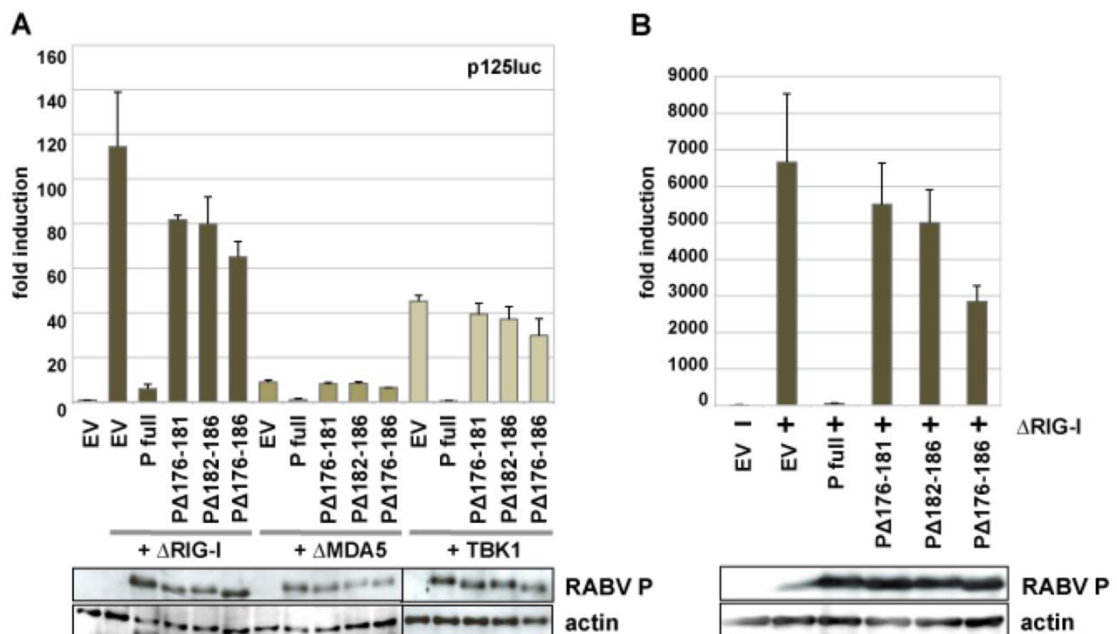


Figure 3-1: RABV P deletion mutants $\Delta 176-181$, $\Delta 182-186$ and $\Delta 176-186$ show decreased ability to inhibit IFN β induction compared to full-length P. (A) In a dual luciferase reporter gene assay, 0.2 μ g full-length RABV P and P deletion plasmids were transfected into HEK 293T cells together with 0.2 μ g Δ RIG-I (aa 1-284), Δ MDA5 (aa 1-350) or TBK1, 50 ng p125-luc reporter plasmid and 1 ng pCMV-*Renilla* control plasmid using Lipofectamine 2000. 24 h p.t. IFN β promoter-dependent FL activation was analyzed. (B) IFN β mRNA levels were analyzed in a qRT-PCR 24 h after coexpression of 0.4 μ g Δ RIG-I and 0.4 μ g of full-length P, P deletion constructs or EV in HEK 293T cells using Lipofectamine 2000. Experiments depicted were carried out in duplicates, with error bars showing standard deviation of the averaged values detected. To prove appropriate protein levels SDS-PAGE was carried out and the Western blots stained against RABV P and actin.

In conclusion, aa 176-186 of RABV P are required for its full capacity to inhibit IFN β induction after stimulation with Δ RIG-I, Δ MDA5, and TBK1 in HEK 293T cells. It is suggested that the inhibition is impeded due to conformational restraints in RABV P caused by the internal deletions.

3.1.1.2 Amino acids 176-186 are essential to efficiently inhibit TBK1- and IKKi-induced IRF3 phosphorylation

As RABV P interferes with IFN induction by inhibiting the phosphorylation and dimerization of IRF3 (Brzózka et al., 2005), the results from the dual luciferase assays and the qRT-PCRs led us to the assumption that the Δ Ind mutants might have lost

their inhibitory potential due to a decreased ability to block IRF3 activation. This was analyzed by native gel electrophoresis and subsequent Western blot analysis after induction of IRF3 activation by overexpressing TBK1 or IKKi from plasmids. Using an antibody specific against phosphorylated IRF3-S386 we could detect phosphorylation after stimulation with TBK1 (Fig. 3-2A) and IKKi (Fig. 3-2B). Dimerization was also seen by using an IRF3 antibody. In case of RABV P coexpression, the S386 phosphorylation and dimerization were not detectable anymore. However, when coexpressing the mutants P Δ Ind1, P Δ Ind2, or P Δ Ind1/2, phosphorylation and dimerization of IRF3 were visible, although to a lesser extent than in the control (EV); this was found in case of activation by both TBK1 and IKKi. Expression of RABV P, P Δ Ind mutants, TBK1 and IKKi was validated in SDS-PAGE and Western blot analysis.

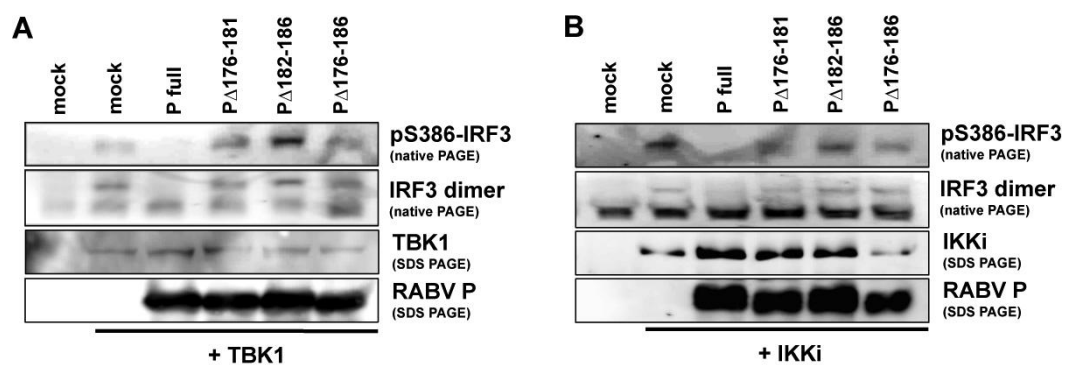


Figure 3-2: Native PAGE showing inhibition of IRF3 dimerization and S386 phosphorylation by RABV P, which is lost when aa 176-186 are deleted. HEK 293T cells were cotransfected with 5 μ g TBK1 (A) or IKKi (B) and 10 μ g full-length RABV P or the deletion mutants P Δ Ind1, P Δ Ind2, or P Δ Ind1/2 using PEI. 24 h p.t. cells were lysed and subjected to native PAGE analysis. Western blotting and subsequent incubation with phospho-IRF3-Ser386 and IRF3 antibody revealed phosphorylation at Ser386 and dimerization of IRF3, respectively. SDS PAGE was undertaken to analyze expression levels of RABV P, P Δ Ind mutants, and TBK1 (A) or IKKi (B).

These findings provide evidence that the individual deletions of aa 176-186 disturb the function of RABV P to inhibit induction of IFN because the P Δ Ind mutants are not able anymore to inhibit IRF3 activation.

3.1.2 Generation of recombinant viruses harboring deletions of amino acids 176-186

Consequential to the findings acquired from plasmid transfection experiments, it was of interest how the deletions of aa 176-181, 182-186, and 176-186 affect the

inhibitory effect of RABV P in a viral context. Therefore, minigenome assays were carried out to initially elaborate whether the P Δ Ind mutants fulfill the functions of wt P necessary for viral RNA synthesis. Subsequently, recombinant RABV were generated carrying the respective deletions.

3.1.2.1 P Δ Ind proteins support viral growth

In a minigenome assay the plasmid constructs P Δ Ind1, P Δ Ind2, and P Δ Ind1/2 were tested for their ability to rescue a RABV minigenome into functional RNPs and to sustain replication and gene expression. The RABV minigenome plasmid pSDI-HH-flash (Ghanem unpublished and (Conzelmann and Schnell, 1994)), which is composed of a FL gene flanked by RABV leader and trailer sequences, was cotransfected together with RABV N, L, P, or P deletion mutants into BSR-T7/5 cells. The DNA dependent T7 RNA polymerase transcribes the minigenome RNA from the plasmid. In case P fulfills its functions as polymerase co-factor, the viral polymerase (L/P) transcribes and replicates the minigenome RNA. The cells were harvested 48 h p.t. and FL activity was measured in a dual luciferase assay. As shown in figure 3-3, the deletion mutants of RABV P were as effective as full-length P to engage into N-P, L-P, and N-L-P complexes, thus, to encapsidate T7 transcripts, transcribe FL mRNAs, and replicate RNPs, respectively.

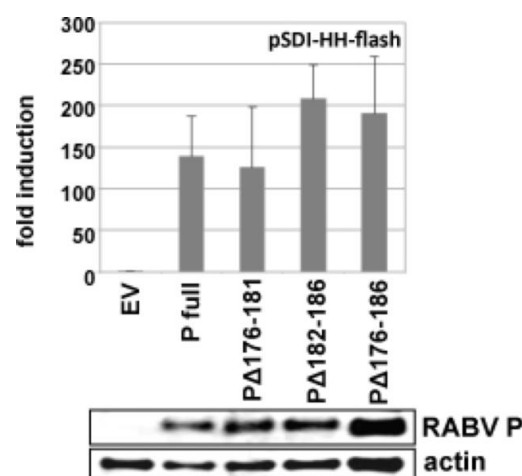


Figure 3-3: RABV P deletion mutants Δ 176-181, Δ 182-186 and Δ 176-186 fulfill essential functions to support expression from the RABV pSDI-HH-flash minigenome. BSR-T7/5 cells were cotransfected with 4 μ g pSDI-HH-flash minigenome and the helper plasmids that express RABV L (2.5 μ g), N (5 μ g), and either full-length P, or the depicted P deletion mutants (2.5 μ g). Transfection of EV instead of P was used as control. 10 ng *Renilla* luciferase was further coexpressed to normalize the FL expression. 48 h p.t. cell lysates were prepared and luciferase activities measured.

This finding indicates that the deletions in P do not greatly affect virus replication and favor the possibility that full-length RABV genomes lacking aa 176-181, 182-186, or 176-186 in their P gene can be rescued.

3.1.2.2 SAD Δ Ind viruses can grow in IFN-incompetent and IFN-competent cells

Using the standard RABV reverse genetics approach (Schnell et al., 1994), viable RABV harboring the P Δ Ind1, P Δ Ind2, and P Δ Ind1/2 mutations could be rescued from cDNA. The generated recombinant viruses were named SAD Δ Ind1, SAD Δ Ind2, and SAD Δ Ind1/2. To initially test the ability of the SAD Δ Ind1 and SAD Δ Ind2 to inhibit IFN induction, as examined by the P Δ Ind plasmid transfection experiments, native PAGE and immune fluorescence experiments were undertaken. These showed that the SAD Δ Ind viruses, like SAD Δ PLP, were incapable of interfering with IRF3 S386 phosphorylation, dimerization, and nuclear translocation (K. Brzózka; shown in (Rieder et al., 2011)).

Growth kinetics of the recombinant viruses were analyzed in IFN-incompetent BSR-T7/5 cells (which do not express IFN in response to RLR induction) (Fig. 3-4A), and in IFN-competent HEp-2 cells (K. Brzózka; shown in (Rieder et al., 2011)). After infection of BSR-T7/5 cells with an MOI of 0.1, the viruses SAD Δ Ind1, SAD Δ Ind2, and SAD Δ Ind1/2 reached titers comparable to parental SAD L16, namely up to 10^8 ffu/ml at day 3 p.i. (Fig. 3-4A). SAD Δ Ind1 and SAD Δ Ind2 (SAD Δ Ind1/2 not analyzed) showed comparable growth kinetics in IFN-competent HEp-2 cells meaning that the recombinant viruses most likely inhibit IFN-mediated JAK/STAT signaling. In contrast, SAD Δ PLP, which expresses only basal levels of full-length P (P gene moved from the second to the most promoter-distal position), showed a marked delay in propagation in HEp-2 cells, yielding 10- to 15-fold lower infectious titers.

Indeed, SDS-PAGE analyses revealed that in HEp-2 cells infected with SAD Δ Ind1 and SAD Δ Ind2 levels of ISGs (such as Mx) were kept at low levels in contrary to cells infected with SAD Δ PLP where ISGs were expressed to higher levels (the control SAD L16 infection strongly blocked ISG accumulation). The ability of the Δ Ind mutant

viruses to still prevent IFN-mediated ISG induction could be corroborated in dual luciferase reporter assays, in which ISRE promoter-controlled FL activities were analyzed. For this experiment, BSR-T7/5 cells were transfected with pISRE-luc and a *Renilla* control plasmid and 6 h later infected with SAD L16, SAD Δ Ind1, SAD Δ Ind2, and SAD Δ PLP at an MOI of 3. 24 h p.i. the cells were stimulated with 1,000 IU/ml IFN α A/D, and FL activities were determined. An IFN-induced FL activity could only be detected in mock- and SAD Δ PLP-infected cells. However, strong inhibition of ISRE-promoter activation was clearly seen after infection with L16, and the Δ Ind mutant viruses (shown in (Rieder et al., 2011)).

To conclude, besides the lack of the Δ Ind mutant viruses to inhibit IFN induction, they are able to replicate in HEp-2 cells because of their remaining capability to inhibit JAK/STAT signaling, thus keeping expression of antiviral ISGs below a critical level. As a consequence we believe that inhibition of IFN induction and IFN signaling are genetically distinct functions of RABV P (also see (Brzozka et al., 2005, 2006)).

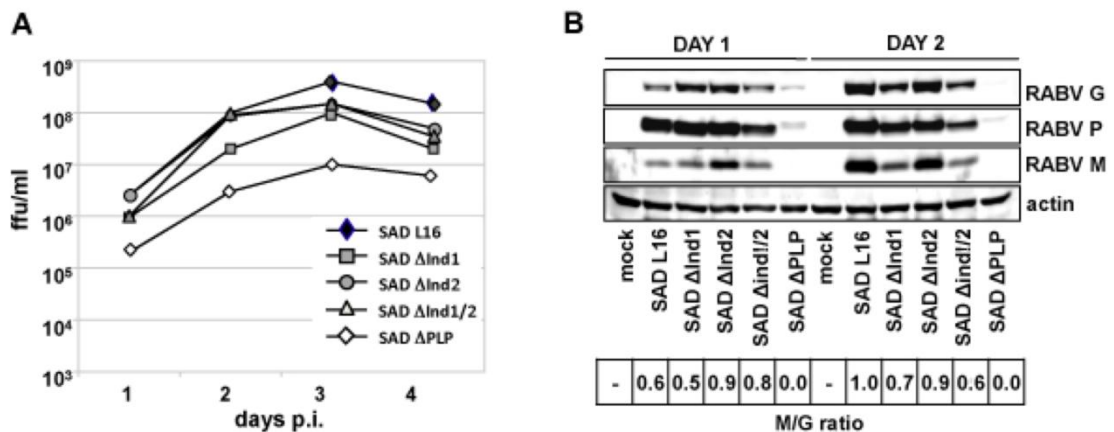


Figure 3-4: Growth kinetics and protein expression of recombinant viruses SAD Δ Ind1, SAD Δ Ind2, and SAD Δ Ind1/2, are comparable to SAD L16. (A) BSR-T7/5 cells were infected with the indicated SAD Δ Ind mutant viruses at an MOI of 0.1, and compared to SAD L16 and SAD Δ PLP. Infectious titers were determined 24, 48, 72 and 96 h p.i. by counting virus foci. (B) For analysis of viral protein expression, HEp-2 cells were infected with SAD L16 and respective mutant viruses at an MOI of 1, and cell lysates prepared 24 and 48 h p.i. Western blots were prepared and stained with antibodies against G, P, and M, and actin as loading control. Using the Bio 1D software of the Fusion molecular imaging device, the chemiluminescent signals were compared and a ratio of M relative to G was calculated (L16 at day 2 set to 1.0).

To further characterize growth of SAD Δ Ind1, Δ Ind2, and Δ Ind1/2, HEp-2 cells were infected with an MOI of 1 and SDS-PAGE and Western blot analysis were performed

to compare protein levels of M, P, and G. In case of SAD Δ Ind1 and Δ Ind1/2, after two days a slight attenuation of M and G protein accumulation was visible compared to SAD L16 and SAD Δ Ind2. In case of SAD Δ PLP, a lack of protein expression was apparent, which is in accordance with its slow growth kinetics in infected HEp-2 cells. In a digital readout of chemiluminescent signals, protein expression was quantified by Fusion Bio 1D software. Indeed, 2 days p.i. SAD L16 and SAD Δ Ind2, show comparable M/G ratios, namely 1.0 and 0.9, respectively. However, SAD Δ Ind1 and SAD Δ Ind1/2 show reduced M levels (M/G ratio of 0.7 and 0.6, respectively), which indicates an influence of deleting aa 176-181 on M protein levels (Fig. 3-4B).

3.1.2.3 SAD Δ Ind viruses are inducers of IFN β , yet with diverging capacities

In order to quantitatively evaluate the induction of IFN β promoter activation and mRNA transcription by Δ Ind mutant viruses, p125-luc dual luciferase reporter assays and qRT-PCRs, respectively, were carried out in HEK 293T cells.

For the luciferase assay, cells were transfected with p125-luc and pCMV-*Renilla* and 6 h p.t. infected with SAD L16, SAD Δ Ind viruses, and Δ PLP at an MOI of 3. 24 h p.i., IFN β promoter-controlled FL activities were inhibited strongest in SAD L16 infected cells. However, a 5-, 3-, and 4-fold increase in FL activities was detected by SAD Δ Ind1, SAD Δ Ind2, and SAD Δ Ind1/2, respectively, and even up to 10-fold by SAD Δ PLP compared to wt virus (Fig. 3-5A).

These data were supported by qRT-PCR after isolation of RNA from infected HEK 293T cells and quantification of IFN β mRNA levels 24 h p.i. As expected, cells infected with Δ Ind viruses showed a markedly increased level of IFN β mRNA transcription, as opposed to SAD L16. However, whilst in case of SAD Δ Ind1 and SAD Δ Ind1/2 the determined IFN β transcription levels were strongly upregulated, namely 8-fold and 4-fold compared to SAD L16, the cells infected with SAD Δ Ind2 only induced a 2-fold increase (Fig. 3-5B).

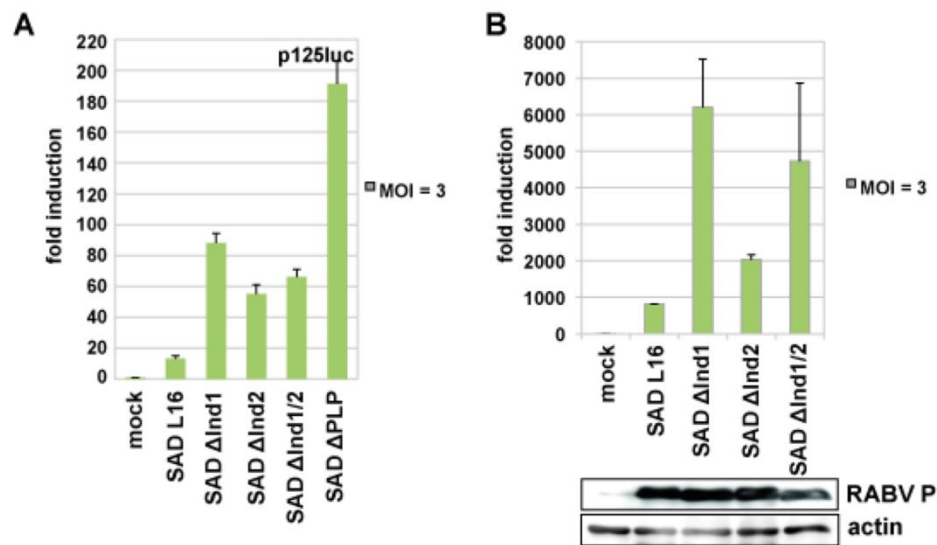


Figure 3-5: Infection of HEK 293T cells with SAD ΔInd1, SAD ΔInd2, and SAD ΔInd1/2 showed an increased induction of IFN β compared to SAD L16. HEK 293T cells were infected with the indicated viruses at an MOI of 3 and investigated for IFN β induction 24 h p.i. (A) For dual luciferase analysis of IFN β promoter activation, 100 ng p125-luc and 2 ng pCMV-*Renilla* were expressed from plasmids and 6 h p.t. cells were infected with ΔInd mutant viruses, SAD L16 and SAD ΔPLP. (B) qRT-PCR of total RNA using primers for IFN β was applied to analyze IFN β mRNA transcription. Western blot analysis was performed to validate comparable expression of RABV P.

These results reveal that in comparison to SAD L16, which powerfully inhibits IFN β induction, the recombinant viruses SAD ΔInd1, SAD ΔInd2, and SAD ΔInd1/2, which lack the aa 176-181, 182-186, and 176-186 in their P gene, respectively, lost the ability to effectively interfere with IFN β induction. SAD ΔInd1 and SAD ΔInd1/2 are more potent inducers of IFN β than SAD ΔInd2.

3.1.2.4 SAD ΔInd1, a strong inducer of IFN β , has a characteristic transcription and replication profile, and is highly attenuated *in vivo*

The distinct properties of the SAD ΔInd viruses concerning the level of IFN induction and their protein expression profile were intriguing and further characterization was needed. Therefore, Northern blot experiments from total RNA were undertaken to investigate transcription (N mRNA) and replication (vRNA) patterns of the respective viruses, after infection of HEK 293T and BSR-T7/5 cells at an MOI of 3, by using a probe against the nucleoprotein N. As depicted (Fig. 3-6), it could be confirmed that correctly sized N mRNA and vRNA but apparently no defective interfering particles (inducers of RIG-I activation) were made. Interestingly, calculating the ratio between

N mRNA and vRNA using ImageQuant, SAD Δ Ind1 and SAD Δ Ind1/2 apparently accumulate more mRNAs per genome than SAD L16 and SAD Δ Ind2 in both HEK 293T and BSR-T7/5 cells. Furthermore, SAD Δ Ind1 shows a 4-fold induction of N mRNA/vRNA compared to SAD Δ Ind2 in both HEK 293T and BSR-T7/5 cells. SAD Δ Ind1/2 also accumulates more N mRNAs per genome than SAD Δ Ind2, namely 2-fold in HEK 293T cells and 4-fold in BSR-T7/5 cells.

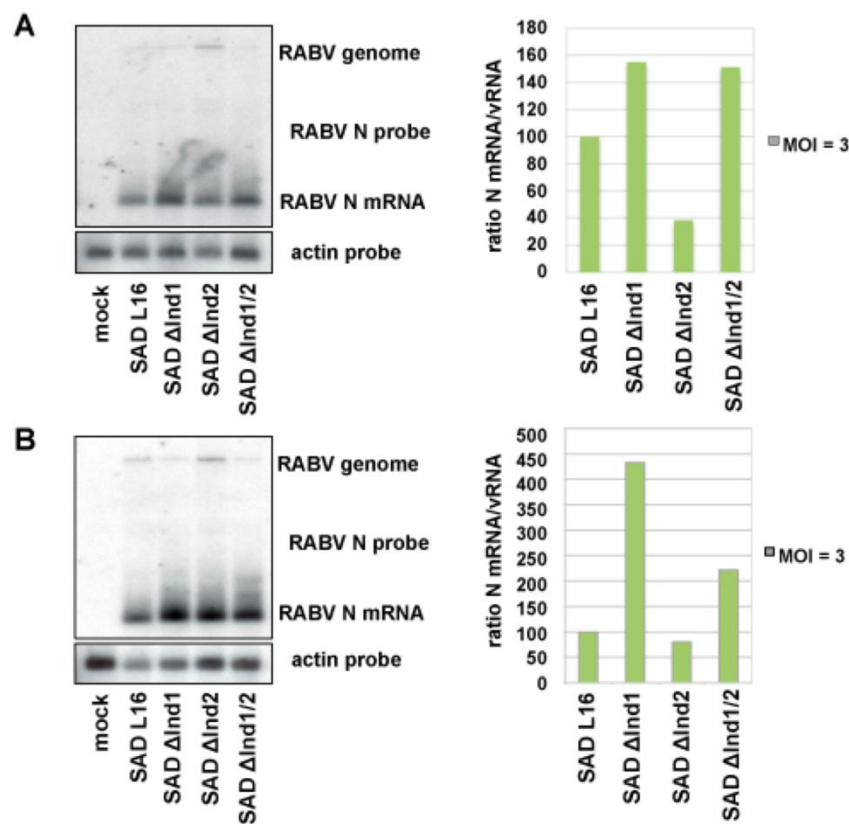


Figure 3-6: Northern blot analysis of SAD L16 and recombinant SAD Δ Ind viruses. HEK 293T (A) and BSR-T7/5 (B) cells, infected with indicated viruses at an MOI of 3, were analyzed for N mRNA transcription and vRNA replication, after isolation of total RNA 24 h p.i. An N probe was applied and the signals were detected using ImageQuant. The ratio between N mRNA and genome vRNA was calculated and depicted in histograms as the percentage of the SAD L16 ratio (set to 100%).

In conclusion, the above shown cell culture experiments demonstrated a loss of function of the P deletion mutants P Δ 176-181, P Δ 182-186 and P Δ 176-186, and the corresponding recombinant viruses SAD Δ Ind1, SAD Δ Ind2 and SAD Δ Ind1/2, in preventing induction of IFN β after transfection or infection, respectively. However, the ability to prevent JAK/STAT signaling and to support virus growth was not

compromised. A particularly strong IFN induction by SAD Δ Ind1 and SAD Δ Ind1/2 may be due to transcription of IFN-stimulating RNAs.

A biological relevance has been disclosed after investigating the effect of enhanced IRF3 activation of SAD Δ Ind viruses on their pathogenicity *in vivo*, after intracerebral (i.c.) injection into mice (Rieder et al., 2011). Wt mice with a functional IFN α / β -receptor (IFNAR^{+/+}) or mice lacking the receptor (IFNAR^{-/-}) were infected with 10⁵ ffu of SAD L16, SAD Δ Ind1, SAD Δ Ind2 and SAD Δ PLP and survival of mice was monitored over 18 days. As one would expect, all IFNAR^{-/-} mice succumbed to infection by any of the viruses, with one day delay in case of SAD Δ Ind1 and SAD Δ PLP. However, the wt mice showed a strong difference in their reactions to the distinct viruses. Wt mice succumbed to SAD L16 infection already after 9 days, while SAD Δ Ind2 required 13 days to cause death. On the contrary, SAD Δ Ind1 and SAD Δ PLP infections remained completely apathogenic, and all mice survived without showing clinical symptoms.

These experiments provide evidence that the recombinant virus SAD Δ Ind1, which lacks the amino acids 176-181, is as attenuated as SAD Δ PLP, while it grows to much higher titers in IFN-competent cells (like SAD L16). As the previous experiments showed that SAD Δ Ind1 has a higher intrinsic capacity to induce IFN, it is assumed that the level of IRF3 activation and IFN expression is the major attenuating factor of the virus. The threshold of IFN production might decide whether a virus is apathogenic, like SAD Δ Ind1, or lethal, such as SAD Δ Ind2 and SAD L16.

3.1.3 RABV P interacts with proteins of the RLR signaling cascade: Interaction with RLRs

RABV P has been identified as potent antagonist of the cellular IFN system being able to interfere with both induction of IFN β transcription (Brzózka et al., 2005) and IFN-mediated JAK/STAT signaling (Brzózka et al., 2006; Vidy et al., 2005). The inhibition of IFN signaling occurs via interaction of C-terminal aa of RABV P to activated STAT, preventing binding of the transcription factor to its promoters. However, a direct interaction of P to a cellular protein that explains the inhibition of IRF3 S386 phosphorylation, dimerization and nuclear import, was not identified so far. In this

study potential candidates of the RLR signaling cascade were investigated for their interaction with RABV P.

The RLRs RIG-I, MDA5, and Lgp2, the downstream adaptor proteins IPS-1, Rip-1, Sintbad, NEMO, and Nap1, the kinases TBK1 and IKKi, and the transcription factor IRF3 were individually coexpressed with RABV P in HEK 293T cells and were analyzed for co-precipitation in Co-IP experiments. Strikingly, although repeated experiments in resting cells did not identify a clear interaction of RABV P with the proteins downstream of the RLRs, as was predicted from the ability of P to prevent TBK1-mediated IRF3 phosphorylation, an interaction of P with the RLRs themselves, the receptors that recognize RABV RNA, was obtained. Functional assays, such as ATPase assays, were undertaken to investigate a biochemical relevance of these interactions.

3.1.3.1 RABV P interacts with MDA5 and to a lesser extent Lgp2

To analyze the interaction of RABV P with Flag-tagged RLRs in resting cells, 3 μ g of RABV P and 3 μ g of either one of the Flag-tagged RLRs were transfected into HEK 293T cells and 24 h p.t. subjected to Co-IP analysis. In individual experiments, the ability of Flag-tagged RIG-I, MDA5, and Lgp2 to co-precipitate P on the Flag-matrix, or the ability of P to pulldown Flag-tagged RIG-I or MDA5 on SepharoseA beads (coated with antibody against P) were investigated. Proteins captured on the matrix (IP, Co-IP) and total protein in the expression control (WCL) were analyzed by SDS-PAGE.

First interesting results revealed an interaction of RABV P with the RIG-I-like helicase MDA5, and to a lesser extent with Lgp2, but not with RIG-I (Fig. 3-7B/C). The interaction of MDA5 and RABV P seems to be rather strong, considering a rather poor precipitation of MDA5 by the Flag-matrix compared to RIG-I and Lgp2. All RLRs contain a C-terminal RD and a HD with its motifs I-VI. RIG-I and MDA5 additionally have two C-terminal CARDS for downstream signaling (Fig. 3-7A). The activation of RIG-I and MDA5 by specific ligands induces conformational changes that ultimately influence their capacity for downstream signaling. This fact may influence access and possible interaction of RABV P to distinct RLR domains.

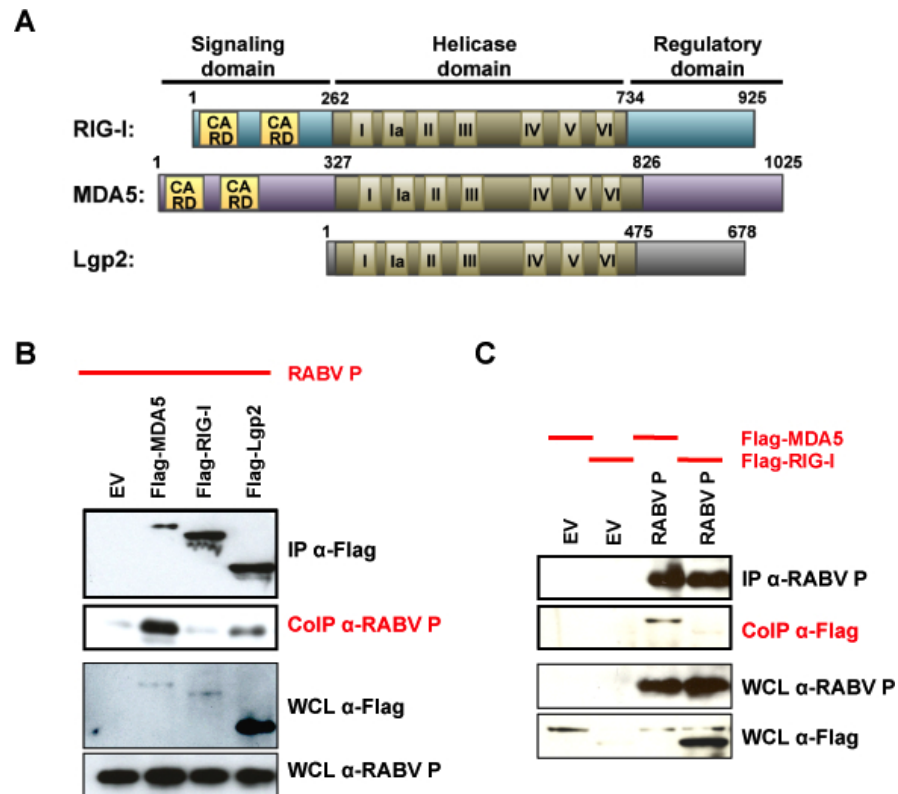


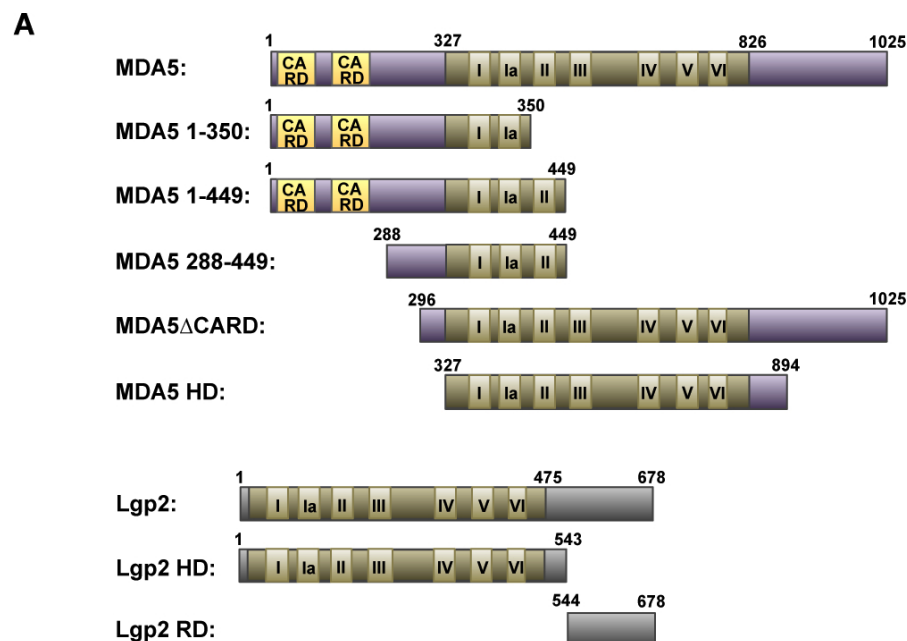
Figure 3-7: RABV P interacts with MDA5, and to a lesser extent Lgp2. (A) Schematic illustration of RIG-I, MDA5 and Lgp2. All RLRs contain a C-terminal RD and a HD with the motifs I-VI (beige). RIG-I and MDA5 additionally have two C-terminal CARDs (yellow) for downstream signaling. In Co-IP assays Flag-MDA5, Flag-RIG-I, and Flag-Lgp2 were examined for interaction with RABV P. 3 μ g plasmids containing cDNA of Flag-tagged RLRs were cotransfected with 3 μ g RABV P expression plasmid (pCR3-RABV P) into HEK 293T cells. Cells were lysed 24 h p.t. and 10 % of the lysate served as expression control (WCL; bottom panels). (B) 90 % of the cell lysate was incubated with a Flag-matrix. Precipitation of Flag-tagged proteins by the matrix (upper panel) and co-precipitation of RABV P (second panel) were analyzed by SDS-PAGE and Western blot. (C) 90 % of the lysate was incubated with SepharoseA beads coated with an antibody against RABV P. RABV P protein precipitation by the SepharoseA beads (upper panel) and co-precipitation of Flag-tagged proteins (second panel) were analyzed by SDS-PAGE and Western blot. The blots were stained with α -RABV P or α -Flag antibody.

3.1.3.2 RABV P interacts with the CARD/HD junction of MDA5 and the HD of Lgp2

To characterize the region(s) of MDA5 and Lgp2 responsible for interaction with RABV P in more detail, constructs of Flag-tagged MDA5 and Lgp2 were generated comprising (or lacking) specific domains, such as MDA5 1-350, which contains the CARD domain and the helicase domain (HD) motif I, and MDA5 1-449, which contains the CARD domain and the HD motifs I, Ia and II. Furthermore, MDA5 HD, MDA5 Δ CARD, Lgp2 HD, and Lgp2 RD were generated (Fig. 3-8A). The Flag-tagged proteins were analyzed for interaction with RABV P in Co-IP experiments.

In case of MDA5, all constructs containing aa 1-350 were able to interact with RABV P, and in a construct where the CARD domain is missing, the interaction was lost. Interestingly, an MDA5 deletion construct comprising only aa 288-449, hence the CARD/HD junction and HD motifs I, Ia and II, was found sufficient for interaction with RABV P. However, the MDA5 HD (aa 327-894) was not able to associate with P which implicates an essential role of aa 288-327 for MDA5/P interaction (Fig. 3-8B). Furthermore, the abilities of Lgp2 domains (HD and RD) to interact with RABV P were analyzed. Obviously, RABV P rather interacts with the N-terminal part of Lgp2, thus the HD (Fig. 3-8C).

Taken together, it seems that binding of RABV P involves the CARD/HD junction of MDA5, and the HD of Lgp2. It has to be mentioned that amino acid sequence comparison of the RLRs revealed that Lgp2 HD shares 30 % identity to the RIG-I HD and 40 % identity the MDA5 HD. If only HD motif I (Walker A motif), and motif I/II (Walker A and B motifs) are considered, sequence identities of 87.5 % and 81.25 %, respectively, exist between MDA5 and Lgp2, but only 75 % and 68.75 % between RIG-I and Lgp2.



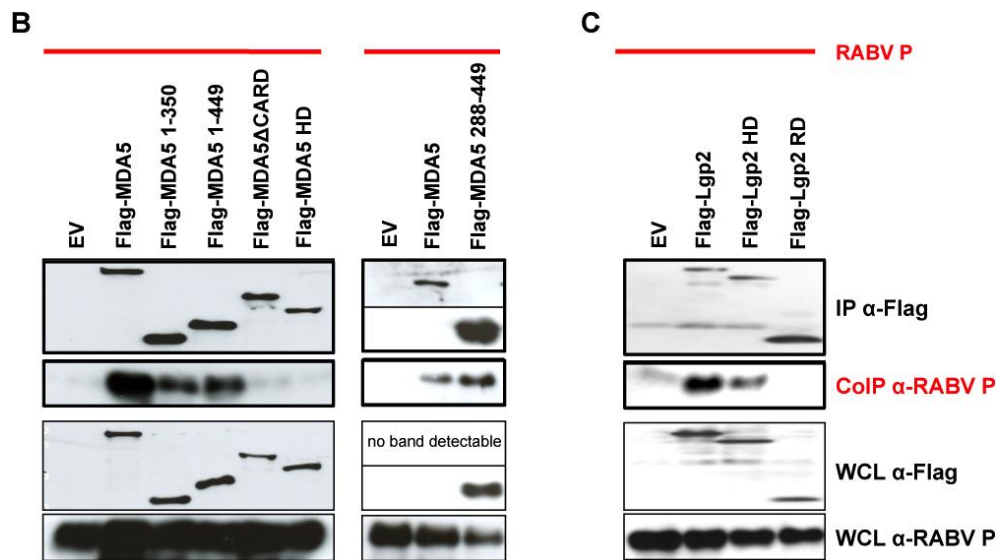


Figure 3-8: RABV P interacts with the MDA5 CARD/HD junction and with an Lgp2 N-terminal domain. (A) Schematic overview of MDA5 and Lgp2 mutants that were tested for interaction with RABV P. CARDs are depicted in yellow and HD motifs in beige. (B) Flag-MDA5, Flag-MDA5 1-350, Flag-MDA5 1-449, Flag-MDA5 ΔCARD, Flag-MDA5 HD, Flag-MDA5 288-449 or (C) Flag-Lgp2 HD and Flag-Lgp2 RD were examined for interaction with RABV P in Co-IP assays. 3 μg plasmids containing cDNA of Flag-tagged RLRs and RLR-constructs were cotransfected with 3 μg RABV P expression plasmid (pCR3-RABV P) into HEK 293T cells and lysed 24 h p.t. The Co-IP was carried out as described in Fig. 3-7.

3.1.3.3 RABV P_{CTD} and P_{NTD} regions confer interaction with MDA5

As the interaction with MDA5 seems to be rather strong compared to Lgp2 and as the question arose whether lyssavirus P proteins act on MDA5 like paramyxovirus V proteins, the interaction of RABV P to MDA5 was further elaborated. To restrict the interaction interface of RABV P required for MDA5 binding, full-length P (N- or C-terminal Ig-tag) and the smaller P-forms, P₂ (aa 19-297), P₃ (aa 52-297) and P₄ (aa 69-297) (N-terminal Ig-tag) were expressed from respective plasmids in HEK 293T cells and analyzed 24 h p.t. for interaction with transfected Flag-MDA5 using the Flag-matrix. Notably, the presence of an N-terminal Ig-tag on P interfered with co-precipitation by Flag-MDA5, while a C-terminal Ig-tag allowed strong interaction. The strength of interaction decreased further when the N-terminal aa 1-52 were lacking, such as in P₃ and P₄ (Fig. 3-9A). These findings point towards an important role of a RABV P N-terminal region in MDA5 interaction.

Further Co-IP experiments were performed to investigate C-terminally truncated RABV P constructs, with deletions of aa 191-297, 199-297, 217-297, and 245-297 for their interaction with Flag-MDA5 288-449 after cotransfection into HEK 293T cells.

Here, a drastic loss of co-precipitation by Flag-MDA5 288-449 was apparent in RABV P constructs that lack the C-terminal 80 aa or more (217-297). However, when only aa 245-297 of P were deleted, a strong interaction with MDA5 288-449 could be detected. It seems that the loss of RABV P aa 217-245 was decisive in the loss of interaction (Fig. 3-9B).

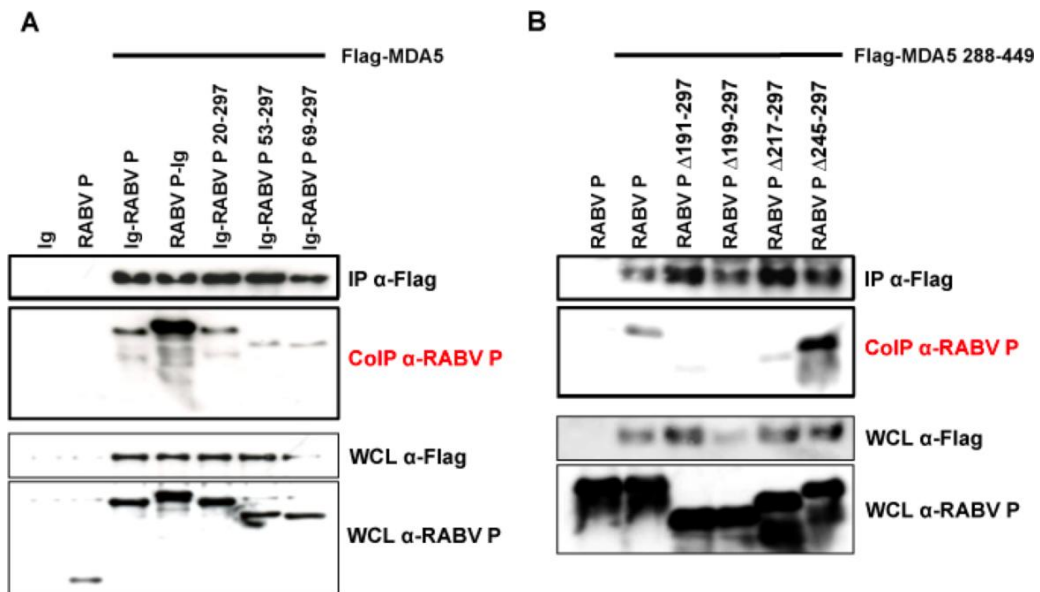


Figure 3-9: RABV P lacking aa 20-52 and 217-245 show a reduced interaction with MDA5. 3 µg Flag-MDA5 or Flag-MDA5 288-449 and 3 µg RABV P constructs were coexpressed in HEK 293T cells and subjected to Co-IP experiments 24 h p.t. (A) Ig-RABV P (6630 nt), RABV P-Ig (6679 nt), Ig-RABV P₂ (aa 19-297), Ig-RABV P₃ (aa 52-297) and Ig-RABV P₄ (aa 69-297) were coexpressed with Flag-MDA5. Ig and RABV P were cotransfected with EV to exclude unspecific interactions with the matrix. (B) RABV P, RABV P Δ191-297, RABV P Δ199-297, RABV P Δ217-297 and RABV P Δ245-297 were cotransfected with MDA5 288-449. The Co-IPs were carried out as described in Fig. 3-7.

Taken these results together, it seems that not only the P_{NTD} but also aa 217-245 of the P_{CTD} are important for MDA5 binding. It is possible that certain regions of RABV P are only brought into proximity upon tertiary structure formation, hereby displaying an interface that recognizes MDA5. Further constructs are generated to elucidate the precise binding interface.

3.1.3.4 RABV PΔInd1 is able to interact with MDA5

In chapter 3.1.1 of this thesis, a domain in RABV P was described that is required for inhibition of IRF3 activation, namely aa 176-186. If this stretch of eleven amino acids is directly required for interaction with MDA5, or if this deletion renders the protein

shape sterically unfavorable for P interaction, was investigated in a further Co-IP assay. Initially, interaction of MDA5 and RABV P Δ Ind1 (P Δ 176-181) was analyzed. As seen in figure 3-10, the amounts of P and RABV P Δ Ind1 that were pulled down with Flag-MDA5 on the Flag-matrix were comparable, thus the deletion of aa 176-181 did not disturb P/MDA5 interaction. The addition of poly(I:C), a ligand of MDA5 that induces its activation and signaling capacity, also had no effect on interaction. Therefore, both wt P and P Δ Ind1 are able to interact with MDA5 in its basal and activated state. Consequently, as P Δ Ind1 lost its ability to block RLR signaling, P binding to MDA5 alone seems not to be sufficient to prevent IFN induction.

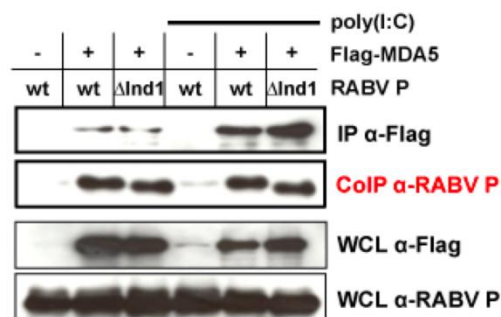


Figure 3-10: RABV P Δ Ind1 still interacts with MDA5 and strength of interaction is independent of poly(I:C) stimulation. In Co-IP assays RABV P or P Δ Ind1 were analyzed for interaction with Flag-MDA5. 3 μ g of respective plasmids were transfected into HEK 293T cells using PEI. 6 h p.t. cells were further transfected with poly(I:C) or with EV. 24 h after poly(I:C) transfection, cell lysates were prepared and analyzed. The Co-IP was carried out as described in Fig. 3-7.

3.1.3.5 Activation of RIG-I allows for RABV P association

In previous experiments investigating P/RLR interactions the transfected cells generally had not been treated with immune stimulating agents. Only in case of MDA5, poly(I:C) was applied to activate MDA5, which, as already mentioned, did not result in an increased interaction with P. However, the interaction of RABV P with RLRs was revisited in a situation where the cells were alerted. Therefore, Flag-RIG-I or Flag-Lgp2 were coexpressed with RABV P and the interaction analyzed in a Co-IP in absence or presence of Sendai virus DI (SeV DI-H4) infection. As positive control, a Co-IP of Flag-MDA5 1-350 and RABV P was carried out without stimulation of the cells. Indeed, the situation of P/RLR interaction intriguingly changes if the IFN induction pathway was stimulated by incubation of the cells with SeV DI-H4. Compared to unstimulated cells, where no or only weak interaction of RIG-I or Lgp2

with RABV P was observed, in stimulated cells P effectively interacted with RIG-I and Lgp2. The efficiency of activated RIG-I and Lgp2 to pull-down P was just as strong as by the positive control MDA5 1-350 which does not need to be activated (Fig. 3-11A).

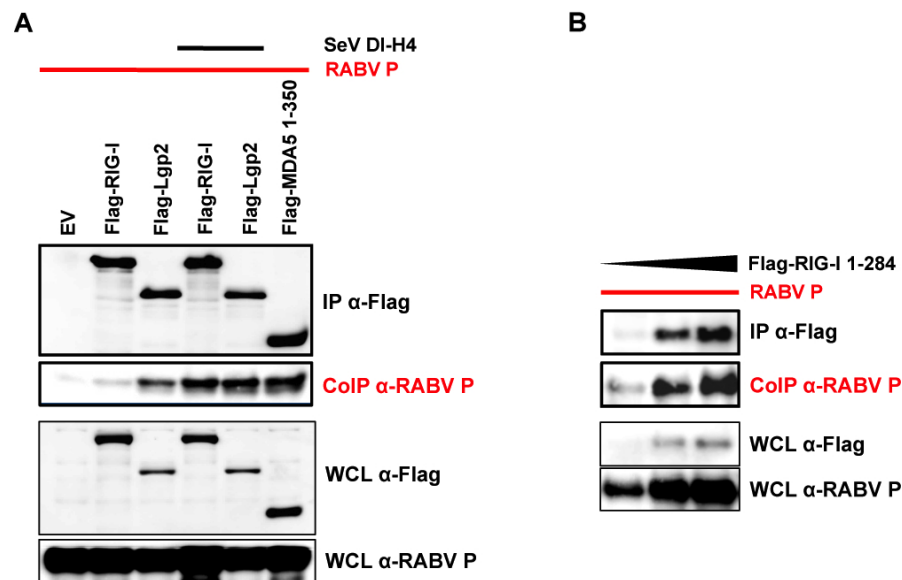


Figure 3-11: RABV P interacts with activated RIG-I and Lgp2 and with RIG-I CARDS. (A) In Co-IP assays Flag-RIG-I and Flag-Lgp2 were examined for interaction with RABV P with or without SeV DI stimulation. FI-MDA5 1-350 was transfected as positive control without SeV DI stimulation. 3 μ g of the Flag-tagged constructs were cotransfected with 3 μ g RABV P expression plasmid (pCR3-RABV P) into HEK 293T cells using PEI, and analyzed 24h p.t. (B) RABV P was coexpressed with increasing amounts of Flag-RIG-I 1-284 (1, 2 and 4 μ g) in HEK 293T cells and interaction analyzed by Co-IP 24 h p.t. The Co-IP was carried out as described in Fig. 3-7.

As already mentioned, in resting cells the RIG-I signaling activity is repressed by interactions of the HD (or also RD) with the CARDS, masking the CARD domains from crucial activation modifications and from subsequent interaction with IPS-1. Upon ligand binding, a conformational change occurs that releases the CARDS which then convey downstream signaling. Concerning the previous findings, it seems that RABV P exclusively targets the activated conformations of RIG-I and preferentially of Lgp2. It was therefore of interest if a RIG-I construct lacking the repressive domain(s) can interact with RABV P without further stimulation. For this purpose, a RIG-I construct only composed of the CARDS and the HD motif I (known to be constitutively active), named Flag-RIG-I 1-284, was generated. Increasing amounts of Flag-RIG-I 1-284 (1, 2 and 4 μ g) were coexpressed with RABV P in HEK 293T cells without further stimulation and interaction analyzed in Co-IP assays. As anticipated, Flag-RIG-I 1-284 was able to co-precipitate RABV P in a dose dependent manner and without activation by a ligand (Fig. 3-11B).

Taken together, RABV P is able to interact with MDA5 independent of its activation while interaction with Lgp2 is markedly induced upon its activation. In case of RIG-I an interaction with RABV P is only observed when a ligand is present. As an interaction of P with the RIG-I CARD/HD motif I could be observed without stimulation, it seems that only activation of RIG-I allows access to this region, while in MDA5 and Lgp2 this region is accessible without stimulation.

These results were puzzling, yet they fit to findings observed in dual luciferase assays which revealed diverse abilities of RIG-I and MDA5 to induce IFN β in presence or absence of certain stimuli. Therefore, p125-luc and pCMV-*Renilla* were transfected into HEK 293T cells and induction of the IFN β promoter was analyzed.

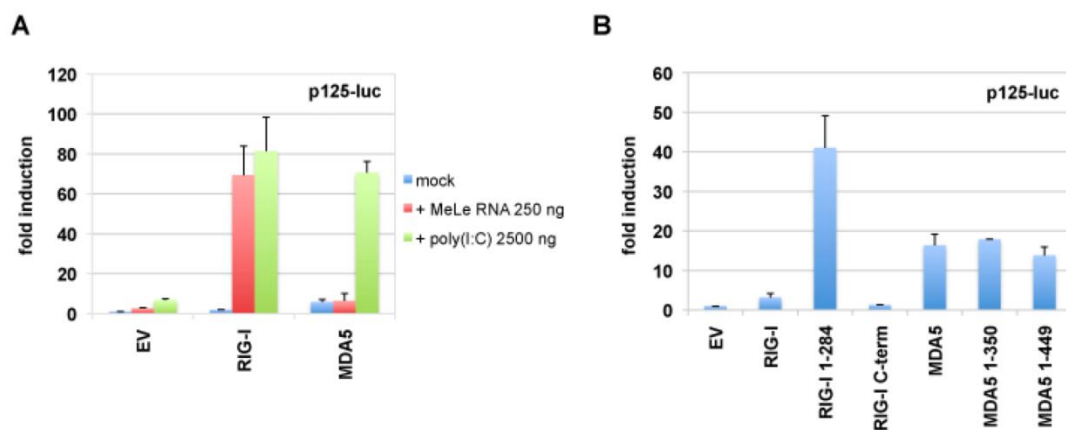


Figure 3-12: Activation of IFN β promoter is induced by RIG-I and MDA5 depending on their activation. HEK 293T cells were transfected with 50 ng p125-luc reporter plasmid and 1 ng pCMV-*Renilla* using Lipofectamine 2000. (A) 10 ng RIG-I, MDA5 or EV were cotransfected and 6 h p.t. either 250 ng MeLe RNA or 2500 ng poly(I:C) transfected further. (B) 0.2 μ g RIG-I, RIG-I 1-284, RIG-I C-terminus, MDA5, MDA5 1-350, MDA5 1-449 or EV were cotransfected. After 24 h FL activities were measured and corrected to the *Renilla* luciferase activity in order to normalize the results.

To identify specific ligands that activate RIG-I or MDA5, HEK 293T cells were transfected with RIG-I or MDA5 plasmids and 6 h p.t. they were further transfected with measles virus leader (MeLe) RNA or poly(I:C). As depicted in figure 3-12A, HEK 293T cells showed a very low endogenous response to MeLe RNA or poly(I:C) in the dual luciferase assays. Pre-existing findings (Yoneyama et al., 2004, 2005) were corroborated that on the one hand MeLe RNA specifically induces RIG-I- (23-fold) but not MDA5-dependent IFN β promoter activation. Poly(I:C) on the other hand is recognized by both RIG-I and MDA5 which leads to a 12- and 10-fold induction of the

IFN β promoter, respectively. Interestingly, transfection of MDA5 without activation by a ligand (compared to EV w/o stimulation) already led to a 8-fold increase in IFN β promoter induction. This finding indicates a basal activity of MDA5, inducing weak downstream signaling independent of ligand binding (Fig. 3-12A).

This ligand independent IFN β induction by MDA5 was addressed in further dual luciferase assays. Here RIG-I and MDA5 were transfected into HEK 293T cells and compared to the constitutively active forms RIG-I 1-284 (Δ RIG-I), MDA5 1-350 (Δ MDA5), and MDA5 1-449 (all exhibiting a signaling CARD), regarding their intrinsic abilities to induce IFN β without activation by their ligands. Expression of the RIG-I C-terminal domain served as negative control. As expected, full-length RIG-I and RIG-I C-terminus did not induce luciferase levels, while RIG-I 1-284 induced the IFN β promoter 50-fold. However, MDA5, like MDA5 1-350 or MDA5 1-499, induced the IFN β promoter activity 20-fold (Fig. 3-12B).

These data imply that RIG-I activity depends on a conformational change, which ultimately releases previously masked CARDS for downstream interactions, and which can then be targeted by RABV P. Full-length MDA5 on the other hand did not seem to fully depend on activation by a ligand and holds a conformation that allows for basal signaling, also exposing an interface for RABV P binding.

3.1.3.6 Interaction of RABV P with RIG-I or MDA5 does not inhibit their ATPase activity

Although an interaction of RABV P with RLRs is apparent, the functional relevance remains unclear. Previous experiments revealed a strong inhibition of IFN β induction by RABV P after TBK1 was overexpressed (Fig. 3-1), therefore, an inhibition must occur downstream of TBK1. However, it is possible that RIG-I and MDA5 are additional targets of P to reinforce its blockage of the RLR signaling cascade. RIG-I and MDA5 are ATPase helicases and in previous studies it was implied that ATP driven helicase activity plays a role in their activation (Cui et al., 2008). To investigate an effect of RABV P on the ATPase activity of RIG-I and MDA5, thus inhibiting their full activation, ATPase assays were undertaken with respective purified proteins. In

ATPase assays, the ability of RIG-I and MDA5 to hydrolyze radioactively labeled γ - 32 ATP to ADP and γ - 32 Pi was measured.

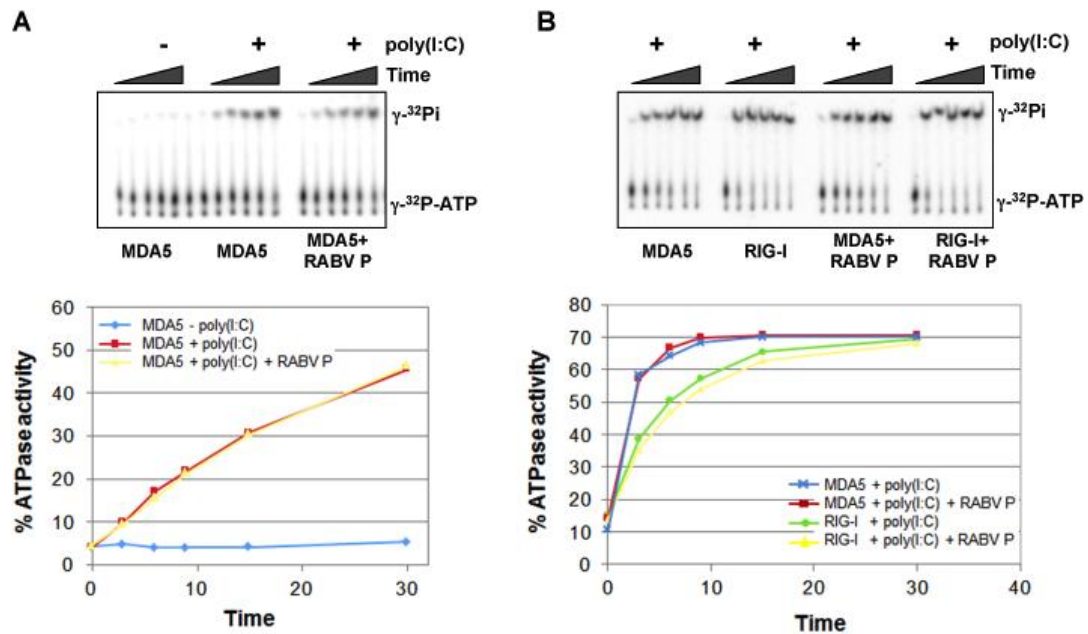


Figure 3-13: RIG-I and MDA5 ATPase activity depends on poly(I:C) stimulation and is not inhibited by RABV P. ATPase activity was measured in an ATPase assay by analyzing the conversion of radioactively labeled γ - 32 ATP to ADP and γ - 32 Pi. By thin layer chromatography γ - 32 ATP and γ - 32 Pi were separated and visualized with a phosphoimager (upper panel). Bands were quantified by Image Quant software and reaction velocities illustrated in a histogram (γ - 32 Pi/time; lower panel). (A) 0.5 μ M purified MDA5 was stimulated with 0.1 μ M poly(I:C) and compared to unstimulated MDA5. Influence of 1 μ M purified RABV P on the activated MDA5 was studied in a third sample. (B) 2 μ M purified MDA5 and RIG-I were stimulated with 0.1 μ M poly(I:C) in the presence or absence of RABV P.

Initially, ATP hydrolysis by 0.5 μ M MDA5 was investigated in the absence or presence of its ligand poly(I:C) (0.1 μ M). As illustrated in Fig. 3-13A, in a time course of 30 min MDA5 does not show any ATPase activity without poly(I:C). However, if poly(I:C) was added a 45-fold increase in conversion of γ - 32 ATP to γ - 32 Pi was obtained. Thus, poly(I:C) is necessary for ATPase activity of MDA5. To test whether RABV P inhibits this activity, 1 μ M purified P protein was added and ATP hydrolysis was measured under the same conditions. It was found that *in vitro* ATPase activity of purified MDA5 was not affected in the presence of purified P. To investigate the effect of RABV P on RIG-I ATPase activity in comparison to MDA5, a further ATPase assay was performed using 2 μ M purified RIG-I and MDA5. The RLRs were stimulated with poly(I:C), an effective ligand of both RLRs (as seen in Fig. 3-12), and ATPase activity was analyzed in the absence or presence of P. RIG-I hydrolyzed ATP to similar level as

MDA5 (10 % less), and the presence of RABV P did again not reduce ATPase activity (Fig. 3-13B). The steeper increase of ATPase activity and the earlier saturation in figure 3-13B compared to figure 3-13A, can be explained by the usage of different enzyme concentrations (RIG-I/MDA5), namely 2 μ M and 0.5 μ M, respectively, while substrate (poly(I:C)) concentration was kept constant.

Taken together, RABV P seems not to interfere with RLR ATPase activity. Our working hypothesis is that P binding prevents conformational changes or associates to domains of RLRs required for association with downstream molecules like IPS-1 and/or eventually with other RLRs.

3.1.4 RABV P interacts with proteins of the RLR signaling cascade: Interaction with (partially) activated IRF3

As mentioned previously, overexpression of TBK1 and IKKi effectively induces IRF3 phosphorylation at S386, dimerization and transcriptional activity. Coexpression of RABV P abrogates this activation (Fig. 3-2 or (Rieder et al., 2011)). This indicates that RABV P not only targets RLRs, but must interfere at the step of IRF3 phosphorylation; possibly by association with the kinases or with IRF3 directly. However, neither in Co-IP experiments nor in conventional mass spectrometry analyses an interaction was detected (K. Brzózka dissertation). However, in this study I provide evidence for a conditional interaction of RABV P with IRF3 and describe a novel activation intermediate form of IRF3.

3.1.4.1 RABV P interacts with IRF3 depending on its activation

In Co-IP experiments, Flag-tagged IRF3, TBK1 or IKKi were coexpressed with RABV P in HEK 293T cells and interaction was investigated using a Flag-matrix 24 h p.t. In non-activated cells IRF3, TBK1 or IKKi did not purify P on the Flag-matrix. Remarkably, however, in cells expressing Δ RIG-I, a stimulator of the IFN induction pathway, a strong interaction of Flag-IRF3 with RABV P, but not with TBK1 or IKKi was apparent, indicating a direct interaction with IRF3 after its activation (Fig. 3-14A). Thus,

although P is known to effectively prevent activation of IRF3, the decisive step that revealed the interaction partner of RABV P was the stimulation of the IFN induction cascade.

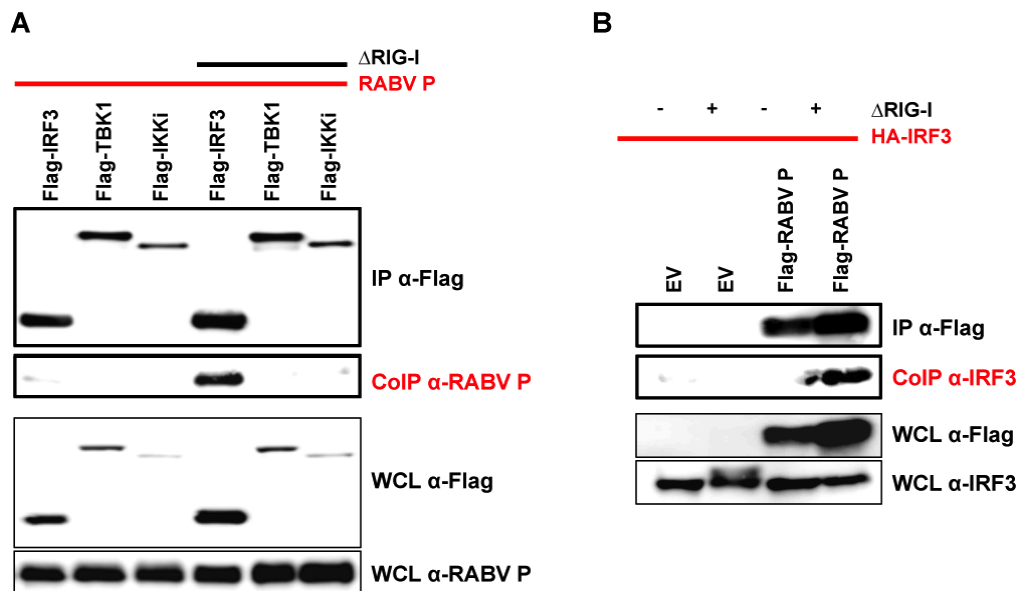


Figure 3-14: RABV P interacts with IRF3 depending on its activation. HEK 293T cells were transfected with 2 μ g of displayed plasmids and Co-IP assays were undertaken. A) Flag-IRF3, Flag-TBK1 and Flag-IKKi were examined for interaction with RABV P (pCR3-RABV P) 24 h p.t., in absence or presence of Δ RIG-I coexpression. (B) Plasmids containing cDNA of Flag-tagged RABV P was coexpressed with HA-IRF3 expression plasmid, in absence or presence of Δ RIG-I coexpression. EV was coexpressed with HA-IRF3 to exclude the possibility of unspecific interactions of HA-IRF3 with the matrix. The Co-IP was carried out as described in Fig. 3-7.

In further Co-IPs, Flag-RABV P was used as the “bait” and the pull down of HA-IRF3 was analyzed 24 h p.t. of respective plasmids into HEK 293T cells. Again, only in cells where Δ RIG-I was coexpressed, an association of HA-IRF3 with RABV P was detected. Interestingly, in the expression control (WCL) an increase of IRF3 molecular weight could be seen after stimulation with Δ RIG-I. However, this shift was not detected in the presence of RABV P. The shift might be due to phosphorylations in the C-terminal domain of IRF3, such as S386, which is inhibited by RABV P (Fig. 3-14B).

The observed P/IRF3 interaction was further investigated by Co-IP experiments in which equal levels of Flag-IRF3 and RABV P were expressed (2 μ g of each), however, with increasing levels of Δ RIG-I (0.1, 0.25, 0.5, 1, 2, 4 μ g) activating cells to different degrees. To exclude unspecific binding of RABV P to the Flag-matrix a control was included where EV was transfected instead of Flag-IRF3. To furthermore exclude an

indirect association of Δ RIG-I (non-tagged) with the Flag-matrix (and a P pull down via Δ RIG-I) the control was in addition transfected with 4 μ g Δ RIG-I.

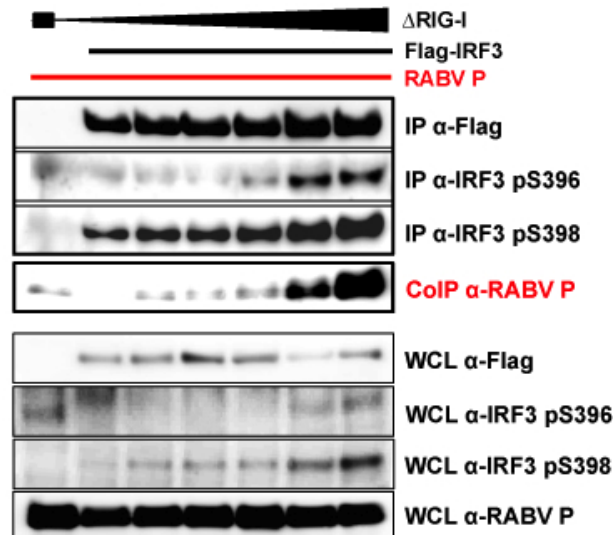


Figure 3-15: RABV P/IRF3 interaction correlates with the degree of IRF3 activation. HEK 293T cells were transfected with 3 μ g of Flag-IRF3 and RABV P expression plasmids. Increasing amounts of Δ RIG-I was coexpressed (0.1, 0.25, 0.5, 1, 2, 4 μ g). 2 μ g EV was coexpressed with 2 μ g RABV P and 4 μ g Δ RIG-I to exclude the possibility of unspecific interactions of Δ RIG-I or P with the matrix. The Co-IP was carried out 24 h p.t. as described in Fig. 3-7.

Using phosphospecific antibodies against phosphorylated serines 396 and 398, it was shown that these phosphorylations accumulated with increasing amounts of Δ RIG-I, while levels of IRF3 were constant (Fig. 3-15). Therefore, although RABV P inhibits phosphorylation at S386, phosphorylations at S396 and S398 are apparently not affected. Strikingly, the amount of RABV P that associated to IRF3 increased drastically with an increased amount of transfected Δ RIG-I, showing a peak in cells stimulated with 4 μ g Δ RIG-I.

These experiments clearly show an interaction of RABV P and IRF3 that depends on activation of the RLR signaling cascade in the transfected cells. As no interaction was apparent in case of TBK1 or IKKi, an indirect association of RABV P with the signaling complex via Δ RIG-I is unlikely. It further seems that P/IRF3 interaction increases according to increased IRF3 activation and that P does not interfere with S396 and S398 phosphorylation.

3.1.4.2 RABV P/IRF3 interaction inhibits phosphorylation of IRF3 at serine 386 while allowing phosphorylation at serines 396 and 398

To address the highly discussed question of how phosphorylation and therefore activation of IRF3 actually takes place, expression profiles of phosphorylated IRF3 forms over time were generated using commercially available antibodies against phosphorylated S386, S396 and S398. HEK 293T cells were transfected with equal amounts of Flag-IRF3 and 6 h p.t infected with SeV DI-H4, a potent activator of RIG-I-dependent IFN β induction. Cells were harvested at different time points (0, 4, 6, 8, 10, 12, 24 h p.i.) and expression levels were analyzed by Western blot and subsequent staining with the above mentioned phosphospecific antibodies. Phosphorylation of IRF3 S386 (site 1), which serves as an indicator for activation, emerged after 8 h, peaked at 10-12 h and vanished 24 h after SeV DI-H4 stimulation. However, phosphorylation at serines 396 and 398 (site 2) appeared to occur at earlier time points, peaking already 8-10 h p.i.

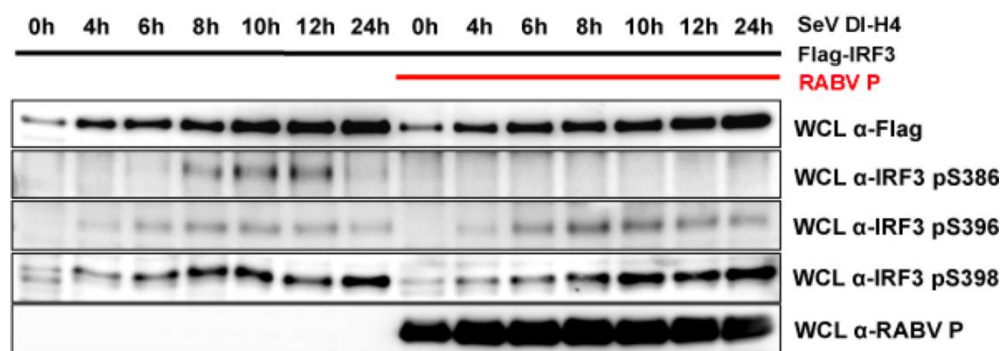


Figure 3-16: IRF3 phosphorylation of serine 398 and 396 occurs prior to serine 386 phosphorylation. Only serine 386 phosphorylation is inhibited by RABV P. HEK 293T cells were transfected with 3 μ g Flag-IRF3 in absence or presence of RABV P, and stimulated with SeV DI-H4. Lysates were prepared 0, 4, 6, 8, 10, 12, and 24 h after infection and subjected to SDS-PAGE and Western blot. Phosphorylation of S386, S396 and S398 was detected using phosphospecific antibodies.

The influence of RABV P on IRF3 phosphorylation was investigated by coexpressing RABV P under the same experimental set-up. Inhibition of S386 phosphorylation by P was evident at all time points whilst phosphorylation at S396 and S398 appeared to be unaffected (Fig. 3-16).

To identify if the IRF3 phosphorylation profile at distinct time points somehow affects the interaction between IRF3 and P, the lysates generated for figure 3-16, were used in a Co-IP experiment. Thus, Flag-IRF3, stimulated for different periods of time and either coexpressed with RABV P or EV, was precipitated by the Flag-matrix, leading to a high protein yield. The precipitate was stained with phosphospecific antibodies, and the efficiency to pull-down P was investigated. When no P is present, phosphorylation at S386, S396 and S398 was nicely detectable, fortifying results from the expression control of figure 3-16. In P-expressing cells phospho-S386 was not detectable at any time point, however, phospho-S396 and -S398 bands were visible. Association of P and IRF3 clearly accumulated over time although P expression levels were constant throughout the time course (WCL). This indicates a correlation between the IRF3 activation kinetics and P binding.

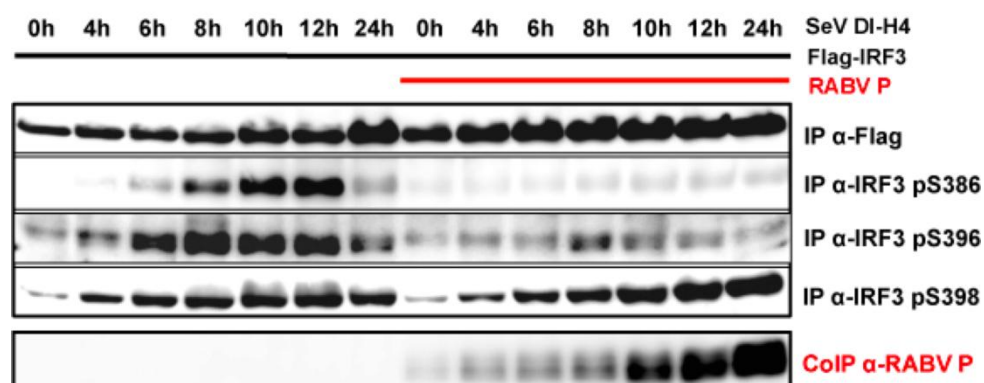


Figure 3-17: RABV P interaction with IRF3 increases according to time of activation. Serine 386 phosphorylation is inhibited by IRF3/P interaction. HEK 293T cells were transfected with 3 µg Flag-IRF3 in absence or presence of RABV P, and stimulated with SeV DI-H4 for 24 h. Lysates were prepared at 0, 4, 6, 8, 10, 12, and Co-IP carried out as described in Fig. 3-7. Phosphorylation of S386, 396 and 398 were detected using phosphospecific antibodies.

In conclusion, RABV P binds IRF3 in an activation-dependent manner, leading to inhibition of S386 whilst leaving S396 and S398 phosphorylations predominantly unaffected. These findings corroborate the proposed model of a two-step, phosphorylation dependent IRF3 activation. Hereby, initially site 2 residues are phosphorylated, leading to conformational changes allowing for site 1 phosphorylation in the absence of P, but inhibition of site 1 phosphorylation in the presence of P.

3.1.4.3 Site directed mutagenesis of IRF3 serines 396/398 to alanine reduces interaction with RABV P

Regarding the previous findings, it seems that the interaction of P/IRF3 is proportional to site 2 phosphorylations, specifically at S398. The possibility arose that RABV P might interact with IRF3 at specific site 2 phosphate moieties or that these phosphorylations induce an IRF3 conformation that allows for P binding. Therefore, mutants were generated where combinations of individual site 2 serines or threonines (S396, S398, S402, T404, S405) were exchanged to non-phosphorylatable alanine (S/T→A). In a Co-IP assay, Flag-tagged mutants called IRF3 2A (S396, S398→A), IRF3 3A (S402, T404, S405→A), or IRF3 5A (all site 2 residues→A), were analyzed for interaction with RABV P in the absence or presence of SeV DI-H4 infection. The interaction of wt IRF3 and IRF3 3A with RABV P was increased upon infection, however, IRF3 2A and IRF3 5A, both harboring mutations of serines 396/398 to alanine, showed a decrease in IRF3/P interaction after stimulation with SeV DI-H4 (Fig. 3-18).

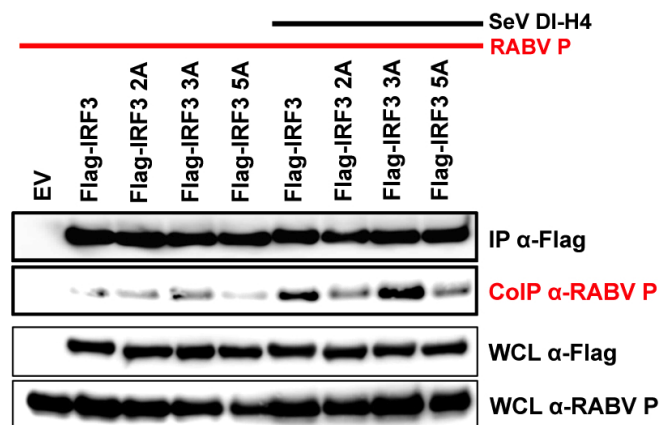


Figure 3-18: Mutation of serines 396/398 to alanine reduces RABV P binding after SeV DI-H4 infection. HEK 293T cells were transfected with 3 μ g Flag-IRF3, Flag-IRF3 IRF3 2A (S396A, S398A), IRF3 3A (S402A, T404A, S405A), and IRF3 5A (S396A, S398A, S402A, T404A, S405A) and 3 μ g RABV P. 6 h p.t. cells were infected with SeV DI-H4 for 24 h and compared to unstimulated cells. Lysates were prepared and Co-IP carried out as described in Fig. 3-7.

This indicates that phosphate moieties known to be a prerequisite for IRF3 activation are either targeted by RABV P directly or that phosphorylation of S396/S398 induces a specific conformation facilitating P binding.

Additionally, mutants of IRF3 were generated in which site 2 residues were replaced by a phosphomimetic aspartic acid, such as IRF3 5D (all site 2 phosphosites \rightarrow D). IRF3 5D was characterized to be constitutively active to induce IFN β transcription without stimulation of the cells (Lin et al., 1999). Actually, already overexpression of IRF3 S396D was previously identified to be sufficient to induce IFN β (Servant et al., 2003). It is believed that the charges introduced by these mutations relieve auto-inhibitory structures and thus allows access for kinases that phosphorylate S385/S386. In Co-IP experiments IRF3 5D was analyzed for RABV P binding in non-activated cells and in cells stimulated with SeV DI-H4. As in previous experiments, IRF3/P interaction could only be observed in stimulated cells. Strikingly, P showed only residual binding to “constitutively active” IRF3 5D, which is assumed to hold a confirmation that enables S386 phosphorylation without stimulation. Interestingly, in stimulated cells IRF3 5D co-precipitated P much stronger, and stimulation even further increased S386 phosphorylation. Furthermore, RABV P does not seem to effectively inhibit S386 phosphorylation in case of IRF3 5D as opposed to wt IRF3 (Fig. 3-19A).

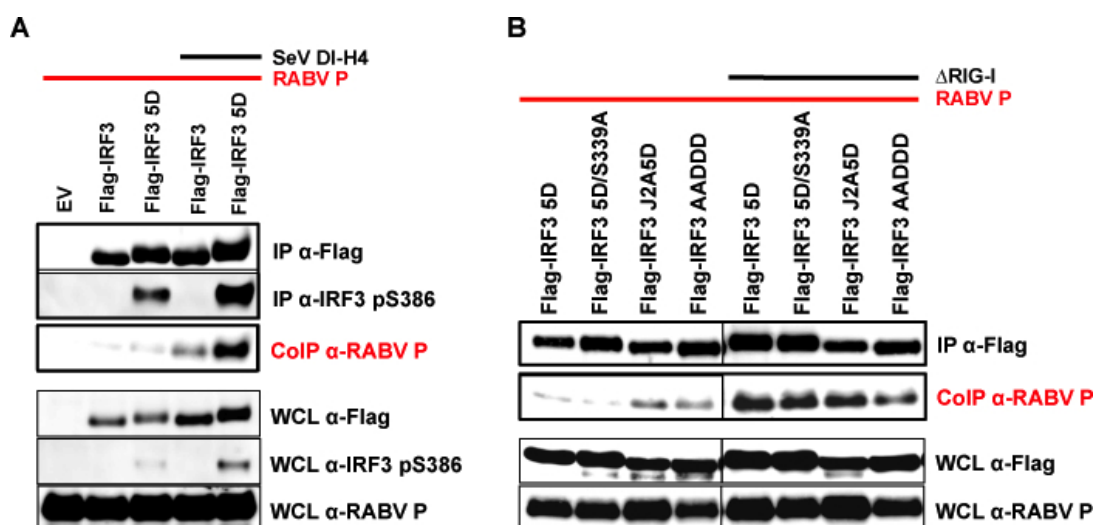


Figure 3-19: Interaction of RABV P with phosphomimetic, constitutively active IRF3 is potentiated by SeV DI-H4 and Δ RIG-I stimulation. HEK 293T cells were transfected with 3 μ g Flag-IRF3 or Flag-IRF3 constructs and coexpressed with 3 μ g RABV P. Transfected cells were stimulated with SeV DI-H4 or Δ RIG-I for 24 h subjected to Co-IP and compared to unstimulated cells. (A) IRF3 and IRF3 5D (S396D, S398D, S402D, T404D, S405D) were analyzed for interaction with RABVP. (B) IRF3 5D, IRF3 5D/S339A, IRF3 J2A5D and IRF3 AADDD (S396A, S398A, S402D, T404D, S405D) mutants were analyzed for interaction with RABV P. Lysates were prepared and Co-IP carried out as described in Fig. 3-7.

This indicates that IRF3 5D holds a stable conformation that allows for S386 phosphorylation, which cannot be effectively inhibited by RABV P despite a strong

interaction. The fact that S386 phosphorylation but also P interaction is further induced by stimulation, implies that P does not directly bind to site 2 phosphate moieties and that S386 phosphorylation must be induced by further, so far unknown modifications beside site 2 phosphorylation, which also favor P binding.

As IRF3 S396/S398 seem to have a certain role in IRF3 activation and P binding, a mutant called IRF3 AADDD was included harboring S396/S398→A and S402/T404/S405→D mutations. Furthermore, IRF3 5D mutants that additionally lack S339 and S385/S386 phosphosites were included in the study. RABV P showed only residual binding to all of these mutants, however, efficient binding occurred upon activation by ΔRIG-I. Only the mutant IRF3 AADDD displayed a weak reduction in P interaction which again implies a role of S396/S398 for P binding. However, phosphorylation of S339 and S385/S386 seem to be dispensable for P binding. The results also indicate an involvement of other residues, and/or additional activation mechanisms of IRF3 that lead to conformational changes that allow for P binding.

3.1.4.4 RABV P/IRF3 interaction involves helices H3/H4 of the IRF association domain

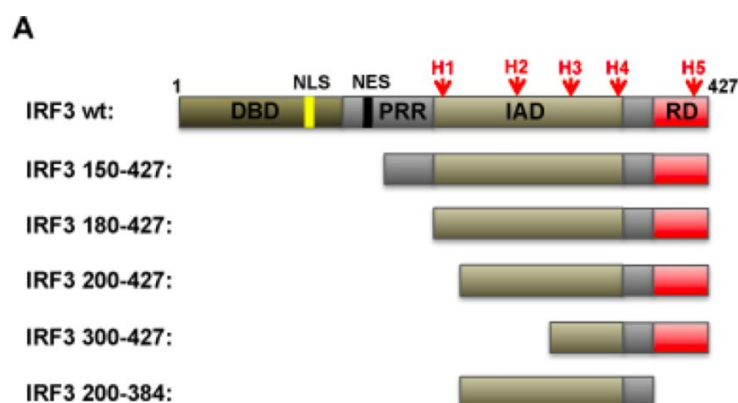
As IRF3/P binding is induced by S396/S398 phosphorylation, which probably supports activation of IRF3 by releasing inhibitory structures, the interaction was further characterized by generating Flag-tagged deletion constructs lacking specific domains (such as H1 and/or H5) to investigate their ability to co-precipitate RABV P on a Flag-matrix (Fig. 3-20A). Due to our previous findings, we support a sequential phosphorylation but also suggest that further phosphorylations or regulatory mechanisms are involved.

To characterize the IRF3/P interface, interaction of the distinct IRF3 constructs with P was analyzed with or without SeV DI-H4 infection. As could be expected for full-length IRF3 and IRF3 180-427, comprising all helices of the IAD and RD, interaction was only induced by SeV DI-H4 infection. However, the shorter constructs lacking auto-inhibitory structures H1 (IRF3 200-427), H1 and H2 (IRF3 300-427), or H1 and H5 (IRF3 200-384), already displayed increased interaction with P in uninfected cells.

Interestingly, although H1 and H5 were lacking, these interactions increased even further in activated cells. The constructs comprising the H1 helix (IRF3 and IRF3 185-427), showed a reduced interaction compared to mutants lacking H1, supporting an inhibitory function of H1. Additional deletion of H2 in IRF3 300-427, even further increased the efficiency of IRF3 to pull-down RABV P, although expression of this mutant was very low (Fig. 3-20B), suggesting a further inhibitory role of H2.

Interestingly, deletion of the H5 helix in the mutant IRF3 200-384 did not substantially decrease strength of interaction with P, which supports the finding that H5 is not directly involved in P binding. Furthermore, besides phosphosite S339 that is also involved in IRF3 activation, this mutant lacks the C-terminal site 1 and 2 residues, as well as the constitutively phosphorylated S173/S175. As IRF3 200-384/P interaction is also induced after activation only a partial contribution of these residues to the conformational rearrangements favoring P binding is probable. Eventually, intramolecular displacements must occur that allow for an interaction with P even upon removal of inhibitory regions, potentiated by stimulation of the cells due to so far unknown activation mechanisms around H3 and H4.

Taken together, these data indicate that IRF3 helices H3 and H4, which are also involved in IRF3 dimerization and CBP interaction, are required for P binding. Access of P to these helices is obtained upon removal of H1/H2 and H5 and increased by activation. Therefore, a very specific IRF3 activation intermediate that seems not to solely rely on phosphorylation of C-terminal residues but on further modifications favors P binding.



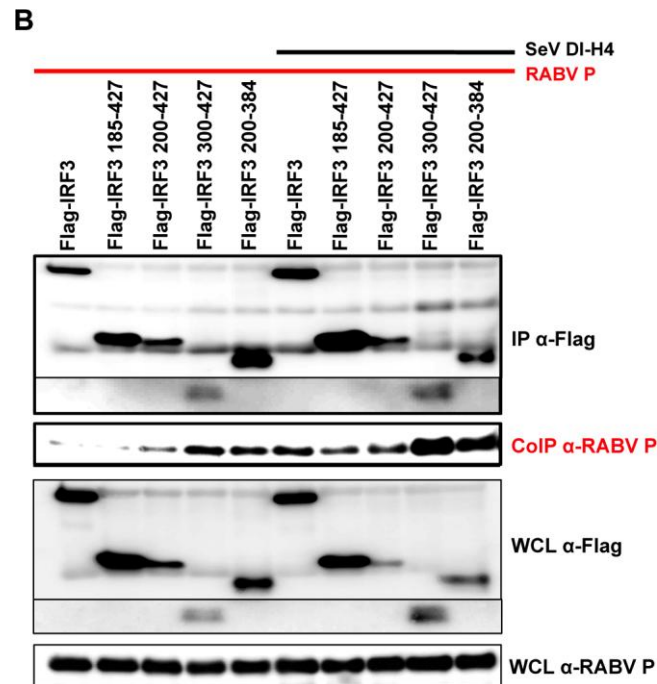


Figure 3-20: RABV P/IRF3 interaction is induced by the lack of IRF3 IAD H1/H2 and H5 helices. (A) Schematic overview of IRF3 constructs. IRF3 wt is composed of a DNA-binding domain (DBD), a proline rich domain (PRR), an IRF association domain (IAD) and a regulatory domain (RD). The nuclear localization signal (NLS; yellow stripe), nuclear export signal (NES; black stripe), and auto-inhibitory helices H1 and H5 are assigned (red arrows). (B) HEK 293T cells were transfected with 3 μ g of assigned Flag-IRF3 constructs and coexpressed with 3 μ g RABV P. Transfected cells were infected with SeV DI-H4 and compared to unstimulated cells. Lysates were prepared and Co-IP carried out as described in Fig. 3-7.

3.1.4.5 RABV P Δ Ind mutants unable to inhibit serine 386 phosphorylation can still interact with IRF3

In the first part of this thesis, mutants of RABV P were presented that have lost the ability to interfere with activation of IRF3, namely RABV P Δ Ind1, P Δ Ind2 and P Δ Ind1/2 (see Fig. 3-1). These mutants lost the ability to inhibit IRF3 S386 phosphorylation, dimerization and transcriptional activity. To investigate whether this loss of inhibition results from a loss of IRF3/P interaction, further Co-IP assays were carried out.

Flag-IRF3 was coexpressed with full-length P and P Δ Ind1, and the interaction was compared in cells stimulated with SeV DI-H4 and unstimulated cells. To elaborate effects on S386, S396, and S398 phosphorylation, phosphospecific antibodies were used. As displayed in figure 3-21, in unstimulated cells Flag-IRF3 did not co-precipitate RABV P. However, upon stimulation a strong pull-down of RABV P was

detected. Strikingly, interaction with IRF3 was also observed for P Δ Ind1 which was pulled down by Flag-IRF3 as efficiently as wt P. However, in spite of IRF3 binding, P Δ Ind1 has lost its ability to inhibit phosphorylation of S386, as observed in previous experiments. As expected, phosphorylation of S396/S398 remained unaffected (Fig. 3-21).

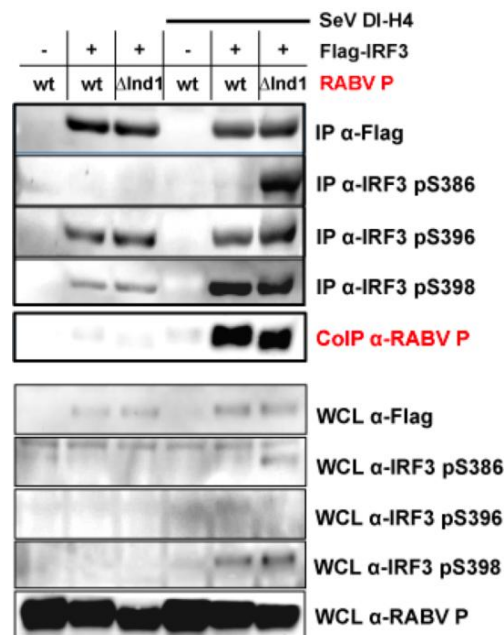


Figure 3-21: RABV P lacking aa 176-181 is incapable of inhibiting IRF3 phosphorylation and dimerization but can still interact with IRF3. HEK 293T cells were transfected with 3 μ g of Flag-IRF3 and 3 μ g RABV P or RABV P Δ Ind1. To exclude unspecific binding of P to the matrix, RABV P was also coexpressed with EV. Transfected cells were stimulated with SeV DI-H4 and compared to unstimulated cells. Lysates were prepared and Co-IP carried out as described in Fig. 3-7. Phosphorylation of S386, S396 and S398 were detected using phosphospecific antibodies.

Furthermore, mutants P Δ Ind2 and P Δ Ind1/2 were analyzed for their ability to interact with IRF3 as well as for their properties in inhibiting IRF3 S386 phosphorylation, in comparison to P Δ Ind1 and full-length P. Interactions of P Δ Ind2 and P Δ Ind1/2 with IRF3 in stimulated cells were as strong as in case of wt P and P Δ Ind1. No interaction occurred in unstimulated cells. Phosphorylation of S386 upon activation by SeV DI-H4 infection was inhibited only by wt RABV P. As previously described, P Δ Ind2 and P Δ Ind1/2 largely lost the ability to inhibit S386 phosphorylation, like P Δ Ind1, and almost to levels observed without P expression (Fig. 3-22).

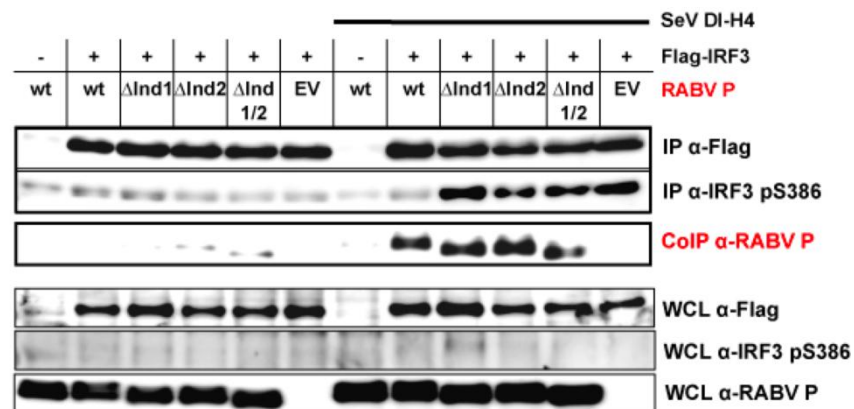


Figure 3-22: RABV P Δ Ind1, P Δ Ind2, and P Δ Ind1/2 mutants can interact with IRF3. HEK 293T cells were transfected with 3 μ g of Flag-IRF3 and 3 μ g RABV P, RABV P Δ Ind1, RABV P Δ Ind2, or RABV P Δ Ind1/2. To exclude unspecific binding of P to the matrix, RABV P was also coexpressed with EV. Transfected cells were stimulated with SeV DI-H4 and compared to unstimulated cells. Lysates were prepared and Co-IP carried out as described in Fig. 3-7. Phosphorylation of IRF3 S386 in absence or presence of P, or P Δ Ind mutants, was detected using phosphospecific antibodies.

Therefore, all of the P Δ Ind mutants can still interact with IRF3 yet fail to inhibit S386 phosphorylation and transcriptional activity. This finding also supports the previous notion that deletion of aa 176-186 changes structural conformations in P, leading to a loss of function regarding IFN β induction.

4 Discussion

The details of the interplay of viruses and the host innate immune system are just being discovered. In the past years the importance of viral counteractions against the host type I IFN system in order to establish an infection became evident. The RABV phosphoprotein P has been shown to be a potent antagonist of the innate immune system by inhibiting both arms of the IFN response. RABV P inhibits IFN induction and IFN signaling, by preventing activation of IRF3/7 transcription factors and import of activated STAT1/2 transcription factors, respectively (Brzózka et al., 2006, 2005). This dual mode of inhibition effectively limits expression of IFN, immune stimulatory and antiviral genes and hereby helps RABV to pursue various strategies, such as unhindered growth and maintenance of neuronal circuits for efficient virus spread to the CNS.

As shown previously by Brzózka *et al.*, STAT binding is accomplished by the 10 C-terminal aa of P. However, the mechanisms involved in the inhibition of IFN induction still have to be elaborated. In this study, mutants of RABV P lacking aa 176-186, which lost the ability to inhibit type I IFN induction while leaving inhibition of STAT signaling or other crucial functions of P intact, were characterized *in vitro* and *in vivo*, revealing a critical contribution to pathogenicity (Rieder et al., 2011). In a second part, cellular interaction partners of RABV P could be identified that play major roles in the RLR signaling cascade, namely the receptors RIG-I, MDA5, and Lgp2, and the transcription factor IRF3, thus providing the mechanistic background for the inhibitory effect of P on IFN induction. As RABV P can interact with MDA5 and Lgp2 in their “non-activated” state but RIG-I requires ligand-induced activation to be bound by P, the findings suggest distinct latent conformational states and activation mechanisms of the individual RLRs. Furthermore, RABV P binds an activation intermediate of IRF3, thereby inhibiting IRF3 serine 386 phosphorylation, which is required for full transcriptional activity. This interaction can be used as tool to identify the sequence of events leading to transcriptional activation of IRF3.

4.1 Inhibition of type I IFN induction by RABV P depends on amino acids 176-186

In previous studies, the properties of RABV P were analyzed by generating a mutant virus, named SAD Δ PLP, in which the P gene is shifted to the most promoter distal position (N-M-G-L-P), exhibiting an attenuated P expression due to a possible dissociation of the viral polymerase. It was shown that the marginal P levels are sufficient to fulfill essential functions in viral RNA synthesis, as SAD Δ PLP was only slightly attenuated in IFN incompetent BSR cell lines, with only a 10-fold reduction of maximum virus titer compared to wt RABV (SAD L16). However, in IFN-competent HEp-2 cells it completely failed to replicate, indicating a role of P in counteracting the IFN system. The specific antagonistic role of P on the IFN induction pathway became evident when SAD Δ PLP infected cells induced transcription of IFN β mRNA, whereas in SAD L16 infected cells IFN β transcription was hardly detectable. Furthermore, SAD Δ PLP infection resulted in activation of IRF3, as demonstrated by S386 phosphorylation and IRF3 dimerization, as opposed to SAD L16 where this activation was blocked. Ectopic expression of P from plasmid inhibited transcriptional activation of IRF3, induced by different stimuli (Brzózka et al., 2005).

By direct mutagenesis and transfection experiments, an essential domain of RABV P required for this interference could be identified. As shown in dual luciferase assays and qRT-PCR experiments, the deletion of aa 176-186 in the RABV P gene diminished the inhibitory properties of P regarding IFN induction. Upon transfection of the plasmids RABV P Δ 176-181 (P Δ Ind1), P Δ 182-186 (P Δ Ind2), and P Δ 176-186 (P Δ Ind1/2) into HEK 293T cells and overexpression of distinct stimuli (Δ RIG-I, Δ MDA5, TBK1), the IFN β promoter activation and IFN β mRNA transcription were not inhibited, as opposed to full-length RABV P that strongly inhibited IFN β induction (Fig. 3-1). Furthermore, in native gel analyzes the ability of RABV P and the loss of the P Δ Ind mutants to inhibit IRF3 phosphorylation at S386 and IRF3 dimerization after stimulation by TBK1 or IKKi was revealed (Fig. 3-2). Noteworthy is the observation that the deletion of RABV P aa 176-181 or aa 182-186 resulted in similarly strong defects with respect to IRF3 inhibition, while the combined deletion of the entire

domain aa 176-186 appeared to have a less pronounced defect. It can be therefore hypothesized that the deletions rather affect a specific protein folding required for interference with IRF3 activation than being directly involved in binding targets of the signaling complex. The identified domain is positioned in a part of the protein predicted to be structurally disordered (Gerard et al., 2009). Moreover it is directly adjacent to a region (aa 61-175) nonessential for basic transcription of RABV minigenomes (Jacob et al., 2001).

As indicated by minigenome experiments, the deletions in RABV P Δ 176-181, P Δ 182-186 and P Δ 176-186 did not critically affect crucial functions in transcription and replication (Fig. 3-3). Corresponding recombinant viruses SAD Δ Ind1, SAD Δ Ind2, SAD Δ Ind1/2 were generated and analyzed for growth kinetics and the ability to interfere with IFN β promoter activity and IFN β transcription. As expected from the transfection experiments, the SAD Δ Ind viruses also showed a reduced ability to prevent IFN β induction as shown in dual luciferase assays and qRT-PCR (Fig. 3-5). This data was corroborated by immunofluorescence and native gel analyses of SAD Δ Ind infected IFN-competent cells, where IRF3 nuclear localization, and S386 phosphorylation and dimerization could be detected. Interestingly, all SAD Δ Ind viruses showed a clear growth advantage over the SAD Δ PLP, with infectious titers comparable to the parental SAD L16 in IFN-competent (HEp-2) and IFN-incompetent (BSR-T7/5) cells (Fig. 3-4A). This unhindered growth in IFN-competent cells can be explained by the strong capability of the SAD Δ Ind viruses to interfere with IFN-mediated ISG induction, as confirmed in reporter gene assays and Western blot analysis. Infection of HEp-2 cells with SAD Δ Ind viruses also led to an accumulation of activated STAT, reflecting a retention of STATs in the cytoplasm and hindered STAT recycling (Rieder et al., 2011). This indicates that SAD Δ PLP suffers from induction of greater levels of IFN and ISGs in the initially infected cells, thus a more rapid establishment of an antiviral state, while the SAD Δ Ind viruses, though inducing IFN, can limit this antiviral environment by keeping ISGs low.

In conclusion, the SAD Δ Ind viruses lost the full capacity to inhibit IRF3 activation and IFN induction but are otherwise equipped with the full capacity of IFN resistance and virus propagation.

4.2 Inhibition of IRF3 activation is important for pathogenicity

Interestingly, the recombinant SAD Δ Ind1 and SAD Δ Ind1/2 viruses induced IFN β to significantly higher quantities than SAD Δ Ind2 (Fig. 3-5A/B). To further characterize the viruses, Northern blot experiments were carried out, which revealed that SAD Δ Ind1 and SAD Δ Ind1/2 mutants produce more mRNAs per genome (Fig. 3-6). It is speculated that this could lead to a stronger stimulation of the RIG-I pathway by RABV 5'-pppRNAs and therefore an increased IFN induction. The origin of this distinct phenotype is unclear, yet a correlation with the reduced expression levels of the SAD Δ Ind1 and SAD Δ Ind1/2 M protein seems possible (Fig. 3-4B). The RABV M protein has been shown to regulate the balance of transcription and replication (Finke et al., 2003) and the P protein has been shown to interact with M (A. Kern unpublished). The involvement of an increased transcription level in increased IFN induction would indicate a dominant role of subgenomic RNAs in RLR activation, arguing against a previous finding that genome RNA (here of SeV) is the major RIG-I inducer (Rehwinkel et al., 2010). However, whether the M protein is responsible for distinct transcription levels has to be elucidated further.

In vivo mouse experiments (performed by L. Stitz, FLI Tübingen) revealed the importance of blocking IRF3 activation and IFN induction for RABV pathogenicity (see (Rieder et al., 2011)). SAD Δ PLP injection into wt mice did not cause symptoms, disease, or death, while wt SAD L16 led to death of the mice within a few days. IFNAR $^{-/-}$ mice all succumbed to infection 5 days p.i., yet in case of SAD Δ PLP with one day delay. The SAD Δ Ind2 mutant caused the typical rabies symptoms in wt and IFNAR $^{-/-}$ mice, but in both cases the course of disease was delayed by several days compared to that of SAD L16, approving a protective role of IRF3 activation and IFN induction. Strikingly, a high dose of SAD Δ Ind1 virus did not cause symptoms in wt mice revealing a severely attenuated phenotype of this virus. Like in SAD Δ PLP infection, however, IFNAR $^{-/-}$ mice infected with SAD Δ Ind1 died with one day delay compared to SAD L16 and SAD Δ Ind2.

Taken these results together, SAD Δ Ind recombinant viruses showed growth kinetics comparable to SAD L16, yet SAD Δ Ind1 remained completely apathogenic even after

i.c. injection into mouse brains. Here it seems that activation of IRF3 and induction of IFN by SAD Δ Ind1 is sufficient to activate the host defense system to a protective level. This also indicates that neurovirulence of IFN resistant RABV correlates with the ability to prevent induction of IFN.

4.3 RABV P interacts with RIG-I-like helicases depending on their conformational state

To clarify the mechanisms utilized by RABV P to inhibit IRF3 activation, potential target proteins of RABV P, which function upstream of IRF3 activation in the IFN α / β induction pathway, were screened for interaction with P. Therefore, plasmids of RABV P and potential interaction partners were coexpressed in HEK 293T cells and Co-IP experiments were undertaken. Reproducible interaction of RABV P with various members of the RLR signal cascade such as TANK, SINTBAD, NAP1, and TBK1, in resting cells could not be revealed. However, when RABV P was coexpressed with the RLRs, a co-precipitation of RABV P with MDA5 and to a lesser extent Lgp2, but not RIG-I, was apparent (Fig. 3-7). Interestingly, in the presence of an adequate RIG-I ligand, a substantial interaction of P with RIG-I was detected as well (Fig. 3-11A).

Biochemical and structural analyses have revealed that the C-terminal RD of RIG-I specifically binds 5'-pppRNAs (Cui et al., 2008), whereas the RDs of MDA5 or Lgp2 can accommodate blunt dsRNA ends (Li et al., 2009; Pippig et al., 2009). These studies suggested a model according to which inactive RIG-I is present in a closed conformation where CARDs are masked, but upon 5'-pppRNA binding to the RD and dsRNA binding to the HD, a conformational change occurs allowing the CARDs to interact with the downstream adapter IPS-1. It is probable that in the absence of an adequate ligand, not only RIG-I CARDs are masked but also the domains recognized by RABV P. For MDA5 a similar activation mechanism is probable, however, a distinct conformation is suggested that allows for basal signaling in the inactive state, maybe also exposing domains recognized by P (Bamming and Horvath, 2009). We suggest that RABV P can only interact with the activated open conformation state of RIG-I but

also with the non-stimulated MDA5.

In correlation with this hypothesis, dual luciferase assays revealed differences of RIG-I and MDA5 concerning their intrinsic signaling properties in the absence or presence of specific ligands. In accordance with previous studies, both MDA5 and RIG-I respond to poly(I:C), however, MeLe RNA only activates RIG-I to induce IFN β (Fig. 3-12A). Interestingly, in the absence of a ligand, the transfection of full-length MDA5 and constitutively active MDA5 CARDS induced the IFN β promoter to a similar extend, whereas full-length RIG-I did not induce IFN without a ligand (Fig. 3-12B). The non-ligand dependent IFN induction and the non-ligand dependent P binding of MDA5 observed in this study and findings by others, which also observed elevated IFN β promoter-coupled luciferase activities after ectopic expression of MDA5 (Bamming and Horvath, 2009), suggest that the non-activated structure of MDA5 is different from that of RIG-I.

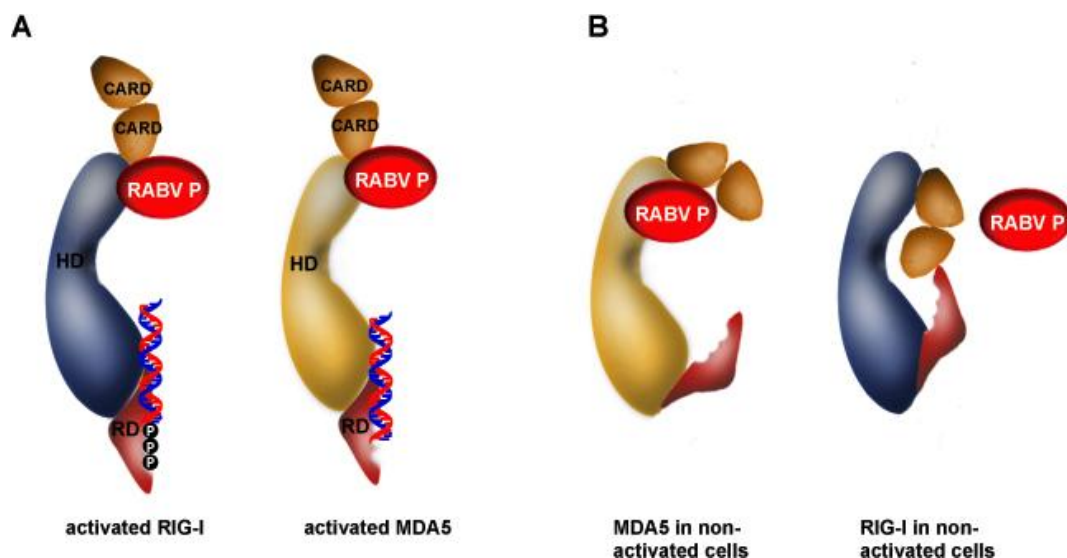


Figure 4-1: Models of RIG-I and MDA5 conformation in their activated and non-activated states and RABV P binding. (A) Illustration of RIG and MDA5 in their activated state upon binding to their ligands 5'-pppRNA (or poly(I:C)) and poly(I:C), respectively. The receptors hold an open conformation with the RD bound to the ligand and the CARDs exposed so that RABV P could associate. (B) Conformation of RIG-I and MDA5 in non-activated cells. It is suggested that RIG-I holds a closed conformation with the CARDs masked by the RD or HD (Cui et al., 2008). MDA5 is tentatively present in a leaky, not completely closed conformation that allows for basal signaling and P binding (Bamming and Horvath, 2009).

The finding that P interacts with MDA5 was surprising as rhabdoviruses are thought to predominantly activate RIG-I and not MDA5. As already described, RABV produces a 5'-pppRNA during its life cycle which is known to be the main ligand for RIG-I.

MDA5, however, was shown to predominantly recognize a picornavirus (EMCV) and the dsRNA analogue poly(I:C), which is also recognized by RIG-I. However, the RABV P/MDA5 interaction might resemble the situation found in paramyxoviruses, which are also recognized mainly by RIG-I but whose V proteins bind MDA5, thus inhibiting RLR signaling (Andrejeva et al., 2004; Ikegame et al., 2010). As the exact mechanism of RLR activation, such as the physiological ligand for MDA5, and an eventual co-operation or interaction of RIG-I and MDA5 is still highly discussed, the RLR/P interaction can be beneficial in elucidating these questions.

To further characterize this interaction, MDA5 constructs composed of distinct (functional) domains were generated and analyzed for interaction with RABV P (Fig. 3-8B). The constructs Flag-MDA5 1-350 and Flag-MDA5 1-449, which contain the CARDS and the HD motif I or the HD motif I/II, respectively, were able to interact with RABV P, whilst the constructs lacking the CARD domain did not pull down RABV P. This initially indicated that for the interaction with RABV P the MDA5 CARD domains are essential. However, a MDA5 construct only composed of aa 288-449, displaying the N-terminal part of the CARDS and HD motifs I/II, was also able to interact with RABV P. As the Flag-MDA5 HD construct did not associate with RABV P, the aa that seem to be decisive for interaction are 288-327, thus, the region of the CARD/HD junction.

Furthermore, Co-IP experiments that analyzed the P/Lgp2 interaction showed that the RD of Lgp2 is dispensable for interaction whilst the HD is required (Fig. 3-8C). This finding also reveals parallels to the paramyxovirus V protein that not only interacts with MDA5 but also with Lgp2 via its HD (Parisien et al., 2009). The V proteins of distinct paramyxoviruses, such as MeV, mumps virus, Hendra virus, Nipah virus, and human parainfluenza virus type 2, target a 130-residue region in the MDA5 HD, which is highly homologous between MDA5 and Lgp2 (Parisien et al., 2009). Also the N-terminal part of the MDA5 HD, shown to be essential for MDA5/P interaction, shows a high homology to Lgp2. However, an indirect interaction of P to Lgp2 cannot be excluded, as Lgp2 itself might bind to MDA5. It also has to be mentioned that a direct MDA5/P interaction has not been proven so far. Thus, a further protein might be interjacent and the interaction indirect.

By the generation of RABV P deletion constructs, regions of P could be revealed that seem crucial for binding to MDA5 (Fig. 3-9, 3-10). Taken the results of diverse Co-IPs together, RABV P mutants that lack the P_{NTD} or the aa 217-245 of the P_{CTD}, exhibited a reduced ability to interact with Flag-MDA5 and Flag-MDA5 288-449. An N-terminal Ig-tag on P also strongly attenuated the interaction, corroborating the importance of the RABV P N-terminus. It is possible that the two RABV P domains identified are brought into close proximity only in the tertiary structure and form an interface for MDA5 binding. As no complete 3D structure of P could be resolved so far, this possibility can only be speculated.

As shown in preceding experiments, the RABV P mutants lacking aa 176-186 lost the ability to interfere with IRF3 activation. Therefore, it was of interest if this specific deletion interferes with MDA5/P interaction. In a Co-IP experiment, MDA5 was coexpressed with RABV P Δ Ind1 and the interaction compared to RABV P wt. Furthermore, the effect of the MDA5 ligand poly(I:C) on the strength of interaction was analyzed. Neither did RABV P Δ Ind1 show a decreased binding to MDA5, nor did poly(I:C) increase the interaction. Therefore, the aa 176-181 are not required for MDA5/P interaction. In addition, it can be concluded that the unstimulated and stimulated conformation of MDA5 interacts with RABV P to comparable levels, most probably by exposing the P interaction interface to similar degrees (Fig. 3-10).

As already mentioned, an interaction of RIG-I with RABV P was only observed in cells infected with SeV DI-H4. This indicates that RIG-I undergoes conformational changes upon ligand binding, allowing for P binding only after activation. This presumption was corroborated by Co-IP experiments that revealed an interaction of RABV P with a constitutively active form of RIG-I, composed of the RIG-I CARDS and HD motif I (Fig. 3-11B).

As reported by Zou *et al* "The RIG-I/MDA5 viral surveillance system is conserved in vertebrates. The RIG-I like helicase family appears to have evolved from a common ancestor that originated from genes encoding different core functional domains" (Zou et al., 2009). It is rather likely that P targets a certain functional domain of the RLRs or aa adjacent to such a domain, which is/are conserved to a higher or lesser

extent, and whose exposure requires distinct conformational changes, determining the possibility of interaction.

4.4 MDA5 ATPase activity is not a prerequisite for downstream signaling

Structural and biochemical analyses of RIG-I suggest that the ligand-induced conformational switch, liberating the CARDS for signaling, depend on ATP-hydrolysis by the HD (Cui et al., 2008). However, it was also shown that the catalytic activity of the HD motifs is not categorically required for downstream signaling. Only specific HD motifs, that differ between MDA5 and RIG-I, correlate with signaling capacity (Bamming and Horvath, 2009). Binding of the paramyxovirus V protein to specific motifs of the MDA5 and Lgp2 HD inhibits ATP hydrolysis. The V/MDA5 interaction is claimed to inhibit MDA5-dependent IFN induction (Parisien et al., 2009).

In contrast to V, P binding does not inhibit poly(I:C) induced ATPase activity of RIG-I or MDA5, as revealed by ATPase assays (Fig. 3-13). As P can inhibit IFN induction downstream of RLRs by blocking IRF3 S386 phosphorylation, an effect on IFN induction due to RLR binding was not detectable. Our working hypothesis is that P binding blocks the N-terminal RLR CARDS or prevents conformational changes required for association with downstream molecules like IPS-1. The finding that RLRs are targeted by P gene products of both paramyxoviruses and rhabdoviruses further emphasizes a general and crucial role of RLRs in the host defense against negative strand RNA virus infection and illustrates the functional similarities of P gene products among these viruses.

Considering the results of the dual luciferase assay and the ATPase assay, where non-stimulated full-length MDA5 has a basal activity to induce signaling but ATPase activity depends on poly(I:C) stimulation, it seems that ATP hydrolysis and downstream signaling are distinct events and that ATP hydrolysis is not a prerequisite for (basal) signaling, as proposed in a recent study (Bamming and Horvath, 2009).

4.5 RABV P interacts with an activation intermediate of IRF3, depending on S396/S398 phosphorylation

In Co-IP experiments evidence was provided that RABV P indeed does not interact with IRF3 in non-stimulated cells; however, in cells where the RLR pathway was activated a strong interaction of RABV P with IRF3 was determined (Fig. 3-14A/B). Coevally, TBK1 and IKKi did not show binding to RABV P, neither in non-stimulated nor in stimulated cells. Therefore, the interaction seems to be direct or tightly interconnected by proteins downstream of TBK1/IKKi in the RLR signaling cascade, such as CypB. CypB knockdown resulted in inhibition of IRF3 phosphorylation, dimerization, DNA and coactivator binding, and IFN-induction, which would make it a hypothetical target for RABV P. However, the interaction must be upstream of nuclear translocation, as IRF3 is accumulated in the cytoplasm in the presence of P (Rieder et al., 2011).

IRF3 is the key regulator of IFN β expression and its activation by the kinases TBK1 or IKKi involves phosphorylation at specific C-terminal Ser and Thr residues (site1: S385/S386; site 2: S396, S398, S402, T404, S405; further residues: S339, S390). A prerequisite for IRF3 transcriptional activity is the phosphorylation of S385/S386. However, the order of phosphorylation events that lead to activation (i.e. S385/S386 phosphorylation) are still highly discussed. Distinct models of an IRF3 phosphorylation sequence have been suggested. On the one hand it is suggested that phosphorylation of site 2 Ser and Thr residues relieve an auto-inhibitory structure of IRF3 that allows for S385/S386 phosphorylation (Servant et al., 2003; Panne et al., 2007). On the other hand, the initial site 2 phosphorylation and auto-inhibition are thought to be irrelevant. Rather the phosphorylation of site 1 only (Takahasi et al., 2010) or an initial phosphorylation of site 1, followed by site 2 phosphorylation (Bergstroem et al., 2010) are proposed to be required for activation of IRF3. The interaction of RABV P with IRF3, depending on its activation, can be used as tool to elucidate the activation mechanism of IRF3.

Recent studies, based on structural data (Qin et al., 2003), biochemical analyses and molecular biological approaches (Servant et al., 2003; Panne et al., 2007; Clément et al., 2008) provide a strong evidence for the auto-inhibitory model of IRF3. In its inactive state, the N- and C-terminal auto-inhibitory segments of the IRF association domain (IAD), such as helices H1 and H5, respectively, interact with each other and together cover a hydrophobic surface on the H3 and H4 helices of the IAD, which is involved in IRF3 dimerization and binding to CBP. Hydrophobic residues on the H3 and H4 helix include L322, P324, I326, V327, L329, I330 and C371, A374, L375, M378 and A379, respectively. These residues are masked by the hydrophobic interactions with L192, L195 and L196 of the H1 helix, V391, L393 and I395 in the L6 loop, T408, L412, L415 and V416 of the H5 helix, and M419 and P421 in the C-terminal extension (the IRF3 aa sequence and a detailed assignment of specific domains can be found in the appendix). As the helices H1 and H5 form an interdigitating interaction, with the aa 192-196 of H1 inserting into a space provided by the β 12-L6- β 13 region and H5, a synergistic effect conferring auto-inhibition is suggested. In a study by Qin *et al.* it was shown that replacement of hydrophobic residues of H1 and H5 to arginine results in IRF3 dimerization without stimulation (Qin et al., 2003).

It is claimed that phosphorylation of IRF3 site 2 Ser/Thr residues by virus-induced kinases triggers a conformational change possibly involving the disruption of the hydrophobic interactions of H1/H5 and H3/H4, allowing for site 1 S385/S386 phosphorylation. It has to be mentioned that site 1 and 2 phospho-sites are located between H4 and H5, in the region of β 12-L6- β 13, where the H1 inserts in the auto-inhibited state. Unmasking of the H3/H4 interface as result of charge repulsions exposes a hydrophobic surface on H3/H4 involved in protein-protein interaction, such as IRF3 dimerization and binding to proteins of the IRF3 enhanceosome, such as CBP (Fig. 4-3). We propose that after the first step of activation RABV P can interact with a (partially) open conformation of IRF3, thereby inhibiting S385/S386 phosphorylation.

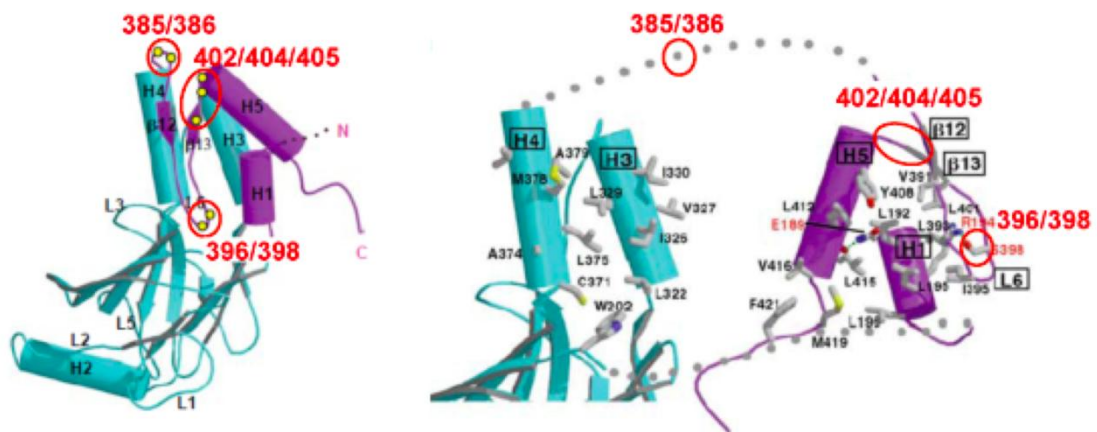


Figure 4-2: Structural model of IRF3 activation upon sequential phosphorylation. Structure of IRF3 C-terminal domain as illustrated in a recent publication (Qin et al., 2003). The left conformation shows the auto-inhibited state, where H1 and H5 helices interact with and shield the H3 and H4 interface. This model suggests an initial phosphorylation of site 2 residues S396, S398, S402, T404 and S405, by virus-induced kinases that lead to conformational changes, unshielding H3 and H4 helices, allowing for S385/S386 phosphorylation and further activation. Location of phosphosites (without S390 and S339) are circled in red.

In all conducted Co-IPs, the coexpression of RABV P and IRF3 only resulted in interaction when the cells were previously stimulated with SeV DI-H4 or by coexpressing Δ IRIG-I. Using phospho-specific antibodies it was revealed that binding of P increased in a time- and dose dependent manner, during a time course of 2 - 24 h p.i. with SeV DI-H4 and after transfection of increasing levels of Δ IRIG-I, respectively. It is obvious that strength/quantity of P/IRF3 interaction correlates with IRF3 stimulation (Fig. 3-15, 3-17). In the time course of IRF3 activation after SeV DI-H4 stimulation and in the absence of RABV P, it was obvious that site 2 residues S396 and S398 (peak at 8-10 h p.i.) are phosphorylated previously to S386 (peak at 12 h p.i.). Interestingly, RABV P binding inhibited phosphorylation of S386, which is essential for transcription of IFN β , at all time points after IRF3 stimulation, while phosphorylation at phosphosites S396 and S398 seem to be unaffected (Fig. 3-16, 3-17). Therefore, these experiments not only show activation-dependent P/IRF3 interaction but also support the initial phosphorylation of site 2 residues prior to S385/S386 phosphorylation.

As it seems that P/IRF3 interaction depends on IRF3 activation and increases with S396 and S398 phosphorylation, it was of interest whether the phosphates at site 2 residues (or at S386 and S339) are directly involved or a prerequisite for binding of RABV P. Site-directed mutagenesis was carried out to exchange respective Ser/Thr

phospho-sites to non-phosphorylatable Ala or to phosphomimetic Asp. Interestingly, after SeV DI-H4 infection, the IRF3 constructs containing a mutation of S396/S398 to A showed a strong decrease in P interaction compared to wt IRF3, while the other mutations (S402, T404, S405→A) did not seem to affect interaction (Fig. 3-18, 3-19). Therefore, an essential role of S396/S398 phosphorylation with respect to IRF3 activation, but also for RABV P binding was suggested.

In a recent study it was reported that expression of IRF3 holding the minimal mutation of S396 to aspartic acid is sufficient to induce S385/S386 phosphorylation, activation of IRF3 and induction of type I IFN, RANTES, and ISG promoters (Servant et al., 2003). Here we also saw that the mutation of site 2 residues to aspartic acid (IRF3 5D) had an intrinsic potential to phosphorylate S385/S386 residues in the absence of stimulation, probably by kinases other than TBK1, leading to a constitutively active IRF3 form (Fig. 3-19A). However, structural changes in IRF3 5D that would support an auto-inhibitory mechanism were not observed so far (Takahasi et al., 2010). Interestingly, IRF3 5D or IRF3 mutants where single site 2 residues were exchanged to Asp did not lead to an association with RABV P in unstimulated cells, however, upon stimulation an interaction was induced (Fig. 3-19). This further indicates that phosphomimetic forms, which lead to S385/S386 phosphorylation, are not sufficient for P binding. Further activation mechanisms that induce a characteristic conformation for perfect P binding must therefore exist. It is possible, that the described transcriptional activity by the IRF3 S396D or IRF3 5D mutants is reflecting a picture of leaky IRF3 proteins which only reveal their full functional capacities after further stimulation. Taken together, although it seems as if site 2 residues are phosphorylated prior to site 1 residues, the relevance of site 2 phosphorylation, and the complete events leading to IRF3 transcriptional activation after virus infection remain ambiguous.

4.6 RABV P binds to the H3/H4 helix of IRF3

The previous findings indicate that although S396/S398 phosphorylation facilitates P binding, conformational changes independent from phosphorylation at auto-

inhibitory structures occur that allow for P interaction. In further Co-IP experiments, the domain(s) of IRF3 that play a role in RABV P interaction was/were elucidated. Various Flag-IRF3 constructs were generated and coexpressed with RABV P in absence or presence of stimulation by SeV DI-H4 infection.

Strikingly, in case of the IRF3 constructs that lack the H1 helix an association with P could be detected in uninfected cells. This interaction was even increased upon deletion of the H2 helix. This supports an important inhibitory role of H1 (and maybe H2) not only for IRF3 activation but also for P binding. However, the interaction of P with all IRF3 constructs was strongly induced in cells infected with SeV DI-H4. IRF3 constructs that lack the described auto-inhibitory structures, such as IRF3 300-427, which lacks H1/H2, and IRF3 200-384, which lacks H1 and H5, show a substantial increase in P pull-down. IRF3 300-427 associated strongest with P, although the expression level of this mutant was very low (Fig. 3-20). Surprisingly, the construct IRF3 200-427, which also lacks the H1 helix (aa 192-196) showed a weaker interaction for so far unidentified reasons. Full-length IRF3 and IRF3 185-427, which only lacks the DBD/PRR but still contains the H1 and H5, show a reduced interaction in infected and uninfected cells, which again implies a special inhibitory role of the IRF3 IAD H1. As the H2 helix is also dispensable for interaction, RABV P most probably binds at the H3/H4 interface depending on so far unknown modifications and intramolecular displacements.

From these findings it appears that IRF3 H1 confers a quite strong inhibition that is only partially released upon activation of the cells with SeV DI-H4. In case the H1 is lacking, RABV P should have free excess to the IAD H3/H4, which might be further induced by the lack of H2. As the mutant IRF3 200-384 lacks the H5 helix, mechanisms beside the S390, and site 1 and 2 residue phosphorylations must be involved in conformational rearrangements favoring P binding. Furthermore, the contribution of the constitutively phosphorylated upstream S173/S175 was excluded.

An indirect interaction of RABV P and IRF3 bridged by a specific protein, such as a chaperone, is pro forma not ruled out so far. The possibility that the interaction additionally requires a specific activation of RABV P is under investigation.

4.7 RABV P binding to H3/H4 shields adjacent S385/S386 from phosphorylation

The RABV PΔInd1, PΔInd2 and PΔInd1/2 lost their ability to interfere with IRF3 activation. The most logical reason that appeared was that the mutants lost their ability to bind to IRF3. However, PΔInd1, PΔInd2 and PΔInd1/2 were still able to interact with IRF3 in stimulated cells and with intensities comparable to wt RABV P. However, IRF3 S386 phosphorylation was not inhibited. Furthermore, when PΔInd1 is overexpressed in stimulated cells, the S396 and S398 phosphorylation remained unchanged.

These data indicate that PΔInd1 specifically lost the ability to interfere with S386 phosphorylation while binding to IRF3 like wt P. This data indicates that the internal deletions of RABV PΔInd1, PΔInd2 and PΔInd1/2 lead to a changed conformation that is inefficient in blocking S386 phosphorylation.

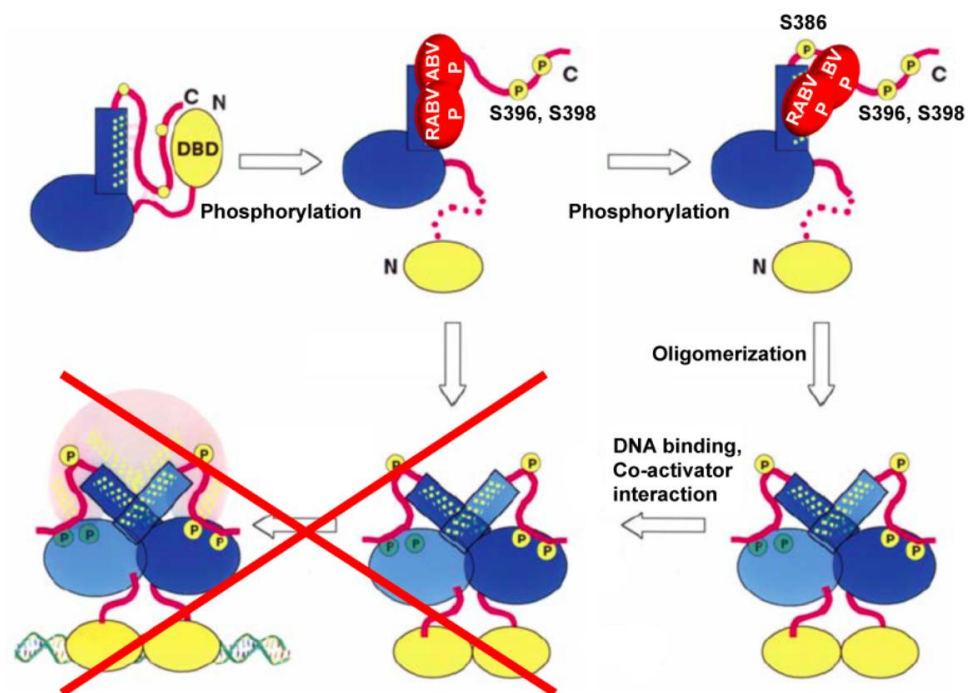


Figure 4-3: Model of IRF3 inhibition by RABV P and loss of inhibition by PΔInd mutants. It is suggested that specific modifications in IRF3 after stimulation, that go along with phosphorylation of site 1 Thr and Ser residues, induce conformational changes in IRF3 that expose certain domains in the region of the H3/H4 region. To these regions RABV P can bind and inhibit S386 phosphorylation, required for full activation of IRF3. In the RABV PΔInd mutants the conformation is probably also altered so that the P mutants can still bind, yet the binding does not inhibit the S386 phosphorylation anymore.

Taking all acquired results into consideration, a model of IRF3 activation and binding by RABV P and P non-inhibiting mutants is suggested. Upon stimulation of the RLR signaling cascade, sequential phosphorylation occurs that takes part in conformational rearrangements of IRF3. However, other, so far unknown alterations are required for inducing a fully active IRF3 form. RABV P targets a very specific activation stage of IRF3, probably due to exposure of an interaction interface in H3/H4 conferred by a defined conformation. It seems that the auto-inhibitory H1 (and possibly H2) of the IRF3 IAD confers a strong blockage of the H3/H4 helix as deletion of H1 increases RABV P binding after activation. In a study by Qin *et al.*, an IRF3 was generated where hydrophobic aa L192, L195, and L196 of H1 were mutated to Arg, leading to homo-dimerization of IRF3 without further stimulation (Qin *et al.*, 2003). In ongoing attempts, this IRF3 H1 mutant, but also mutants where L322, I326 and I330 of the H3 helix and L375, M378 and A379 of the H4 helix were mutated to Arg, are analyzed with respect to P interaction. These mutations might generate an IRF3 that can be bound by RABV P without stimulation (H1 mutant) or which cannot be bound by P anymore (H3/H4 mutants) to give further details on IRF3 activation but also inhibition.

It is assumed that via an interaction with the H3/H4 interface, the P protein shields S386 from phosphorylation whilst leaving S396 and S398 phosphorylations unaffected. Conformational restrictions of P Δ Ind mutants, however, preclude shielding and allow for S386 phosphorylation, hence, IRF3 transcriptional activation.

4.8 Conclusion and future perspectives

As IFN induction is a major target of the RABV countermeasures to avoid an antiviral immune response, it is a potent target for therapeutic approaches. The findings of this thesis strongly point towards a central role of successful IRF3 activation in the defense against RABV and most likely this is also true for many other viruses. Not only RABV P but also the phosphoproteins of related BLVs seem to be a major factor in determining pathogenicity of a lyssavirus in a certain host. In concomitant and ongoing experiments the ability of particular BLV P proteins to inhibit IRF3 activation

in human cells is analyzed. The P protein of EBLV-1, which shows a high phylogenetic relation to RABV P, was able to strongly inhibit IRF3 activation, while P proteins of more distantly related BLVs did not exhibit this inhibitory potential. This adaptation might be decisive in the establishment of a novel human pathogen with altered virulence. Revealing the specific mechanisms of RABV to invade the host IFN system and the virus-host interactions leading to RABV pathogenicity, should help to find biological substances that counteract virus propagation or in designing novel attenuated viruses for immunization, gene therapy or oncolytic approaches. A conversion of the collected data to clinical application could be the development of IRF3-like small molecules that inhibit P binding to IRF3 (antiviral), or the development of P-like small molecules that inhibit IRF3 activation (anti-inflammatory). Furthermore, the generated recombinant virus SAD Δ Ind1, which was highly attenuated in mice because of a strong IFN induction, represents a potential candidate for novel vaccines.

Future research has to be undertaken to unravel the full mechanistic background of the interference of IFN induction by RABV P. The functional relevance of the described P/RLR interaction would be of major interest, such as a possible blockage of RIG-I and MDA5 to bind to downstream molecules like IPS-1. Furthermore, a direct interaction has to be verified or the interjacent protein identified. As P potentially inhibits IFN induction downstream of the RLRs (at IRF3), possible effects of the P/RLR interaction on IFN expression are hard to reveal. In this respect, a P mutant would be helpful that is not able anymore to bind IRF3 but can still interact with MDA5. Furthermore, the specific region of RABV P required for RLR interaction has to be elucidated more precisely. It would also be necessary to identify more defined regions in RIG-I and Lgp2 that confer P binding, and undertake sequence comparisons with the identified MDA5 interaction interface (for alignment of full RLR aa sequences see appendix).

Further experiments also have to be directed at the site of IRF3 inhibition. As already discussed, mutants of IRF3 were generated where hydrophobic residues in the IAD H1, H3, and H4 helices were replaced by Arg (see discussion) to destroy auto-inhibitory hydrophobic interactions or potential P binding sites and analyzed for P

interaction in ongoing attempts. It is also of interest whether IRF3 200-384 or IRF3 300-427 form dimers in the absence of activation due to the lack of H1, if this potential interaction is increased by activation, and if RABV P has an influence on this. In case spontaneous dimerization is lost in the presence of P it might coincide with the ability of P binding. Furthermore, IRF3 has been recently shown to interact with Bax via a BH3 domain in the H4 helix to induce apoptosis. To investigate whether P binds to residues in the H4 helix, it would be interesting if binding of P to IRF3 can outcompete Bax binding, or if presence of Bax inhibits P binding.

To characterize the phosphorylatable sites in IRF3 in the absence or presence of RABV P, a phospho-specific mass spectrometry analysis is undertaken. Further collaborations might allow us to determine a structure of the RABV P/IRF3 complex.

As IRF7, like IRF3, transcribes type I IFN genes in response to RABV infection, and also IRF3/IRF7 heterodimers are formed during innate immune signaling (H3/H4 helix), it is of interest if RABV P can also bind to IRF7 or prevent IRF3/IRF7 dimer formation. As already published (Rieder et al., 2011), RABV P can also inhibit IRF7 induced signaling yet to a lesser degree than IRF3 induced signaling.

In a sequence comparison of human, dog, bat, and mouse IRF3 a high conservation can be seen. Especially the auto-inhibitory structures of the IAD are highly homologous among the species (for sequence comparison see appendix). This conservation further underlines a central role of IRF3 across distinct species. Comparing the ability of RABV P to interact with IRF3 from distinct species and further mutational analyses could unravel particularly essential residues for this association and might partially explain the large reservoir species of RABV.

5 Appendix

Sequence alignments:

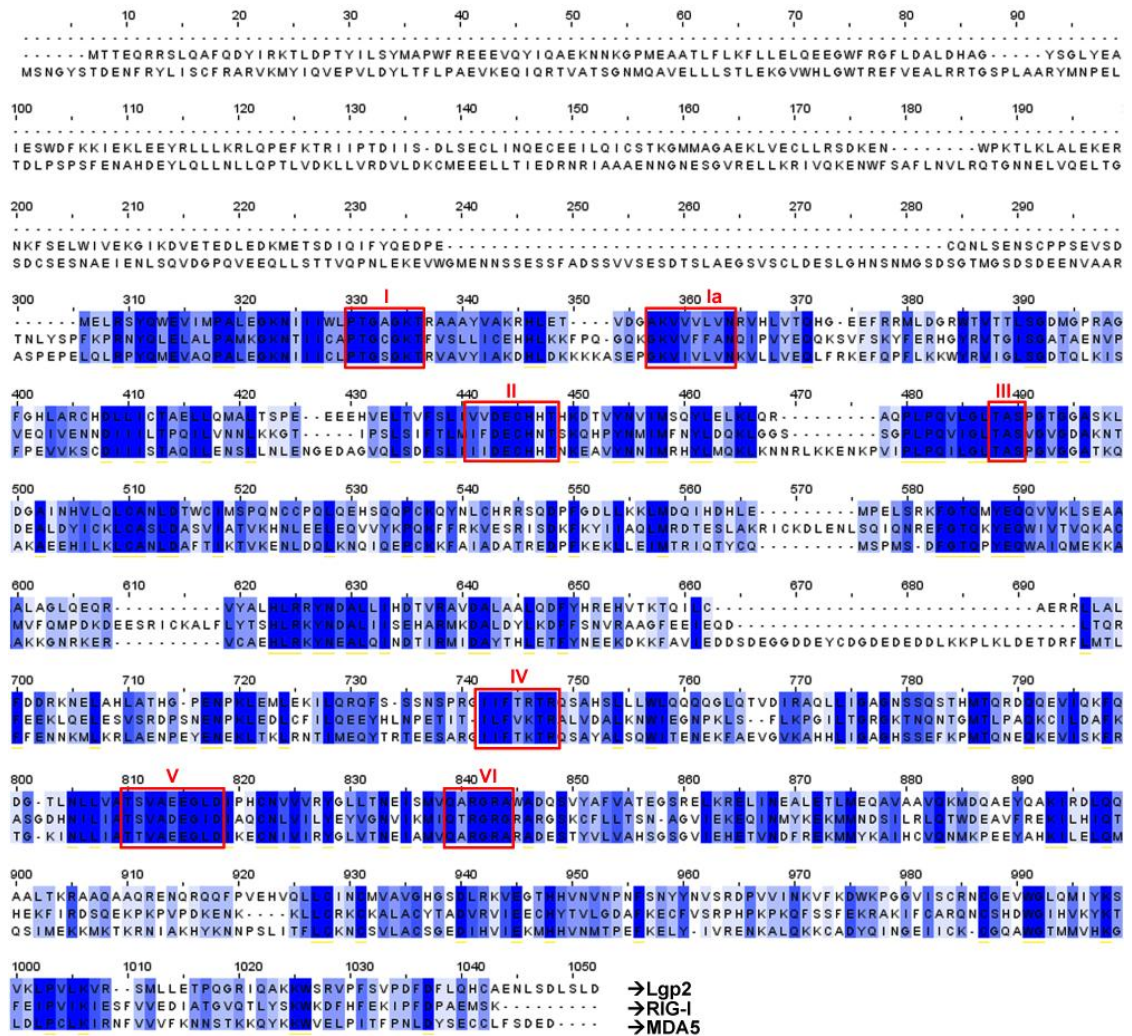


Figure 5-1: Sequence alignment of human Lgp2, RIG-I and MDA5. RLR sequences were aligned with the ClustalW2 software and the conservation was illustrated by blue colors (dark blue: highly conserved). Lgp2 is 678 aa long, RIG-I is 925 aa long and MDA5 is 1025 aa long. The numbers above the alignment do not correspond to the aa positions but are generated by the software. The motifs I, Ia, II, III, IV, V, and VI are outlined by red boxes.

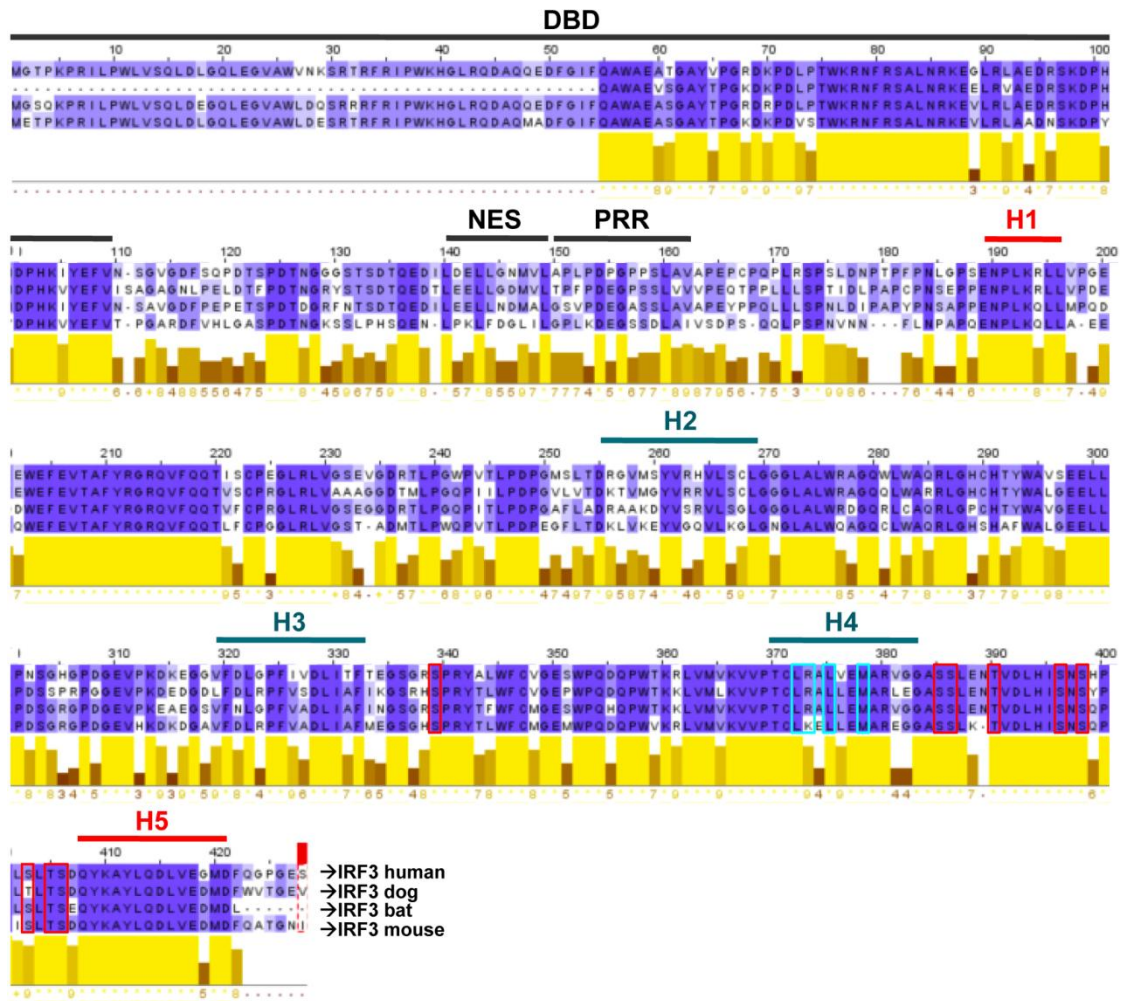


Figure 5-2: Sequence comparison of IRF3 from human, dog, bat, and mouse. IRF3 sequences were aligned with the ClustalW2 software and the conservation was illustrated by blue colors (dark blue: highly conserved). IRF3 is composed of an N-terminal DBD, a central IAD and N-terminal regulatory domain, as illustrated in a recent publication (Qin et al., 2003). The auto-inhibitory helices H1 and H5 helices are indicated in red writing. H2, H3 and H4 helices are indicated in blue writing. The known phospho-sites involved in IRF3 activation are illustrated in red boxes. The residues of the IRF3 BH3 domain in the H4 helix that are required for Bax binding are marked by turquoise boxes.

Buffers and Solutions:

Mini Preparation:

Flexi I:

- 100 mM Tris-HCl pH 7.5
- 10 mM EDTA
- 200 µg/ml RNase

Flexi II:

- 200 mM NaOH

1 % (w/v) SDS

Flexi III:

3 M potassium acetate

2 M acetic acid, pH 5.75

Agarose gel electrophoresis:**10 x TAE:**

2 M Tris-HCl, pH 7.8

0.25 M Sodium acetate x 3 H₂O

0.25 M EDTA

1 x TAE + EtBr:

100 ml 10 x TAE

150 µl Ethidium bromide solution 1%

to 1 l H₂O

OG loading buffer:

50 % (v/v) 10x TAE

15 % (w/v) Ficoll 400

0.125 % (w/v) Orange G

10x TE:

100 mM Tris-HCl, pH 7.5

10 mM EDTA

Blue juice:

0.125 % (w/v) Bromphenol blue

0.125 % (w/v) xylene cyanol

0.125 % (w/v) Orange G

15 % (w/v) Ficoll 400

50 % (v/v) 10 x TAE

1 kb marker:

380 µl 1 x TE

100 µl Blue juice

20 µl 1 kb DNA ladder

PCR marker:

167 µl Gel loading dye blue (6x)

733 µl H₂O

100 µl PCR Marker

SDS-PAGE:**Jagow gel buffer:**

3 M Tris-HCl, pH 8.45

0.3 % (w/v) SDS

Jagow anode buffer:

200 mM Tris-HCl, pH 8.9

Jagow kathode buffer:

100 mM Tris-HCl, pH 8.25

100 mM Tricine

0.1.1 % (w/v) SDS

SDS sample buffer:

62.5 mM Tris-HCl, pH 6.8

2 % (w/v) SDS

10 % (w/v) glycerol

6 M Urea

5 % (v/v) β-mercaptoethanol

0.01 % (w/v) Bromphenol blue

0.01 % (w/v) Phenol red

10% APS 10 % (w/v) ammonium persulfate

Stacking gel 4%:

3.5 ml Jagow gel buffer

1.4 ml acrylamide 29:1 Rotiphorese Gel 40

18 µl TEMED

116 µl APS

9 ml H₂O

Separating gel 10%:

12 ml Jagow gel buffer

9 ml acrylamide 29:1 Rotiphorese Gel 40
2 ml glycerol
17 μ l TEMED
175 μ l APS
12.9 ml H₂O

Coomassie staining:**Staining solution:**

50 % (v/v) methanol
10 % (v/v) acetic acid
0.1.1 % (w/v) Brilliant blue

Wash solution:

50 % (v/v) methanol
10 % (v/v) acetic acid

Western blot:**10 x Semi dry buffer:**

480 mM Tris-HCl, pH 8.6
390 mM Glycine
0.05 % (w/v) SDS

1 x Semi dry buffer:

100 ml 10x Semi dry buffer
180 ml methanol
to 1 l H₂O

1 x PBS:

1.37 M NaCl
27 mM KCl
12 mM KH₂PO₄
65 mM Na₂HPO₄ x 2H₂O (pH 7.4)

PBS-Tween:

1 x PBS
0.05 % (v/v) Tween-20

Northern blot:**RNA agarose gel:**

- 2 g agarose (RNA grade)
- 4 ml 50 x phosphate buffer
- 26.7 ml formaldehyde, 37 %
- 167.3 ml H₂O ultra pure

50 x Phosphate buffer:

- 250 mM Na₂HPO₄ x 2H₂O (pH 6.8-7.0)
- 250 mM NaH₂PO₄ x H₂O

Glyoxal solution:

- 8.8 M glyoxal

Acridine orange solution:

- 1 x Phosphate buffer
- 33.3 M Acridine orange

10 x SSC:

- 1.5 M NaCl
- 150 mM Na-citrate x 2H₂O (pH 7.0)

Zeta hybridizing buffer:

- 250 mM Na₂HPO₄ x 2H₂O (pH 7.2)
- 250 mM NaH₂PO₄ x H₂O
- 1 mM EDTA
- 7 % (w/v) SDS

Zeta wash buffer 5 %:

- 8 % (v/v) 50 x phosphate buffer
- 1 mM EDTA
- 5 % (w/v) SDS

Zeta wash buffer 1 %:

- 8 % (v/v) 50 x phosphate buffer
- 1 mM EDTA
- 1 % (w/v) SDS

Native Gel:**2x Native sample buffer:**

125 mM Tris-Cl, pH 6,8
30 % glycerol
0.01 % (w/v) Bromphenol blue

Lysis buffer:

50 mM Tris-Cl, pH 8,0
1% NP-40
150 mM NaCl
5 mM orthovanadate
100 µg/ml leupeptin
1mM PMSF

Gel buffer:

1,5 M Tris, pH 8,8

Native gel 7,5%:

3,5 ml acrylamide
5 ml Tris (1,5 M)
20 ml TEMED
200 µl 10% APS
11,3 ml H₂O d.

Lower chamber buffer:

25 mM Tris-Cl, pH 8,4
192 mM glycine

Upper chamber buffer:

25 mM Tris-Cl, pH 8,4
192 mM glycine
1% DOC

Co-IP:**Standard Co-IP buffer:**

50 mM Tris-HCl pH 7.5
150 mM NaCl

2 mM EDTA
1 mM Na₃VO₄
0.5 % (v/v) NP-40
1 mM NaVO₄
1 x Complete Protease Inhibitor

Sepharose A Co-IP Buffers:

Buffer A:
100 mM Tris pH 8.0
Buffer B:
10 mM Tris pH 7.4

PBS 5mM EDTA:

1 x PBS
5mM EDTA

Immunofluorescence:**3 % PFA/PBS:**

1 x PBS
3 % (w/v) paraformaldehyde

PBS/0.5 % Triton X-100:

1 x PBS
0.5 % (v/v) Triton X-100

PBS/2 %BSA/0.1 % Triton X-100:

1 x PBS
0.1 % (v/v) Triton X-100
2 % BSA

PBS/0.1 % Triton X-100:

1 x PBS
0.1 % (v/v) Triton X-100

His-tag protein purification:**5 x Buffer A:**

250 mM KH₂PO₄, pH 7.5

1000 mM NaCl
75 mM Imidazol

5 x Buffer B:

250 mM KH₂PO₄, pH 7.5
1000 mM NaCl
1500 mM Imidazol

1 x Buffer A or B:

50ml 5 x Buffer A/B
200ml H₂O d.
0.07 % (v/v) β-Mercaptoethanol

10 x Dialysis buffer:

500 mM Tris-HCl, pH 8.0
1500 mM NaCl
50 mM DTT

1 x Dialysis Buffer:

500 ml 10 x Dialysis buffer
10 % (v/v) Glycerol
to 5 l H₂O d.

In vitro* ATPase assay:*5 x ATPase buffer:**

100 mM Tris, pH 7.5
100 mM NaCl
5 mM MgCl₂
100 µg/ml BSA
1 mM DTT

ATPase dilution buffer:

10 µl 5 x ATPase buffer
2,5 µl ATP (2 mM)
1 µl RNaseIN
5 µl poly(I:C) (0.1 µM)
20 nM γ-³²P-ATP

to 40 µl H₂O

General solutions:

70% Ethanol:

700 ml ethanol p.a.

to 1 l H₂O d.

80 % Acetone:

800 ml acetone p.a.

to 1 l H₂O d.

Primer sequences:

Table 2. Primer sequences PCR primer

Primer	Sequence ^{a,b}	Origin
FI-MDA5 1-350 XhoI 3'	5'-TAT <u>CTC GAG</u> TTA CTT CTT GTC TAA GTG ATC-3'	human
FI-MDA5 1-449 XhoI 3'	5'-TAT <u>CTC GAG</u> TTA GTT GGT GTG ATG ACA TTC-3'	human
FI-MDA5 287-449 Acc65I 5'	5'-ATA <u>GGT ACC</u> ATG GAC TAC AAA GAC GAT GAC GAT AAA GGA AGT GAT TCA GAT GAA-3'	human
His6-MDA5 Acc65I 5'	5'-ATA <u>GGT ACC</u> ATG CAT CAT CAT CAT CAT CAT TCG AAT GGG TAT TCC-3'	human
FI-RIG-I CD Acc65I 5'	5'-ATA <u>GGT ACC</u> GCC ACC ATG GAC TAC AAA GAC GAT GAC GAT AAA ACC ACC GAG CAG CGA-3'	human
RIG-I HD 3'	5'-GCC TCT GGT TTG GAT CAT-3'	human
RIG-I RD 5'	5'-AGA GGA AGA GCA AGA GGT-3'	human
RIG-I RD XhoI 3'	5'-TAT <u>CTC GAG</u> TCA TTT GGA CAT TTC-3'	human
FI-MDA5 CD Acc65I 5'	5'-ATA <u>GGT ACC</u> GCC ACC ATG GAC TAC AAA GAC GAT GAC GAT AAA TCG AAT GGG TAT TCC-3'	human
MDA5 HD 3'	5'-ACC ACG GGC CTG GAC CAT-3'	human
MDA5 RD 5'	5'-CGA GCC AGA GCT GAT GAG-3'	human
MDA5 RD XhoI 3'	5'-TAT <u>CTC GAG</u> CTA ATC CTC ATC ACT-3'	human
FI-Lgp2 HD Acc65I 5'	5'-ATA <u>GGT ACC</u> GCC ACC ATG GAC TAC AAA GAC GAT GAC GAT AAA GAG CTT CGG TCC TAC-3'	human
Lgp2 HD 3'	5'-GCC CCT GGC CTG GAC CAT-3'	human
Lgp2 RD 5'	5'-CGT GCC TGG GCC GAT CAG-3'	human
Lgp2 RD XhoI 3'	5'-TAT <u>CTC GAG</u> TCA GTC CAG GGA GAG-3'	human
RIG-I CD 3'	5'-TGG AAT CGT TCC CTT TTT-3'	human
MDA5 HD 5'	5'-GAT GCT GGT GTT CAA TTG-3'	human
MDA5 CD 3'	5'-TTC TCC ATT TTC CAA GTT-3'	human
RIG-I HD 5'	5'-TCA CTA TCC ATC TTT ACT-3'	human
FI-RIG-I CD Acc65I 5'	5'-ATA <u>GGT ACC</u> GCC ACC ATG GAC TAC AAA GAC GAT GAC GAT AAA ACC ACC GAG CAG CGA-3'	human
RIG-I HD 3'	5'-GCC TCT GGT TTG GAT CAT-3'	human
RIG-I RD 5'	5'-AGA GGA AGA GCA AGA GGT-3'	human
RABV P Acc65I 5'	5'-ATA <u>GGT ACC</u> AGC AAG ATC TTT GTC AAT-3'	human
RABV P XhoI 3'	5'-TAT <u>CTC GAG</u> TTA GCA AGA TGT ATA GCG-3'	human

RABV P Agel 5'	5'-ATA <u>ACC GGT</u> ATG AGC AAG ATC TTT GTC-3'	human
IPS-1 Acc65I 5'	5'-ATA <u>GGT ACC</u> GCC ACC ATG CCG TTT GCT GAA GAC-3'	human
IPS-1 XhoI 3'	5'-TAT <u>CTC GAG</u> CTA GTG CAG ACG CCG CCG GTA-3'	human
FI-TRADD Acc65I 5'	5'-ATA <u>GGT ACC</u> ATG <i>GAC TAC</i> AAA <i>GAC GAT GAC GAT</i> AAA GCA GCT GGG CAA AAT GGG CAC-3'	human
TRADD BglII 3'	5'-TAT <u>AGA TCT</u> C TA GGC CAG GCC GCC ATT-3'	human
FI-Sintbad EcoRI 5'	5'-ATA <u>GAA TTC</u> ATG <i>GAC TAC</i> AAA <i>GAC GAT GAC GAT</i> AAA GAG TCC ATG TTT-3'	mouse
Sintbad NheI 3'	5'-TAT <u>GCT AGC</u> CTA GAT CTT GC T GTT CTC-3'	mouse
FI-Nap1 EcoRI 5'	5'-ATA <u>GAA TTC</u> ATG <i>GAC TAC</i> AAA <i>GAC GAT GAC GAT</i> AAA <i>GAC</i> ACG CTA GTA-3'	mouse
Nap1 NheI 3'	5'-TAT <u>GCT AGC</u> TTA ACT TTT GTA AAG GCA-3'	mouse
FI-NEMO EcoRI 5'	5'-ATA <u>GAA TTC</u> ATG <i>GAC TAC</i> AAA <i>GAC GAT GAC GAT</i> AAA AAT AGG CAC CTC-3'	human
NEMO NheI 3'	5'-TAT <u>GCT AGC</u> CTA CTC AAT GCA CTC CAT-3'	human
Rip1 Acc65I 5'	5'-ATA <u>GGT ACC</u> ATG CAA CCA GAC ATG TCC-3'	human
Rip1 XhoI 3'	5'-TAT <u>CTC GAG</u> TTA GTT CTG GCT GAC GTA-3'	human
Nap1 BamHI 5'	5'-ATA <u>GGA TCC</u> ATG GAC ACG CTA GTA GAA-3'	mouse
FI-Nap1 BamHI 5'	5'-ATA <u>GGA TCC</u> ATG <i>GAC TAC</i> AAA <i>GAC GAT GAC GAT</i> AAA GAC ACG CTA GTA GAA GAT-3'	mouse
Nap1 HindIII 3'	5'-TAT <u>AAG CTT</u> TTA ACT TTT GTA AAG GCA-3'	mouse
TRADD BamHI 5'	5'-ATA <u>GGA TCC</u> ATG GCA GCT GGG CAA AAT-3'	human
FI-TRADD BamHI 5'	5'-ATA <u>GGA TCC</u> ATG <i>GAC TAC</i> AAA <i>GAC GAT GAC GAT</i> AAA GCA GCT GGG CAA AAT GGG-3'	human
TRADD HindIII 3'	5'-TAT <u>AAG CTT</u> CTA GGC CAG GCC GCC ATT-3'	human
Sintbad 5'	5'-ATG <u>GAG TCC</u> ATG TTT GAA-3'	mouse
NEMO BamHI 5'	5'-ATA <u>GGA TCC</u> ATG AAT AGG CAC CTC TGG-3'	human
FI-NEMO BamHI 5'	5'-ATA <u>GGA TCC</u> ATG <i>GAC TAC</i> AAA <i>GAC GAT GAC GAT</i> AAA AAT AGG CAC CTC TGG AAG-3'	human
NEMO HindIII 3'	5'-TAT <u>AAG CTT</u> CTA CTC AAT GCA CTC CAT-3'	human
TBK1 XhoI 3'	5'-TAT <u>CTC GAG</u> CTAAGACAGTCAACGTTGCG-3'	human
FI-IRF3 Acc65I 5'	5'-ATA GGT ACC ATG GAC TAC AAA GAC GAT GAC GAT AAA GGA ACC CCA AAG CCA CGG ATC-3'	human
IRF3 XhoI 3'	5'-TAT CTC GAG TCA GCT CTC CCC AGG GCC CTG-3'	human
RABV P 175 3'	5'-AGC CGC CAT CCT GGC TTT-3'	
RABV P 187 5'	5'-TCG GCT ACC AAT GAA GAG-3'	
FI-RABV P HpaI 5'	5'-ATA <u>GTT AAC</u> ATG <i>GAC TAC</i> AAA <i>GAC GAT GAC GAT</i> AAA <i>AGC</i> AAG ATC TTT GTC AAT CCT AGT GCT-3'	
IRF3 150 Acc56I 5'	5'-ATA <u>GGT ACC</u> ATG GAC TAC AAA GAC GAT GAC GAT AAA GCC CCA CTC CCA GAT CCG GGA CCC-3'	human
IRF3 185 Acc56I 5'	5'-ATA <u>GGT ACC</u> ATG GAC TAC AAA GAC GAT GAC GAT AAA CTG GGG CCC TCT GAG AAC CCA CTG-3'	human
IRF3 200 Acc56I 5'	5'-ATA <u>GGT ACC</u> ATG GAC TAC AAA GAC GAT GAC GAT AAA CCG GGG GAA GAG TGG GAG TTC GAG-3'	human
IRF3 300 Acc56I 5'	5'-ATA <u>GGT ACC</u> ATG GAC TAC AAA GAC GAT GAC GAT AAA CTC CCC AAC AGC GGG CAT GGG CCT-3'	human
IRF3 384 XhoI 3'	5'-TAT <u>CTC GAG</u> TCA GGC ACC CCC TAC CCG GGC-3'	human

^a Underlined nucleotides: cleavage sites for restriction enzymes

^b Italic nucleotides: protein tags

Table 3. Primer sequences mutagenesis PCR primer

Primer	Sequence	Origin
IRF3 5ADDDD 5'	5'-AAT ACT GTG GAC CTG CAC ATT GCC AAC GAC CAC CCA CTC-3'	human
IRF3 5ADDDD 3'	5'-GAG TGG GTG GTC GTT GGC AAT GTG CAG GTC CAC AGT ATT-3'	human
IRF3 5DADDD 5'	5'-AAT ACT GTG GAC CTG CAC ATT GAC AAC GCC CAC CCA CTC-3'	human
IRF3 5DADDD 3'	5'-GAG TGG GTG GGC GTT GTC AAT GTG CAG GTC CAC AGT ATT-3'	human
IRF3 5AADDD 5'	5'-AAT ACT GTG GAC CTG CAC ATT GCC AAC GCC CAC CCA CTC GAC CTC GAC GAC-3'	human
IRF3 5AADDD 3'	5'-GTC GTC GAG GTC GAG TGG GTG GGC GTT GGC AAT GTG CAG GTC CAC AGT ATT-3'	human
IRF3 5DDAAA 5'	5'-ATT GAC AAC GAC CAC CCA CTC GCC CTC GCC GCC GAC CAG TAC AAG GCC TAC-3'	human
IRF3 5DDAAA 3'	5'-GTA GGC CTT GTA CTG GTC GGC GGC GAG GGC GAG TGG GTG GTC GTT GTC AAT-3'	human
IRF3 5ADAAA 5'	5'-ATT GCC AAC GAC CAC CCA CTC GCC CTC GCC GCC GAC CAG TAC AAG GCC TAC-3'	human
IRF3 5ADAAA 3'	5'-GTA GGC CTT GTA CTG GTC GGC GGC GAG GGC GAG TGG GTG GTC GTT GGC AAT-3'	human
IRF3 398D 5'	5'-ACT GTG GAC CTG CAC ATT TCC AAC GAC CAC CCA CTC TCC CTC ACC TCC-3'	human
IRF3 398D 3'	5'-GGA GGT GAG GGA GAG TGG GTG GTC GTT GGA AAT GTG CAG GTC CAC AGT-3'	human
IRF3 398A 5'	5'-ACT GTG GAC CTG CAC ATT TCC AAC GCC CAC CCA CTC TCC CTC ACC TCC-3'	human
IRF3 398A 3'	5'-GGA GGT GAG GGA GAG TGG GTG GGC GTT GGA AAT GTG CAG GTC CAC AGT-3'	human
IRF3 S339A 5'	5'-ACG GAA GGA AGC GGA CGC GCA CCA CGC TAT GCC CTC TGG-3'	human
IRF3 S339A 3'	5'-CCA GAG GGC ATA GCG TGG TGC GCG TCC GCT TCC TTC CGT-3'	human
IRF3 S339D 5'	5'-ACG GAA GGA AGC GGA CGC GAC CCA CGC TAT GCC CTC TGG-3'	human
IRF3 S339D 3'	5'-CCA GAG GGC ATA GCG TGG GTC GCG TCC GCT TCC TTC CGT-3'	human
IRF3 wt (revert 339S) 5'	5'-ACG GAA GGA AGC GGA CGC TCA CCA CGC TAT GCC CTC TGG-3'	human
IRF3 wt (revert 339S) 3'	5'-CCA GAG GGC ATA GCG TGG TGA GCG TCC GCT TCC TTC CGT-3'	human
IRF3 T395I 5'	5'-ACT GTG GAC CTG CAC ATT TCC AAC AGC CAC-3'	human
IRF3 T395I 3'	5'-GTG GCT GTT GGA AAT GTG CAG GTC CAC AGT-3'	human
IRF3 revert 415/419 5'	5'-CTG CAG GAC TTG GTG GAG GGC ATG GAT TTC CAG GGC-3'	human
IRF3 revert 415/419 3'	5'-GCC CTG GAA ATC CAT GCC CTC CAC CAA GTC CTG CAG-3'	human
IRF3 396A 5'	5'-ACT GTG GAC CTG CAC ATT GCC AAC AGC CAC CCA CTC TCC CTC ACC TCC-3'	human
IRF3 396A 3'	5'-GGA GGT GAG GGA GAG TGG GTG GCT GTT GGC AAT GTG CAG GTC CAC AGT-3'	human
IRF3 T390A 5'	5'-GCC TCC TCC CTG GAG AAT GCT GTG GAC CTG CAC ATT TCC-3'	human
IRF3 T390A 3'	5'-GGA AAT GTG CAG GTC CAC AGC ATT CTC CAG GGA GGA GGC--3'	human
IRF3 3A 5'	5'-CAC ATT TCC AAC AGC CAC CCA CTC GCC CTC GCC GCC GAC CAG TAC AAG GCC TAC CTG-3'	human
IRF3 3A 3'	5'-CAG GTA GGC CTT GTA CTG GTC GGC GGC GAG GGC GAG TGG GTG GCT GTT GGA AAT GTG-3'	human
IRF3 2A 5'	5'-GAG AAT ACT GTG GAC CTG CAC ATT GCC AAC GCC CAC CCA CTC TCC CTC ACC TCC-3'	human
IRF3 2A 3'	5'-GGA GGT GAG GGA GAG TGG GTG GGC GTT GGC AAT GTG CAG	human

	GTC CAC AGT ATT CTC-3'	
IRF3 revert 5'	5'-AAT ACT GTG GAC CTG CAC ATT TCC AAC AGC CAC CCA CTC TCC CTC-3'	human
IRF3 revert 3'	5'-GAG GGA GAG TGG GTG GCT GTT GGA AAT GTG CAG GTC CAC AGT ATT-3'	human
IRF3 192-95-96A 5'	5'-CCC TCT GAG AAC CCA GCG AAG CGG GCG GCG GTG CCG GGG GAA GAG TGG GAG-3'	human
IRF3 192-95-96A 3'	5'-CTC CCA CTC TTC CCC CGG CAC CGC CGC CCG CTT CGC TGG GTT CTC AGA GGG-3'	human
IRF3 192-95-96R 5'	5'-CCC TCT GAG AAC CCA AGG AAG CGG AGG AGG GTG CCG GGG GAA GAG TGG GAG-3'	human
IRF3 192-95-96R 3'	5'-CTC CCA CTC TTC CCC CGG CAC CCT CCT CCG CTT CCT TGG GTT CTC AGA GGG-3'	human
IRF3 322-26-30R 5'	5'-GGC GTG TTT GAC AGG GGG CCC TTC AGG GTA GAT CTG AGG ACC TTC ACG GAA-3'	human
IRF3 322-26-30R 3'	5'-TTC CGT GAA GGT CCT CAG ATC TAC CCT GAA GGG CCC CCT GTC AAA CAC GCC-3'	human
IRF3 375-78-79R 5'	5'-ACG TGC CTC AGG GCC AGG GT A GAA AGG AGG CGG GTA GGG GGT GCC-3'	human
IRF3 375-78-79R 3'	5'-GGC ACC CCC TAC CCG CCT CCT TTC TAC CCT GGC CCT GAG GCA CGT-3'	human

Table 4. Primer sequences qRT-PCR primer

Primer	Sequence	Origin
hIFN β 5'	5'-TCC AAA TTG CTC TCC TGT TG-3'	human
hIFN β 3'	5'-GCA GTA TTC AAG CCT CCC AT-3'	human
GAPDH 5'	5'-TGG TAT CGT GGA AGG ACT CA-3'	human
GAPDH 3'	5'-CCA GTA GAG GCA GGG ATG AT-3'	human

Table 5. Primer sequences sequencing primer

Primer	Sequence
pCAGGs 5'	5'-GCT CCT GGG CAA CGT GCT GG-3'
pCAGGs 3'	5'-GCT CAA GGG GCT TCA TGA TG-3'
pCMV 5'	5'-CGC AAA TGG GCG GTA GGC GTG-3'
pBGH 3'	5'-TAG AAG GCA CAG TCG AGG-3'
IRF3 middle 3'	5'-CAG AAT GTC TTC CTG GGT ATC-3'
IRF3 middle 5'	5'-TGG CTC TGG GCC CAG CGG CTG GGG-3'
Flag 5'	5'-GAC TAC AAA GAC GAT GAC GAT AAA-3'
TRADD 5'	5'-ATG GCA GCT GGG CAA AAT-3'
TRADD 3'	5'-CTA GGC CAG GCC GCC ATT-3'
NEMO middle 5'	5'-AGC AGG CCG AGG AGG CCC-3'

6 List of figures and tables

Figure 1-1: Phylogenetic tree of the lyssavirus genus.....	2
Figure 1-2: Rabies virus structure, genome and replication.	4
Figure 1-3: Simplified overview of the RABV life cycle.....	10
Figure 1-4: Overview of RABV phosphoprotein P domains and functions.....	11
Figure 1-5: Induction of IFN and proinflammatory cytokines.	14
Figure 1-6: Structure of IRF3.	17
Figure 1-7: IFN α/β - and IFN γ -induced JAK/STAT signaling.....	19
Figure 1-8: Domain structure of RLRs.....	21
Figure 3-1: RABV P deletion mutants Δ 176-181, Δ 182-186 and Δ 176-186 show decreased ability to inhibit IFN β induction compared to full-length P.	67
Figure 3-2: Native PAGE showing inhibition of IRF3 dimerization and S386 phosphorylation by RABV P, which is lost when aa 171-186 are deleted.	68
Figure 3-3: RABV P deletion mutants Δ 176-181, Δ 182-186 and Δ 176-186 fulfill essential functions to support expression from the RABV pSDI-HH-flash minigenome.....	69
Figure 3-4: Growth kinetics and protein expression of recombinant viruses SAD Δ Ind1, SAD Δ Ind2, and SAD Δ Ind1/2, are comparable to SAD L16.	71
Figure 3-5: Infection of 293T cells with SAD Δ Ind1, SAD Δ Ind2, and SAD Δ Ind1/2 showed an increased induction of IFN β compared to SAD L16.	73
Figure 3-6: Northern blot analysis of L16 and recombinant SAD Δ Ind viruses.	74
Figure 3-7: RABV P interacts with MDA5, and to a lesser extent Lgp2.	77
Figure 3-8: RABV P interacts with the MDA5 CARD/HD junction and with an Lgp2 N-terminal domain.	79
Figure 3-9: RABV P lacking aa 20-52 and 217-245 show a reduced interaction with MDA5.	80
Figure 3-10: RABV P Δ Ind1 still interacts with MDA5 and strength of interaction is independent of poly(I:C) stimulation.	81
Figure 3-11: RABV P interacts with activated RIG-I and Lgp2 and with RIG-I CARDS.....	82
Figure 3-12: Activation of the IFN β promoter is induced by RIG-I and MDA5 depending on their activation.	84
Figure 3-13: RIG-I and MDA5 ATPase assay depends on poly(I:C) activation and is not inhibited by RABV P.	85
Figure 3-14: RABV P interacts with IRF3 depending on its activation.....	87

Figure 3-15: RABV P/IRF3 interaction correlates with the degree of IRF3 activation.....	88
Figure 3-16: IRF3 phosphorylation of serine 398 and 396 occurs prior to serine 386 phosphorylation. Only serine 386 phosphorylation is inhibited by RABV P.	89
Figure 3-17: RABV P interaction with IRF3 increases according to time of activation. Serine 386 phosphorylation is inhibited by IRF3/P interaction.	90
Figure 3-18: Mutation of IRF3 serines 396 and 398 to alanine reduces RABV P binding upon SeV DI-H4 infection.....	91
Figure 3-19: Interaction of RABV P with phosphomimetic IRF3 is potentiated by SeV DI-H4 and Δ RIG-I stimulation.....	93
Figure 3-20: RABV P/IRF3 interaction is induced by the lack of IRF3 IAD H1/H2 and H5 helices.	96
Figure 3-21: RABV P lacking aa 176-181 is incapable of inhibiting IRF3 phosphorylation and dimerization but can still interact with IRF3.....	97
Figure 3-21: RABV P lacking aa 176-181 is incapable of inhibiting IRF3 phosphorylation and dimerization but can still interact with IRF3.....	97
Figure 3-21: RABV P lacking aa 176-181 is incapable of inhibiting IRF3 phosphorylation and dimerization but can still interact with IRF3.....	97
Figure 3-21: RABV P lacking aa 176-181 is incapable of inhibiting IRF3 phosphorylation and dimerization but can still interact with IRF3.....	97
Figure 3-22: RABV P Δ Ind1, P Δ Ind2, and P Δ Ind1/2 mutants can interact with IRF3	98
Figure 4-1: Models of RIG-I and MDA5 conformation in their activated and non-activated states and RABV P binding.	107
Figure 4-2: Structural model of IRF3 activation upon sequential phosphorylation.....	111
Figure 4-3: Model of IRF3 inhibition by RABV P and loss of inhibition by P Δ Ind mutants.....	114
Table 1: Lyssavirus genotypes (GT) and epidemiology.....	3
Table 2: Primer sequences PCR primer	127
Table 3: Primer sequences mutagenesis PCR primer.....	129
Table 4: Primer sequences qRT-PCR primer.....	130
Table 5: Primer sequences sequencing primer	130

7 List of abbreviations

A/a	adenine
aa	amino acid
A	ampere
ABLV	Australian bat lyssavirus
abs.	absolute
ARAV	Aravan virus
bp	base pair
BLV	bat lyssavirus
C/c	cytosine
°C	degree Celsius
cDNA	complementary DNA
CARD	caspase activation and recruitment domains
CypB	cyclophilin B
Da	Dalton
DC	dendritic cells
ddH ₂ O	double distilled water
D-MEM	Dulbecco's modified eagle medium
DNA	deoxyribonucleic acid
ds (DNA/RNA)	double strand (DNA/RNA)
DUVV	Duvenhage virus
<i>E.coli</i>	bacteria species <i>Escherichia coli</i>
e.g.	for example (from latin: " <i>exempli gratia</i> ")
EMCV	encephalomyocarditis virus
EBLV-1/2	European bat lyssavirus-1/2
et al.	et alii
EtBr	Ethidium bromide

FADD	Fas-associated protein with death domain
g	gram
G-MEM	Glasgow MEM BHK-21 1x
Fl	Flag
G/g	guanine
GAS	gamma activated sequences
GFP	green fluorescent protein
h	hour
HD	helicase domain
Hsp90	heat shock protein 90
HRP	horse radish peroxidase
i.e.	that is (from latin: " <i>id est</i> ")
IFN	interferon
IFNAR	IFN α/β receptor
IFNGR	IFN γ receptor
IKK	I κ B kinase
IPS-1	IFN β promoter stimulator 1
IRAK	Interleukin-1 receptor associated kinase
IRF	IFN regulating factor
IRKV	Irkut virus
ISG	IFN stimulated gene
ISGF	IFN stimulated gene factor
ISRE	IFN stimulated response element
JAK	Janus kinase
KHUV	Khujand virus
l	liter
LB	Luria Bertani
LBV	Lagos bat virus

LDR	leader sequence
Lgp2	laboratory of genetics and physiology 2
M	molar
mA	milliampere
min	minute
MAL	MyD88 adapter-like
MDA	melanoma differentiation-associated protein
MeV	measles virus
MeLe RNA	MeV leader RNA
mg	milligram
min	minute
MOKV	Mokola virus
mRNA	messenger RNA
MyD88	myeloid differentiation protein 88
Nap-1	NAK-associated protein 1
nc	non-coding
NDV	Newcastle disease virus
NF-κB	nuclear factor κB
NK cells	natural killer cells
NS3/NS4A	non-structural proteins 3/4A
2',5'-OAS	2', 5' oligo-adenylate synthetase
o/n	over night
ORF	open reading frame
p / n / μ / m / k	pico / nano / micro / milli / kilo
PBS	phosphate buffered saline
PCR	polymerase chain reaction
pH	potential hydrogenii
Pin-1	peptidyl-propyl isomerase

PKR	RNA-activated protein kinase
poly(I:C)	polyinosine-polycytidylic acid
5'-pppRNA	5'-triphosphate RNA
P/S	penicillin/streptomycin
p.i.	post infection
p.t.	post transfection
RABV	rabies virus
RD	regulatory domain
RIG	retinoic acid inducible genes
Rip1	receptor interacting protein 1
RLR	RIG-like receptor
RNA	ribonucleic acid
RNase	ribonuclease
RNF125	ring-finger protein 125
rpm	rotations per minute
RT	room temperature
s	second
SAD	Strain Alabama Dufferin
SDS	sodium dodecylsulfate
SeV	Sendai virus
SHIBV	Shimoni bat virus
SIKE	suppressor of IKK ϵ
ss (DNA/RNA)	single strand (DNA/RNA)
STAT	signal transducer and activator of transcription
SV	simian virus
T/t	thymine
TAE	tris acetat EDTA
TANK	TRAF family member-associated NF- κ B activator

TBK1	TANK-binding kinase 1
TBKBP1	TBK1-binding protein 1 (also named Sintbad)
TEMED	N,N,N',N'-tetramethyldiamine
Th-1	T helper cell subset
TICAM	TIR -containing adapter molecule 1
TIR	Toll-IL-1 receptor homology domain
TIRAP	TIR domain-containing adapter protein
TLR	Toll-like receptor
TNF	tumor necrosis factor
TRADD	TNF receptor associated death domain protein
TRAF	TNF receptor associated factor
TRAM	TRIF-related adaptor molecule
TRIF	TIR - domain-containing adaptor-inducing IFN β
TYK2	tyrosine kinase 2
U	units
U/u	uracil
UV	ultraviolet light
V	volt
v/v	volume/volume
w/v	weight/volume
wt	wild type
WCBV	West Caucasian bat lyssavirus

8 References

- Albertini, A. A., Schoehn, G., Weissenhorn, W., and Ruigrok, R. W. (2008). Structural aspects of rabies virus replication. *Cell Mol. Life Sci* 65, 282–294.
- Albertini, A. A., Wernimont, A. K., Muziol, T., Ravelli, R. B., Clapier, C. R., Schoehn, G., Weissenhorn, W., and Ruigrok, R. W. (2006). Crystal structure of the rabies virus nucleoprotein-RNA complex. *Science* 313, 360–363.
- Astic, L., Saucier, D., Coulon, P., Lafay, F., and Flamand, A. (1993). The CVS strain of rabies virus as transneuronal tracer in the olfactory system of mice. *Brain Res* 619, 146–156.
- Badrane, H., Bahloul, C., Perrin, P., and Tordo, N. (2001). Evidence of two Lyssavirus phylogroups with distinct pathogenicity and immunogenicity. *Journal of virology* 75, 3268–3276.
- Baer, G. M., and Smith, J. S. (1991). Rabies in nonhematophagous bats. In “The Natural History of Rabies,” 341–366, CRC Press, Boca Raton, FL, USA.
- Balachandran, S., Thomas, E., and Barber, G. N. (2004). A FADD-dependent innate immune mechanism in mammalian cells. *Nature* 432, 401–405.
- Bamming, D., and Horvath, C. M. (2009). Regulation of signal transduction by enzymatically inactive antiviral RNA helicase proteins MDA5, RIG-I, and LGP2. *The Journal of biological chemistry* 284, 9700–9712.
- Banyard, A. C., Hayman, D., Johnson, N., McElhinney, L., and Fooks, A. R. (2011). Bats and lyssaviruses. *Advances in Virus Research. Research advances in rabies.* 79, 239–289.
- Banyard, A. C., Johnson, N., Voller, K., Hicks, D., Nunez, A., Hartley, M., and Fooks, A. R. (2009). Repeated detection of European bat lyssavirus type 2 in dead bats found at a single roost site in the UK. *Archives of virology* 154, 1847–1850.
- Bibeau-Poirier, A., Gravel, S.-P., Clement, J.-F., Rolland, S., Rodier, G., Coulombe, P., Hiscott, J., Grandvaux, N., Meloche, S., and Servant, M. J. (2006). Involvement of the I κ B Kinase (IKK)-Related Kinases Tank-Binding Kinase 1/IKKi and Cullin-Based Ubiquitin Ligases in IFN Regulatory Factor-3 Degradation. *J. Immunol.* 177, 5059–5067.
- Binder, M., Eberle, F., Seitz, S., Mücke, N., Hüber, C. M., Kiani, N., Kaderali, L., Lohmann, V., Dalpke, A., and Bartenschlager, R. (2011). Molecular mechanism of signal perception and integration by the innate immune sensor retinoic acid inducible gene-I (RIG-I). *The Journal of biological chemistry* 286, 27278–27287.
- Blondel, D., Kheddache, S., Lahaye, X., Dianoux, L., and Chelbi-Alix, M. K. (2010). Resistance to rabies virus infection conferred by the PMLIV isoform. *J. Virol.* 84, 10719–10726.
- Blondel, D., Regad, T., Poisson, N., Pavie, B., Harper, F., Pandolfi, P. P., De The, H., and Chelbi-Alix, M. K. (2002). Rabies virus P and small P products interact directly with PML and reorganize PML nuclear bodies. *Oncogene* 21, 7957–7970.
- Blumberg, B. M., Giorgi, C., and Kolakofsky, D. (1983). N protein of vesicular stomatitis virus selectively encapsidates leader RNA in vitro. *Cell* 32, 559–567.
- Botvinkin, A. D., Poleschuk, E. M., Kuzmin, I. V., Borisova, T. I., Gazaryan, S. V., Yager, P., and Rupprecht, C. E. (2003). Novel lyssaviruses isolated from bats in Russia. *Emerging infectious diseases* 9, 1623–1625.
- Boulger, L. R., and Porterfield, J. S. (1958). Isolation of a virus from Nigerian fruit bats. *Transactions of the Royal Society of Tropical Medicine and Hygiene* 52, 421–424.
- Bowzard, J. B., Ranjan, P., Sambhara, S., and Fujita, T. (2009). Antiviral defense: RIG-Ing the immune system to STING. *Cytokine Growth Factor Rev* 20, 1–5.

- Brzózka, K., Finke, S., and Conzelmann, K. K. (2005). Identification of the rabies virus alpha/beta interferon antagonist: phosphoprotein P interferes with phosphorylation of interferon regulatory factor 3. *J Virol* 79, 7673–7681.
- Brzózka, K., Finke, S., and Conzelmann, K. K. (2006). Inhibition of interferon signaling by rabies virus phosphoprotein P: activation-dependent binding of STAT1 and STAT2. *J Virol* 80, 2675–2683.
- Calam, D. H. (1980). Nomenclature of interferons. *Lancet* 2, 259.
- Chattopadhyay, S., Marques, J. T., Yamashita, M., Peters, K. L., Smith, K., Desai, A., Williams, B. R. G., and Sen, G. C. (2010). Viral apoptosis is induced by IRF-3-mediated activation of Bax. *The EMBO journal* 29, 1762–1773.
- Chelbi-Alix, M. K., Quignon, F., Pelicano, L., Koken, M. H., and De The, H. (1998). Resistance to virus infection conferred by the interferon-induced promyelocytic leukemia protein. *J Virol* 72, 1043–1051.
- Chenik, M., Chebli, K., Gaudin, Y., and Blondel, D. (1994). In vivo interaction of rabies virus phosphoprotein (P) and nucleoprotein (N): existence of two N-binding sites on P protein. *J Gen Virol* 75 (Pt 11, 2889–2896.
- Chenik, M., Chebli, K., and Blondel, D. (1995). Translation initiation at alternate in-frame AUG codons in the rabies virus phosphoprotein mRNA is mediated by a ribosomal leaky scanning mechanism. *J Virol* 69, 707–712.
- Civril, F., Bennett, M., Moldt, M., Deimling, T., Witte, G., Schiesser, S., Carell, T., and Hopfner, K.-P. (2011). The RIG-I ATPase domain structure reveals insights into ATP-dependent antiviral signalling. *EMBO reports* 12, 1127–1134.
- Clément, J.-F., Bibeau-Poirier, A., Gravel, S.-P., Grandvaux, N., Bonneil, E., Thibault, P., Meloche, S., and Servant, M. J. (2008). Phosphorylation of IRF-3 on Ser 339 generates a hyperactive form of IRF-3 through regulation of dimerization and CBP association. *Journal of virology* 82, 3984–3996.
- Conzelmann, K. K., and Schnell, M. (1994). Rescue of synthetic genomic RNA analogs of rabies virus by plasmid-encoded proteins. *J Virol* 68, 713–719.
- Cui, S., Eisenacher, K., Kirchhofer, A., Brzozka, K., Lammens, A., Lammens, K., Fujita, T., Conzelmann, K. K., Krug, A., and Hopfner, K. P. (2008). The C-terminal regulatory domain is the RNA 5'-triphosphate sensor of RIG-I. *Mol. Cell* 29, 169–179.
- Curran, J., and Kolakofsky, D. (2008). Nonsegmented negative-strand RNA virus RNA synthesis in vivo. *Virology* 371, 227–230.
- Dietzschold, B., Li, J., Faber, M., and Schnell, M. (2008). Concepts in the pathogenesis of rabies. *Future Virol* 3, 481–490.
- Edelmann, K. H., Richardson-Burns, S., Alexopoulou, L., Tyler, K. L., Flavell, R. A., and Oldstone, M. B. (2004). Does Toll-like receptor 3 play a biological role in virus infections? *Virology* 322, 231–238.
- Everett, R. D., and Chelbi-Alix, M. K. (2007). PML and PML nuclear bodies: implications in antiviral defence. *Biochimie* 89, 819–830.
- Faul, E. J., Wanjalla, C. N., Suthar, M. S., Gale, M., Wirblich, C., and Schnell, M. J. (2010). Rabies virus infection induces type I interferon production in an IPS-1 dependent manner while dendritic cell activation relies on IFNAR signaling. *PLoS Pathog.* 6, e1001016.
- Field, A. K., Tytell, A. A., Lampson, G. P., and Hilleman, M. R. (1967). Inducers of interferon and host resistance. II. Multistranded synthetic polynucleotide complexes. *Proc Natl Acad Sci U S A* 58, 1004–1010.

- Finke, S., Cox, J. H., and Conzelmann, K. K. (2000). Differential transcription attenuation of rabies virus genes by intergenic regions: generation of recombinant viruses overexpressing the polymerase gene. *J Virol* 74, 7261–7269.
- Finke, S., and Conzelmann, K. K. (1997). Ambisense gene expression from recombinant rabies virus: random packaging of positive- and negative-strand ribonucleoprotein complexes into rabies virions. *J Virol* 71, 7281–7288.
- Finke, S., and Conzelmann, K. K. (2005). Replication strategies of rabies virus. *Virus Res* 111, 120–131.
- Finke, S., and Conzelmann, K. K. (1999). Virus promoters determine interference by defective RNAs: selective amplification of mini-RNA vectors and rescue from cDNA by a 3' copy-back ambisense rabies virus. *J Virol* 73, 3818–3825.
- Fraser, G. C., Hooper, P. T., Lunt, R. A., Gould, A. R., Gleeson, L. J., Hyatt, A. D., Russell, G. M., and Kattenbelt, J. A. (1996). Encephalitis caused by a Lyssavirus in fruit bats in Australia. *Emerging infectious diseases* 2, 327–331.
- Freuling, C. M., Beer, M., Conraths, F. J., Finke, S., Hoffmann, B., Keller, B., Kliemt, J., Mettenleiter, T. C., Mühlbach, E., Teifke, J. P., et al. (2011). Novel lyssavirus in Natterer's bat, Germany. *Emerging infectious diseases* 17, 1519–1522.
- Fu, Z. F. (2005). Genetic comparison of the rhabdoviruses from animals and plants. *Curr Top Microbiol.Immunol* 292, 1–24.
- Fu, Z. F., and Jackson, A. C. (2005). Neuronal dysfunction and death in rabies virus infection. *J.Neurovirol.* 11, 101–106.
- Fujita, F., Taniguchi, Y., Kato, T., Narita, Y., Furuya, A., Ogawa, T., Sakurai, H., Joh, T., Itoh, M., Delhase, M., et al. (2003). Identification of NAP1, a regulatory subunit of IkappaB kinase-related kinases that potentiates NF-kappaB signaling. *Mol.Cell Biol* 23, 7780–7793.
- Gack, M. U., Shin, Y. C., Joo, C. H., Urano, T., Liang, C., Sun, L., Takeuchi, O., Akira, S., Chen, Z., Inoue, S., et al. (2007). TRIM25 RING-finger E3 ubiquitin ligase is essential for RIG-I-mediated antiviral activity. *Nature* 446, 916–920.
- Garoff, H., Hewson, R., and Opstelten, D. J. (1998). Virus maturation by budding. *Microbiology and molecular biology reviews* : MMBR 62, 1171–1190.
- Gaudin, Y. (1995). Photolabeling Identifies a Putative Fusion Domain in the Envelope Glycoprotein of Rabies and Vesicular Stomatitis Viruses. *Journal of Biological Chemistry* 270, 17575–17581.
- Gerard, F. C., Ribeiro Jr., E. A., Leyrat, C., Ivanov, I., Blondel, D., Longhi, S., Ruigrok, R. W., and Jamin, M. (2009). Modular organization of rabies virus phosphoprotein. *J Mol.Biol* 388, 978–996.
- Ghanem, A., Kern, A., and Conzelmann, K.-K. (2011). Significantly improved rescue of rabies virus from cDNA plasmids. *European journal of cell biology* 91, 16–10.
- Gitlin, L., Barchet, W., Gilfillan, S., Cella, M., Beutler, B., Flavell, R. A., Diamond, M. S., and Colonna, M. (2006). Essential role of mda-5 in type I IFN responses to polyriboinosinic:polyribocytidylic acid and encephalomyocarditis picornavirus. *Proceedings of the National Academy of Sciences of the United States of America* 103, 8459–8464.
- Gitlin, L., Benoit, L., Song, C., Cella, M., Gilfillan, S., Holtzman, M. J., and Colonna, M. (2010). Melanoma differentiation-associated gene 5 (MDA5) is involved in the innate immune response to Paramyxoviridae infection in vivo. *PLoS pathogens* 6, e1000734.
- Goodbourn, S., Didcock, L., and Randall, R. E. (2000). Interferons: cell signalling, immune modulation, antiviral response and virus countermeasures. *J.Gen.Virol.* 81, 2341–2364.

- Gupta, A. K., Blondel, D., Choudhary, S., and Banerjee, A. K. (2000). The phosphoprotein of rabies virus is phosphorylated by a unique cellular protein kinase and specific isomers of protein kinase C. *J Virol* 74, 91–98.
- Haller, O., Kochs, G., and Weber, F. (2007a). Interferon, Mx, and viral countermeasures. *Cytokine Growth Factor Rev* 18, 425–433.
- Haller, O., Staeheli, P., and Kochs, G. (2007b). Interferon-induced Mx proteins in antiviral host defense. *Biochimie* 89, 812–818.
- Hiscott, J. (2007). Triggering the innate antiviral response through IRF-3 activation. *J Biol Chem.* 282, 15325–15329.
- Honda, K., Yanai, H., Mizutani, T., Negishi, H., Shimada, N., Suzuki, N., Ohba, Y., Takaoka, A., Yeh, W. C., and Taniguchi, T. (2004). Role of a transductional-transcriptional processor complex involving MyD88 and IRF-7 in Toll-like receptor signaling. *Proc Natl Acad Sci U S A* 101, 15416–15421.
- Honda, K., and Taniguchi, T. (2006). IRFs: master regulators of signalling by Toll-like receptors and cytosolic pattern-recognition receptors. *Nat.Rev.Immunol.* 6, 644–658.
- Hopfner, K. P., and Michaelis, J. (2007). Mechanisms of nucleic acid translocases: lessons from structural biology and single-molecule biophysics. *Curr.Opin.Struct.Biol.* 17, 87–95.
- Hornung, V., Ellegast, J., Kim, S., Brzozka, K., Jung, A., Kato, H., Poeck, H., Akira, S., Conzelmann, K. K., Schlee, M., et al. (2006). 5'-Triphosphate RNA is the ligand for RIG-I. *Science* 314, 994–997.
- Hornung, V., Schlender, J., Guenther-Biller, M., Rothenfusser, S., Endres, S., Conzelmann, K. K., and Hartmann, G. (2004). Replication-dependent potent IFN- α induction in human plasmacytoid dendritic cells by a single-stranded RNA virus. *J Immunol* 173, 5935–5943.
- Hoshino, K., Sugiyama, T., Matsumoto, M., Tanaka, T., Saito, M., Hemmi, H., Ohara, O., Akira, S., and Kaisho, T. (2006). IkappaB kinase- α is critical for interferon- α production induced by Toll-like receptors 7 and 9. *Nature* 440, 949–953.
- Huang, J., Liu, T., Xu, L. G., Chen, D., Zhai, Z., and Shu, H. B. (2005). SIKE is an IKK epsilon/TBK1-associated suppressor of TLR3- and virus-triggered IRF-3 activation pathways. *EMBO J* 24, 4018–4028.
- Hughes, G. J., Orciari, L. A., and Rupprecht, C. E. (2005). Evolutionary timescale of rabies virus adaptation to North American bats inferred from the substitution rate of the nucleoprotein gene. *The Journal of general virology* 86, 1467–1474.
- Ikegame, S., Takeda, M., Ohno, S., Nakatsu, Y., Nakanishi, Y., and Yanagi, Y. (2010). Both RIG-I and MDA5 RNA helicases contribute to the induction of alpha/beta interferon in measles virus-infected human cells. *Journal of virology* 84, 372–379.
- Isaacs, A., and Lindemann, J. (1957). Virus interference. I. The interferon. *Proc.R.Soc.Lond B Biol.Sci.* 147, 258–267.
- Ivanov, I., Crepin, T., Jamin, M., and Ruigrok, R. W. (2010). Structure of the dimerization domain of the rabies virus phosphoprotein. *J.Virol.* 84, 3707–3710.
- Jackson, A. C., Rossiter, J. P., and Lafon, M. (2006). Expression of Toll-like receptor 3 in the human cerebellar cortex in rabies, herpes simplex encephalitis, and other neurological diseases. *J.Neurovirol.* 12, 229–234.
- Jacob, Y., Badrane, H., Ceccaldi, P. E., and Tordo, N. (2000). Cytoplasmic dynein LC8 interacts with lyssavirus phosphoprotein. *J Virol* 74, 10217–10222.

- Jacob, Y., Real, E., and Tordo, N. (2001). Functional interaction map of lyssavirus phosphoprotein: identification of the minimal transcription domains. *J Virol* 75, 9613–9622.
- Janeway Jr., C. A., and Medzhitov, R. (2002). Innate immune recognition. *Annu.Rev Immunol* 20, 197–216.
- Jayakar, H. R., Jeetendra, E., and Whitt, M. A. (2004). Rhabdovirus assembly and budding. *Virus research* 106, 117–132.
- Jelesic, Z., and Nikolic, M. (1956). Isolation of rabies virus from insectivorous bats in Yugoslavia. *Bulletin of the World Health Organization* 14, 801–804.
- Jiang, F., Ramanathan, A., Miller, M. T., Tang, G.-Q., Gale, M., Patel, S. S., and Marcotrigiano, J. (2011). Structural basis of RNA recognition and activation by innate immune receptor RIG-I. *Nature* 479, 423–427.
- Johnson, N., Vos, A., Freuling, C., Tordo, N., Fooks, A. R., and Müller, T. (2010). Human rabies due to lyssavirus infection of bat origin. *Veterinary microbiology* 142, 151–159.
- Kang, D.-chul, Gopalkrishnan, R. V., Wu, Q., Jankowsky, E., Pyle, A. M., and Fisher, P. B. (2002). mda-5: An interferon-inducible putative RNA helicase with double-stranded RNA-dependent ATPase activity and melanoma growth-suppressive properties. *Proceedings of the National Academy of Sciences of the United States of America* 99, 637–642.
- Kato, H., Takeuchi, O., Mikamo-Satoh, E., Hirai, R., Kawai, T., Matsushita, K., Hiiragi, A., Dermody, T. S., Fujita, T., and Akira, S. (2008). Length-dependent recognition of double-stranded ribonucleic acids by retinoic acid-inducible gene-I and melanoma differentiation-associated gene 5. *The Journal of Experimental Medicine* 205, 1601–1610.
- Kato, H., Takeuchi, O., Sato, S., Yoneyama, M., Yamamoto, M., Matsui, K., Uematsu, S., Jung, A., Kawai, T., Ishii, K. J., et al. (2006). Differential roles of MDA5 and RIG-I helicases in the recognition of RNA viruses. *Nature* 441, 101–105.
- Kawai, T., Sato, S., Ishii, K. J., Coban, C., Hemmi, H., Yamamoto, M., Terai, K., Matsuda, M., Inoue, J., Uematsu, S., et al. (2004). Interferon-alpha induction through Toll-like receptors involves a direct interaction of IRF7 with MyD88 and TRAF6. *Nat Immunol* 5, 1061–1068.
- Kawai, T., Takahashi, K., Sato, S., Coban, C., Kumar, H., Kato, H., Ishii, K. J., Takeuchi, O., and Akira, S. (2005). IPS-1, an adaptor triggering RIG-I- and Mda5-mediated type I interferon induction. *Nat.Immunol.* 6, 981–988.
- Kawai, T., and Akira, S. (2010). The role of pattern-recognition receptors in innate immunity: update on Toll-like receptors. *Nat.Immunol.* 11, 373–384.
- Kawai, T., and Akira, S. (2008). Toll-like receptor and RIG-I-like receptor signaling. *Ann.N.Y Acad Sci* 1143, 1–20.
- Kerr, I. M., Friedman, R. M., Brown, R. E., Ball, L. A., and Brown, J. C. (1974). Inhibition of Protein Synthesis in Cell-Free Systems from Interferon-Treated, Infected Cells: Further Characterization and Effect of Formylmethionyl-tRNA(F). *J Virol* 13, 9–21.
- Kim, T. W., Staschke, K., Bulek, K., Yao, J., Peters, K., Oh, K.-H., Vandenburg, Y., Xiao, H., Qian, W., Hamilton, T., et al. (2007). A critical role for IRAK4 kinase activity in Toll-like receptor-mediated innate immunity. *The Journal of experimental medicine* 204, 1025–1036.
- Kim, T., Kim, T. Y., Lee, W. G., Yim, J., and Kim, T. K. (2000). Signaling pathways to the assembly of an interferon-beta enhanceosome. *Chemical genetic studies with a small molecule. The Journal of biological chemistry* 275, 16910–16917.

- Klingen, Y., Conzelmann, K. K., and Finke, S. (2007). Double-Labeled Rabies Virus Live tracking of enveloped virus transport. *J Virol*.
- Kowalinski, E., Lunardi, T., McCarthy, A. A., Louber, J., Brunel, J., Grigorov, B., Gerlier, D., and Cusack, S. (2011). Structural Basis for the Activation of Innate Immune Pattern-Recognition Receptor RIG-I by Viral RNA. *Cell* 147, 423–435.
- Kumar, H., Kawai, T., Kato, H., Sato, S., Takahashi, K., Coban, C., Yamamoto, M., Uematsu, S., Ishii, K. J., Takeuchi, O., et al. (2006). Essential role of IPS-1 in innate immune responses against RNA viruses. *J Exp. Med* 203, 1795–1803.
- Kumar, K. P., McBride, K. M., Weaver, B. K., Dingwall, C., and Reich, N. C. (2000). Regulated nuclear-cytoplasmic localization of interferon regulatory factor 3, a subunit of double-stranded RNA-activated factor 1. *Molecular and cellular biology* 20, 4159–4168.
- Kuzmin, I. V., Botvinkin, A. D., and Khabilov, T. K. (2002). A lyssavirus was isolated from a whiskered bat in Northern Tajikistan. *Plecotus et al.* 4, 75–81.
- Kuzmin, I. V., Mayer, A. E., Niezgodna, M., Markotter, W., Agwanda, B., Breiman, R. F., and Rupprecht, C. E. (2010). Shimoni bat virus, a new representative of the Lyssavirus genus. *Virus research* 149, 197–210.
- Kuz'min, I. V., Botvinkin, A. D., Rybin, S. N., and Baialiev, A. B. (1992). [A lyssavirus with an unusual antigenic structure isolated from a bat in southern Kyrgyzstan]. *Voprosy virusologii* 37, 256–259.
- Lafon, M. (2008). Immune evasion, a critical strategy for rabies virus. *Dev Biol (Basel)* 131, 413–419.
- Lafon, M. (2005). Rabies virus receptors. *Journal of neurovirology* 11, 82–87.
- Lebleu, B., Sen, G. C., Shaila, S., Cabrer, B., and Lengyel, P. (1976). Interferon, double-stranded RNA, and protein phosphorylation. *Proc Natl Acad Sci U S A* 73, 3107–3111.
- Leppert, M., Rittenhouse, L., Perrault, J., Summers, D. F., and Kolakofsky, D. (1979). Plus and minus strand leader RNAs in negative strand virus-infected cells. *Cell* 18, 735–747.
- Leroy, M., Pire, G., Baise, E., and Desmecht, D. (2006). Expression of the interferon-alpha/beta-inducible bovine Mx1 dynamin interferes with replication of rabies virus. *Neurobiol. Dis* 21, 515–521.
- Li, J., Wang, J. T., and Whelan, S. P. (2006). A unique strategy for mRNA cap methylation used by vesicular stomatitis virus. *Proc Natl Acad Sci U S A* 103, 8493–8498.
- Li, X., Lu, C., Stewart, M., Xu, H., Strong, R. K., Igumenova, T., and Li, P. (2009). Structural basis of double-stranded RNA recognition by the RIG-I like receptor MDA5. *Arch. Biochem. Biophys.* 488, 23–33.
- Lin, R., Heylbroeck, C., Pitha, P. M., and Hiscott, J. (1998). Virus-dependent phosphorylation of the IRF-3 transcription factor regulates nuclear translocation, transactivation potential, and proteasome-mediated degradation. *Molecular and cellular biology* 18, 2986–2996.
- Lin, R., Mamane, Y., and Hiscott, J. (1999). Structural and Functional Analysis of Interferon Regulatory Factor 3: Localization of the Transactivation and Autoinhibitory Domains. *Mol. Cell. Biol.* 19, 2465–2474.
- Liu, X.-Y., Wei, B., Shi, H.-X., Shan, Y.-F., and Wang, C. (2010). Tom70 mediates activation of interferon regulatory factor 3 on mitochondria. *Cell research* 20, 994–1011.
- Lumio, J., Hillbom, M., Roine, R., Ketonen, L., Haltia, M., Valle, M., Neuvonen, E., and Lahdevirta, J. (1986). Human rabies of bat origin in Europe. *The Lancet* 327, 378.
- Lund, J. M., Alexopoulou, L., Sato, A., Karow, M., Adams, N. C., Gale, N. W., Iwasaki, A., and Flavell, R. A. (2004). Recognition of single-stranded RNA viruses by Toll-like receptor 7. *Proc Natl Acad Sci U S A* 101, 5598–5603.

- Luo, D., Ding, S. C., Vela, A., Kohlway, A., Lindenbach, B. D., and Pyle, A. M. (2011). Structural Insights into RNA Recognition by RIG-I. *Cell* 147, 409–422.
- Mavrakis, M., McCarthy, A. A., Roche, S., Blondel, D., and Ruigrok, R. W. (2004). Structure and function of the C-terminal domain of the polymerase cofactor of rabies virus. *J Mol.Biol* 343, 819–831.
- Mavrakis, M., Mehoulas, S., Real, E., Iseni, F., Blondel, D., Tordo, N., and Ruigrok, R. W. (2006). Rabies virus chaperone: identification of the phosphoprotein peptide that keeps nucleoprotein soluble and free from non-specific RNA. *Virology* 349, 422–429.
- Mebatsion, T., Konig, M., and Conzelmann, K. K. (1996). Budding of rabies virus particles in the absence of the spike glycoprotein. *Cell* 84, 941–951.
- Mebatsion, T., Weiland, F., and Conzelmann, K.-K. (1999). Matrix Protein of Rabies Virus Is Responsible for the Assembly and Budding of Bullet-Shaped Particles and Interacts with the Transmembrane Spike Glycoprotein G. *J. Virol.* 73, 242–250.
- Menager, P., Roux, P., Megret, F., Bourgeois, J. P., Le Sourd, A. M., Danckaert, A., Lafage, M., Prehaud, C., and Lafon, M. (2009). Toll-like receptor 3 (TLR3) plays a major role in the formation of rabies virus Negri Bodies. *PLoS.Pathog.* 5, e1000315.
- Meredith, C. D., Prossouw, A. P., and Koch, H. van P. (1971). An unusual case of human rabies thought to be of chiropteran origin. *South African medical journal = Suid-Afrikaanse tydskrif vir geneeskunde* 45, 767–769.
- Michallet, M. C., Meylan, E., Ermolaeva, M. A., Vazquez, J., Rebsamen, M., Curran, J., Poeck, H., Bscheider, M., Hartmann, G., Konig, M., et al. (2008). TRADD protein is an essential component of the RIG-like helicase antiviral pathway. *Immunity* 28, 651–661.
- Moseley, G. W., Filmer, R. P., Dejesus, M. A., and Jans, D. A. (2007a). Nucleocytoplasmic Distribution of Rabies Virus P-Protein Is Regulated by Phosphorylation Adjacent to C-Terminal Nuclear Import and Export Signals. *Biochemistry*.
- Moseley, G. W., Lahaye, X., Roth, D. M., Oksayan, S., Filmer, R. P., Rowe, C. L., Blondel, D., and Jans, D. A. (2009). Dual modes of rabies P-protein association with microtubules: a novel strategy to suppress the antiviral response. *J.Cell Sci.* 122, 3652–3662.
- Moseley, G. W., Roth, D. M., Dejesus, M. A., Leyton, D. L., Filmer, R. P., Pouton, C. W., and Jans, D. A. (2007b). Dynein light chain association sequences can facilitate nuclear protein import. *Mol.Biol.Cell* 18, 3204–3213.
- Naeve, C. W., Kolakofsky, C. M., and Summers, D. F. (1980). Comparison of vesicular stomatitis virus intracellular and virion ribonucleoproteins. *J Virol* 33, 856–865.
- Obata, Y., Yamamoto, K., Miyazaki, M., Shimotohno, K., Kohno, S., and Matsuyama, T. (2005). Role of cyclophilin B in activation of interferon regulatory factor-3. *J Biol.Chem.* 280, 18355–18360.
- Oganesyan, G., Saha, S. K., Guo, B., He, J. Q., Shahangian, A., Zarnegar, B., Perry, A., and Cheng, G. (2006). Critical role of TRAF3 in the Toll-like receptor-dependent and -independent antiviral response. *Nature* 439, 208–211.
- Ogino, T., and Banerjee, A. K. (2007). Unconventional mechanism of mRNA capping by the RNA-dependent RNA polymerase of vesicular stomatitis virus. *Mol.Cell* 25, 85–97.
- Okumura, A., and Harty, R. N. (2011). Rabies virus assembly and budding. *Advances in virus research* 79, 23–32.
- Parisien, J.-P., Bamming, D., Komuro, A., Ramachandran, A., Rodriguez, J. J., Barber, G., Wojahn, R. D., and Horvath, C. M. (2009). A shared interface mediates paramyxovirus interference with antiviral RNA helicases MDA5 and LGP2. *Journal of virology* 83, 7252–7260.

- Pasdeloup, D., Poisson, N., Raux, H., Gaudin, Y., Ruigrok, R. W., and Blondel, D. (2005). Nucleocytoplasmic shuttling of the rabies virus P protein requires a nuclear localization signal and a CRM1-dependent nuclear export signal. *Virology* 334, 284–293.
- Peluso, R. W., and Moyer, S. A. (1988). Viral proteins required for the in vitro replication of vesicular stomatitis virus defective interfering particle genome RNA. *Virology* 162, 369–376.
- Perkins, N. D. (2007). Integrating cell-signalling pathways with NF-kappaB and IKK function. *Nat.Rev.Mol.Cell Biol.* 8, 49–62.
- Pichlmair, A., and Sousa, R. e (2007). Innate recognition of viruses. *Immunity* 27, 370–383.
- Pippig, D. A., Hellmuth, J. C., Cui, S., Kirchhofer, A., Lammens, K., Lammens, A., Schmidt, A., Rothenfusser, S., and Hopfner, K.-P. (2009). The regulatory domain of the RIG-I family ATPase LGP2 senses double-stranded RNA. *Nucleic acids research* 37, 2014–2025.
- Pomerantz, J. L., and Baltimore, D. (1999). NF-kappaB activation by a signaling complex containing TRAF2, TANK and TBK1, a novel IKK-related kinase. *EMBO J* 18, 6694–6704.
- Prehaud, C., Wolff, N., Terrien, E., Lafage, M., Megret, F., Babault, N., Cordier, F., Tan, G. S., Maitrepierre, E., Menager, P., et al. (2010). Attenuation of rabies virulence: takeover by the cytoplasmic domain of its envelope protein. *Sci.Signal.* 3, ra5.
- Qin, B. Y., Liu, C., Lam, S. S., Srinath, H., Delston, R., Correia, J. J., Derynck, R., and Lin, K. (2003). Crystal structure of IRF-3 reveals mechanism of autoinhibition and virus-induced phosphoactivation. *Nature structural biology* 10, 913–921.
- Raux, H., Flamand, A., and Blondel, D. (2000). Interaction of the rabies virus P protein with the LC8 dynein light chain. *J Virol* 74, 10212–10216.
- Ribeiro Jr., E. A., Favier, A., Gerard, F. C., Leyrat, C., Brutscher, B., Blondel, D., Ruigrok, R. W., Blackledge, M., and Jamin, M. (2008). Solution structure of the C-terminal nucleoprotein-RNA binding domain of the vesicular stomatitis virus phosphoprotein. *J.Mol.Biol.* 382, 525–538.
- Rieder, M., Brzozka, K., Pfaller, C. K., Cox, J. H., Stitz, L., and Conzelmann, K. K. (2011). Genetic dissection of interferon antagonistic functions of rabies virus phosphoprotein: Inhibition of interferon regulatory factor 3 activation is important for pathogenicity. *Journal of virology* Vol. 85, 842–852.
- Rieder, M., and Conzelmann, K.-K. (2011). Interferon in rabies virus infection. *Advances in virus research* 79, 91–114.
- Rothenfusser, S., Goutagny, N., DiPerna, G., Gong, M., Monks, B. G., Schoenemeyer, A., Yamamoto, M., Akira, S., and Fitzgerald, K. A. (2005). The RNA helicase Lgp2 inhibits TLR-independent sensing of viral replication by retinoic acid-inducible gene-I. *J Immunol* 175, 5260–5268.
- Rudd, B. D., Smit, J. J., Flavell, R. A., Alexopoulou, L., Schaller, M. A., Gruber, A., Berlin, A. A., and Lukacs, N. W. (2006). Deletion of TLR3 alters the pulmonary immune environment and mucus production during respiratory syncytial virus infection. *J.Immunol.* 176, 1937–1942.
- Rupprecht, C. E., Hanlon, C. A., and Hemachudha, T. (2002). Rabies re-examined. *Lancet Infect Dis* 2, 327–343.
- Ryzhakov, G., and Randow, F. (2007). SINTBAD, a novel component of innate antiviral immunity, shares a TBK1-binding domain with NAP1 and TANK. *EMBO J* 26, 3180–3190.
- Saitoh, T., Tun-Kyi, A., Ryo, A., Yamamoto, M., Finn, G., Fujita, T., Akira, S., Yamamoto, N., Lu, K. P., and Yamaoka, S. (2006). Negative regulation of interferon-regulatory factor 3-dependent innate antiviral response by the prolyl isomerase Pin1. *Nature immunology* 7, 598–605.

- Sandrock, M., Frese, M., Haller, O., and Kochs, G. (2001). Interferon-induced rat Mx proteins confer resistance to Rift Valley fever virus and other arthropod-borne viruses. *J Interferon Cytokine Res* 21, 663–668.
- Schafer, S. L. (1998). Regulation of Type I Interferon Gene Expression by Interferon Regulatory Factor-3. *Journal of Biological Chemistry* 273, 2714–2720.
- Schmidt, A., Schwerd, T., Hamm, W., Hellmuth, J. C., Cui, S., Wenzel, M., Hoffmann, F. S., Michallet, M. C., Besch, R., Hopfner, K. P., et al. (2009). 5'-triphosphate RNA requires base-paired structures to activate antiviral signaling via RIG-I. *Proc Natl Acad Sci U S A*.
- Schneider, L. G., and Cox, J. H. (1994). Bat lyssaviruses in Europe. *Current topics in microbiology and immunology* 187, 207–218.
- Schneider, L., Barnard, B., and Schneider, H. (1985). Application of monoclonal antibodies for epidemiological investigations and oral vaccination studies. In: Kuwert E, Merieux C, Koprowski H, Bagel K, editors. *Rabies in the tropics*, p. 47–59.
- Schnell, M. J., McGettigan, J. P., Wirblich, C., and Papaneri, A. (2010). The cell biology of rabies virus: using stealth to reach the brain. *Nature reviews. Microbiology* 8, 51–61.
- Schnell, M. J., Mebatsion, T., and Conzelmann, K. K. (1994). Infectious rabies viruses from cloned cDNA. *EMBO J* 13, 4195–4203.
- Schoehn, G., Iseni, F., Mavrakis, M., Blondel, D., and Ruigrok, R. W. (2001). Structure of recombinant rabies virus nucleoprotein-RNA complex and identification of the phosphoprotein binding site. *J. Virol.* 75, 490–498.
- Sen, G. C., and Peters, G. A. (2007). Viral stress-inducible genes. *Adv. Virus Res* 70, 233–263.
- Shi, H.-X., Yang, K., Liu, X., Liu, X.-Y., Wei, B., Shan, Y.-F., Zhu, L.-H., and Wang, C. (2010). Positive regulation of interferon regulatory factor 3 activation by Herc5 via ISG15 modification. *Molecular and cellular biology* 30, 2424–2436.
- Shope, R. E., Murphy, F. A., Harrison, A. K., Causey, O. R., Kemp, G. E., Simpson, D. I., and Moore, D. L. (1970). Two African viruses serologically and morphologically related to rabies virus. *Journal of virology* 6, 690–692.
- Silverman, R. H. (2007). Viral Encounters with OAS and RNase L during the IFN Antiviral Response. *J Virol.*
- Takahasi, K., Horiuchi, M., Fujii, K., Nakamura, S., Noda, N. N., Yoneyama, M., Fujita, T., and Inagaki, F. (2010). Ser386 phosphorylation of transcription factor IRF-3 induces dimerization and association with CBP/p300 without overall conformational change. *Genes to cells : devoted to molecular & cellular mechanisms* 15, 901–910.
- Takahasi, K., Kumeta, H., Tsuduki, N., Narita, R., Shigemoto, T., Hirai, R., Yoneyama, M., Horiuchi, M., Ogura, K., Fujita, T., et al. (2009). Solution structures of cytosolic RNA sensor MDA5 and LGP2 C-terminal domains: identification of the RNA recognition loop in RIG-I-like receptors. *The Journal of biological chemistry* 284, 17465–17474.
- Tan, G. S., Preuss, M. A., Williams, J. C., and Schnell, M. J. (2007). The dynein light chain 8 binding motif of rabies virus phosphoprotein promotes efficient viral transcription. *Proc Natl Acad Sci U S A* 104, 7229–7234.
- Theodorides, J. (1986). *Histoire de la rage*. p. 289.
- Traenckner, E. B., Pahl, H. L., Henkel, T., Schmidt, K. N., Wilk, S., and Baeuerle, P. A. (1995). Phosphorylation of human I kappa B-alpha on serines 32 and 36 controls I kappa B-alpha proteolysis and NF-kappa B activation in response to diverse stimuli. *The EMBO journal* 14, 2876–2883.
- Tuffereau, C., Schmidt, K., Langevin, C., Lafay, F., Dechant, G., and Koltzenburg, M. (2007). The rabies virus glycoprotein receptor p75NTR is not essential for rabies virus infection. *Journal of virology* 81, 13622–13630.

- Uematsu, S., Sato, S., Yamamoto, M., Hirotsu, T., Kato, H., Takeshita, F., Matsuda, M., Coban, C., Ishii, K. J., Kawai, T., et al. (2005). Interleukin-1 receptor-associated kinase-1 plays an essential role for Toll-like receptor (TLR)7- and TLR9-mediated interferon- α induction. *The Journal of experimental medicine* 201, 915–923.
- Vidal, S., and Kolakofsky, D. (1989). Modified model for the switch from Sendai virus transcription to replication. *J. Virol.* 63, 1951–1958.
- Vidy, A., Chelbi-Alix, M., and Blondel, D. (2005). Rabies virus P protein interacts with STAT1 and inhibits interferon signal transduction pathways. *J Virol* 79, 14411–14420.
- Vidy, A., El Bougrini, J., Chelbi-Alix, M. K., and Blondel, D. (2007). The nucleocytoplasmic rabies virus P protein counteracts interferon signaling by inhibiting both nuclear accumulation and DNA binding of STAT1. *J Virol* 81, 4255–4263.
- Weber, F., Wagner, V., Rasmussen, S. B., Hartmann, R., and Paludan, S. R. (2006). Double-stranded RNA is produced by positive-strand RNA viruses and DNA viruses but not in detectable amounts by negative-strand RNA viruses. *J Virol* 80, 5059–5064.
- Whelan, S. P. (2008). Response to “Non-segmented negative-strand RNA virus RNA synthesis in vivo.” *Virology* 371, 234–237.
- Whelan, S. P., Barr, J. N., and Wertz, G. W. (2004). Transcription and replication of nonsegmented negative-strand RNA viruses. *Curr Top Microbiol. Immunol* 283, 61–119.
- Williams, B. R. (1999). PKR; a sentinel kinase for cellular stress. *Oncogene* 18, 6112–6120.
- Yang, K., Shi, H., Qi, R., Sun, S., Tang, Y., Zhang, B., and Wang, C. (2006). Hsp90 regulates activation of interferon regulatory factor 3 and TBK-1 stabilization in Sendai virus-infected cells. *Mol. Biol. Cell* 17, 1461–1471.
- Yang, K., Shi, H.-X., Liu, X.-Y., Shan, Y.-F., Wei, B., Chen, S., and Wang, C. (2009). TRIM21 is essential to sustain IFN regulatory factor 3 activation during antiviral response. *Journal of immunology (Baltimore, Md. : 1950)* 182, 3782–3792.
- Yoneyama, M., Kikuchi, M., Matsumoto, K., Imaizumi, T., Miyagishi, M., Taira, K., Foy, E., Loo, Y. M., Gale Jr., M., Akira, S., et al. (2005). Shared and unique functions of the DExD/H-box helicases RIG-I, MDA5, and LGP2 in antiviral innate immunity. *J Immunol* 175, 2851–2858.
- Yoneyama, M., Kikuchi, M., Natsukawa, T., Shinobu, N., Imaizumi, T., Miyagishi, M., Taira, K., Akira, S., and Fujita, T. (2004). The RNA helicase RIG-I has an essential function in double-stranded RNA-induced innate antiviral responses. *Nat Immunol* 5, 730–737.
- Yoneyama, M., Suhara, W., Fukuhara, Y., Fukuda, M., Nishida, E., and Fujita, T. (1998). Direct triggering of the type I interferon system by virus infection: activation of a transcription factor complex containing IRF-3 and CBP/p300. *The EMBO journal* 17, 1087–1095.
- Yoneyama, M., and Fujita, T. (2010). Recognition of viral nucleic acids in innate immunity. *Rev. Med. Virol.* 20, 4–22.